Theoretical Studies of Ultracold Atoms in Optical Lattices and Superlattices

THESIS

Submitted

In partial fulfillment of the requirement for the degree of

Doctor of Philosophy

To

INDIRA GANDHI NATIONAL OPEN UNIVERSITY

By

Manpreet Singh

School of Inter-Disciplinary and Trans-Disciplinary Studies,

Indira Gandhi National Open University,

New Delhi – 110 068

April, 2015

DECLARATION

I, Manpreet Singh, do hereby solemnly declare that the Thesis entitled "Theoretical Studies of Ultracold Atoms in Optical Lattices and Superlattices" is a faithful record of the work carried out by me under the supervision of Professor Bhanu Pratap Das of Indian Institute of Astrophysics, Bangalore. I further declare that I have not submitted any part of this Thesis for the award of any other degree of the Indira Gandhi National Open University, New Delhi or any other university in India or abroad.

(Manpreet Singh)
Place : New Delhi
Date : 20 April, 2015

CERTIFICATE

This is to certify that the Thesis entitled "Theoretical Studies of Ultracold Atoms in Optical Lattices and Superlattices" submitted for the award of the degree of Doctor of Philosophy in Astrophysics of Indira Gandhi National Open University, is actual record of bonafide work carried out by Mr. Manpreet Singh under our guidance and supervision. To the best of our knowledge the Thesis is an original work and it has not been submitted for the award of any other degree or diploma in any institution in India or abroad. The Thesis is worthy of consideration for the award of the degree of Doctor of Philosophy (Ph.D.) in Astrophysics.

(Prof. Bhanu Pratap Das) Supervisor
Indian Institute of Astrophysics
2nd Block, Koramangala
Bangalore

(Dr. Nandini Sinha Kapur)
Director,
School of Inter-Disciplinary and
Trans-Disciplinary Studies (SOITS),
IGNOU, New Delhi

(Dr. C. K. Ghosh)
Program Coordinator and Nodal Officer,
IGNOU-IIA Int. M.Sc.-PhD. in
Physics and Astrophysics
IGNOU, New Delhi

List of Publications

1. *Mean-field analysis of quantum phase transitions in a periodic optical superlattice.*
Arya Dhar, **Manpreet Singh**, Ramesh V. Pai, and B. P. Das
Physical Review A **84**, 033631 (2011).

2. *Three-body on-site interactions in ultracold bosonic atoms in optical lattices and superlattices.*
Manpreet Singh, Arya Dhar, Tapan Mishra, R. V. Pai, B. P. Das
Physical Review A (Rapid Communication) **85**, 051604 (2012).

3. *Quantum phases of attractive bosons on a Bose-Hubbard ladder with three-body constraint.*
Manpreet Singh, Tapan Mishra, Ramesh V. Pai, and B. P. Das.
Physical Review A **90**, 013625 (2014).

Acknowledgements

First and foremost, I offer my sincerest gratitude to my thesis supervisor, Professor Bhanu Pratap Das, who has supported me throughout my thesis with his patience, knowledge and encouragement to develop my skills. Without his support and effort this thesis would not have been written or completed. He is the one who first introduced me to the dynamic field of ultracold atoms as well as high-performance computing. He made sure that I met the right people and visited the right places, like C-DAC, to enhance my skills, especially in these two areas. He has been and will remain a father figure, friend and a mentor to me. He sacrificed his weekends to come to the institute and have discussions. Even when he was given an additional responsibility as an acting Director of the institute, he made room in his busy schedule to have regular interactions. Our discussions were not limited to science, at times we talked about history, politics, sports and a lot of other relevant things. All in all, I will be indebted to him my entire life for all that he has given me within a short span of just five years and I am sure he will stand by my side in my future endeavours.

I am grateful to Dr. Ramesh V. Pai for sharing his expertise on ultracold atoms and numerical techniques used to study these systems. Although he resides in Goa and works with the Goa University, he tried to visit our group in Bangalore whenever possible and discuss the problems I have worked upon. He also arranged my visit to Goa University during which he helped me develop cluster mean-field codes and also explained the DMRG method in details. He has been kind enough to collaborate and share his codes for

numerical calculations. He has been very co-operative and always made time for clearing my doubts over phone and online chats. I can never thank him enough for this.

I would also like to acknowledge Dr. Tapan Mishra, my senior and an ex-student of Professor Bhanu Pratap Das. Along with my supervisor and Dr. Ramesh V. Pai, he has been instrumental in teaching me the DMRG basics. He showed a lot of patience during the discussions. While he was a post-doctoral fellow at International Centre for Theoretical Sciences (Bangalore), I used to visit him often and we had lengthy discussions about the DMRG method and problems I have been working on. I greatly admire his qualities not only as a researcher but also as a friend.

I would like to thank the other group members, Dr. Arya Dhar and Srinivasa Prasannaa. Arya helped me to learn the Matrix Product States method and start our group's collaboration with Rosario Fazio and Davide Rossini at SNS, in Pisa (Italy). Prasannaa also has been very active and we had many useful discussions.

My sincere and heartfelt thanks to Professor Kapur Mal Jain, for his excellent guidance and support during my B.Sc. He inspired me a lot and and encouraged me to join for Ph.D.. He understood my interests and provided all the necessary training and resources to keep those interests alive, especially in experimental physics. I would also like to thank Professor Anuj Hundeit, Dr. Shreyas Pitale, Dr. Harsha Jalori, Dr. Rinku Verma and other staff members of Institute for Excellence in Higher Education (Bhopal), for not only taking our courses but also for creating a very friendly and learning atmosphere. It helped me to have open discussions with them without any hesitation or second thoughts. Also, I can never forget my friends at IEHE, especially Anjana, Jasmeet, Juhi, Nidhisha, Divy Jot Jain, Shatrughan and Sumit for providing a home like atmosphere. Because of them, I never felt lonely or lost even though I was staying alone in Bhopal, far from my native place, Lalitpur.

I would like to thank my batch mates Avijeet Prasad and Ramesh Pandey for all their help. They have been very co- operative and I learnt a lot from them. Special thanks

to my M.Tech.-Ph.D.. batch mates Anantha Chanumolu, Arun Surya and Sajal Dhara for letting me borrow their laptops when I wanted to work from the hostel late night and Vineeth Valsan who made my visit to Italy very easy and comfortable. I would also like to thank my other colleagues in IIA, especially Susmitha, Preethi, Honey, Tanmoy, Samyaday, Sangeetha, Sowmya, and Supriya. I would also like to thank all my seniors Blesson, Sreeja, Veeresh, Nataraj, Anusha, Jayashree, Madhulita, Krishna, Indu, Ramya, Hema, Pradeep, Smitha, Prashanth, and Athiray. I indeed feel lucky to have so wonderful juniors and would like to express my thanks to Ambily, Annu, Avinash, Hemanth, Joby, Joice, Mayuresh, Mugundhan, Nancy, Nirmal, Prasanna, Priyanka, Ramya, Shubham, Panini, Phanindra, Anshu, Sireesha, Sreekanth, Subhamoy, Sudip, Tarun, Mageshwaran, Vaibhav, Vaidehi, Varun, Vidhya, Avrajit, Anirban, Chayan, Deepanwita, Megha, Prasanta, Rubinur, Samrat, Snehalata, Tridib and the internship students Amruta, Athira, Deepthi, Estrella, Jaya, Julius, Keyuri, Maitrayee, Manasa, Ragadeepika, Smitha and Sripathy.

I am thankful to the Director of IIA, the Dean and the Board of Graduate Studies (BGS) for facilitating all academic matters during my Ph.D. tenure. I am also thankful to all the faculty members who taught during the M.Sc. and who took the lab courses. I am thankful to Dr. Baba Varghese, Dr. Dipankar Banerjee, Anish, Rekhesh, Fayaz and Ashok for helping me extensively with computer related issues. I am grateful to Dr. Sachin Nanavati from C-DAC Pune for teaching me parallel programming.

I would like to thank Prof. M. Aslam (Vice Chancellor, IGNOU), Prof. Vijayshri (Director, SOS, IGNOU), Dr. Nandini Sinha Kapur (Director, SOITS, IGNOU), Dr. C. K. Ghosh (Program Coordinator and Nodal Officer, IGNOU-IIA Integrated M.Sc.-PhD. in Physics and Astrophysics Programme), and other staff members of the Research Unit and SOITS for helping me with various academic procedures.

I am grateful to the administrative staff at IIA for their co-operation in all matters. In particular I would like to thank Dr. Kumaresan, Mr. Narasimha Raju, Mr. S. B. Ramesh, Mr. Valsalan, Mr. Parthasarathy, Mr. Lakshmaiah, Mr. Sankar, Ms. Meena,

Mr. Rajendran, Mr. Mohan, Ms. Pramila (Director's office), Ms. Malini, Ms. Pramila (Dean's office), and Mr. Suresh for their kind help and support, which enabled me to proceed through administrative activities without any hassles.

Of course this acknowledgements would be incomplete without giving thanks to my parents, uncle, aunty, my brothers and sisters. I extend my respect to my parents, my paternal and maternal grand parents and all elders to me in the family. I don't imagine a life without their love and blessings. I can't thank them enough for showing faith in me and giving me liberty to choose what I desired. I consider myself the luckiest in the world to have such a supportive family, standing behind me with their love and support.

Abstract

The study of ultracold atoms is one of the frontier research areas of modern physics. The ability to control precisely the interactions between the ultracold atoms in optical lattices has led to the prediction and in some cases observation of different phases of matter at ultracold temperatures. Further investigations in this area could lead to the realization of quantum computers and a better understanding of high temperature superconductivity. The applications of ultracold atoms are not restricted to the field of condensed matter physics. These systems can be used to simulate the physics of the early universe and also some astrophysical phenomena.

This thesis reports on certain specific theoretical studies of ultracold atoms in optical lattices and superlattices. Ultracold atoms can exhibit different kinds of phases depending on the strengths of various interactions, densities and geometry of the system. We investigate some of these phases primarily using the mean-field theory and the density matrix renormalization group (DMRG) method. In Chapter 1, we give a brief introduction to the field of ultracold atoms. In Chapter 2, we give a description of the theoretical tools used to obtain quantitative results for the problems studied in this thesis work. In Chapter 3, we focus on the well known superfluid to Mott-insulator phase transition of ultracold atoms in optical lattices. We obtained the transition critical points as well as the phase diagram using perturbation theory first and then mean-field theory, to compare the two methods. We then present our results for ultracold atoms in optical superlattices. Chapters 4 and 5 are based on the study of ultracold atoms in optical lattices and superlattices with the

on-site three body interaction, using mean-field and DMRG methods, respectively. In Chapter 6, we report our findings on the quantum phases of attractive bosons in two coupled one -dimensional optical lattices. In Chapter 7, we discuss our results obtained for a non-equilibrium study of ultracold atoms in optical lattices within the frame work of the extended Bose-Hubbard model. Finally, in Chapter 8 we summarize our findings for the above mentioned problems and suggest scope for future work in this field.

Contents

List of Figures

List of Tables

Chapter 1

Introduction

1.1 Ultracold atoms

The field of ultracold atoms is an area at the cutting edge of modern physics. The study of these systems can be used for providing insights into a large range of condensed matter phenomena. Ultracold atomic and molecular gases are much larger than nanoscale systems. In Bose-Einstein condensation (BEC), for example, thousands of atoms collapse into a single one millimeter wave that is large enough for observations in the laboratory. Degenerate Fermi quantum gases have also been observed using a high-resolution optical microscope [1, 2]. A gas of ultracold atoms can be modeled in a manner similar to electrons in a crystal [3]. Atom lasers have been demonstrated using Bose-Einstein condensates [4, 5]. As a result of these properties ultracold atoms provide unique insights into the microscopic quantum world.

The inception of the field of the ultracold atoms dates back to 1925, when Albert Einstein completed his seminal work on the theory of the phenomenon that we know as BEC [6]. This work was based on the novel ideas on photon statistics from Satyendra Nath Bose, who had sought Einstein's advice. Today, we know that BEC is based on

quantum statistics and is intimately connected to the wave nature of particles. Einstein predicted the phenomenon of BEC without the knowledge of any quantum mechanics, which was in fact just being discovered during that time.

An atom has certain energy levels. The distribution of atoms (for bosons) in these energy levels is governed by the Bose-Einstein distribution:

$$\langle n_i \rangle = \frac{1}{exp[(\epsilon_i - \mu)/k_B T] - 1} \tag{1.1}$$

where n_i is the number of particles in state i, ϵ_i is the energy of the i^{th} state, μ is the chemical potential, k_B is the Boltzmann constant, and T is absolute temperature. Based on this statistics Einstein showed that with the onset of ultracold temperatures ($10^{-9}K$), a very large fraction of atoms will occupy the lowest energy state. This phenomenon is called BEC, which corresponds to a state of matter in which all the atoms are in the same quantum state. The remarkable property of a BEC is that all the atoms which make it up exhibit identical quantum behavior, i.e. they are all in the same phase below a critical temperature.

After the seminal work of Einstein, BEC was first observed by Eric Cornell and Carl Wieman in 1995 at the University of Colorado at Boulder NIST-JILA lab, using a gas of rubidium atoms cooled to 170 nanokelvin (nK) ($1.7 \times 10^{-7}K$). They used the technique of laser cooling followed by evaporative cooling and magnetic confinement to trap the atoms at such low temperatures [7]. The 1997 Nobel prize in Physics was awarded to Chu, Cohen-Tannoudji and Phillips for their pioneering work on laser cooling of atoms [8] and subsequently the 2001 Nobel prize in Physics was awarded to Eric Cornell, Carl Wieman, and Wolfgang Ketterle of MIT [9] for the experimental realization and elucidating the properties of BECs. There has been rapid progress in the field of ultracold atoms since that time. Remarkable advances has been made in this field in a very short time. As of today, Bose-Einstein Condensates are readily available in the leading laboratories and more than 30 research groups around the world are carrying out experiments with this new form of quantum matter. BEC has been subsequently achieved in several atomic

species, some of them are: ^{1}H,^{4}He,^{7}Li,^{23}Na,^{39}K,^{41}K,^{52}Cr,^{85}Rb,^{87}Rb, ^{133}Cs,^{170}Yb and ^{174}Yb.

Bose-Einstein Condensates can be moved, shaken and rotated without instantaneously destroying their quantum properties. Therefore Bose-Einstein Condensates are ideal for performing experiments in the context of a number of different physical situations [10]. In ultracold quantum gases (at $\sim 10^{-9}$K temperatures), particles interact mainly by s-wave scattering. In this case one can express the long distance interaction such as the van der Waals interaction in terms of a pseudo potential which is short range and isotropic in nature:

$$U_{int}(r) = \frac{4\pi\hbar^2 a_s}{m}\delta(r) = g\delta(r) \tag{1.2}$$

where a_s is the s-wave scattering length and m is the mass of atom. The magnitude and also the sign of a_s can be varied between a large range of values using the method of Feshbach resonance [11, 12]. In this method, the internal states of the particles and hence the scattering lengths are modified. For example in the case of ^{85}Rb, the scattering length was tuned over several orders of magnitude [13, 14]. The weakly interacting gas can be well understood in the framework of the well known Gross-Pitaevski equation and the Bogoliubov theory [10, 15, 16]. The gas is said to be weakly interacting when the ratio between the interaction energy of uncorrelated atoms (E_{int}) and the quantum kinetic energy (E_{kin}) needed to correlate the atoms within a distance of the order of inter-particle separation is small. For a three dimensional system the interaction energy is given as:

$$E_{int} = n\frac{4\pi\hbar^2 a_s}{m} \tag{1.3}$$

and the kinetic energy is given as:

$$E_{kin} = \frac{\hbar^2}{m}n^{2/3} \tag{1.4}$$

where n is the atomic density and a_s is the scattering length. The ratio between the two quantities turns out to be na_s. In dilute alkali vapors this ratio is typically of the order of

0.02. In order to achieve the strongly correlated regime, either the density of atoms or the scattering length a_s must be increased. But in this regime, the lifetime of the condensate decreases due to naturally occurring three body losses [17]. To overcome this problem, an optical lattice is considered to be the ideal tool to realize the strongly correlated regime. In an optical lattice, the ratio between the potential energy and the kinetic energy can be changed by increasing the depth of the lattice without changing either the density or the scattering length [3]. The ability to precisely control the interaction parameters by tuning the laser intensity and wavelength, makes optical lattice systems an ideal tool to study strongly correlated atomic systems.

1.2 Applications

Ultracold atoms in optical lattices have offered a fresh and new approach to some of the long standing questions in condensed matter and other fields of physics. The merit of these investigations using ultracold atoms in optical lattices is that almost all relevant parameters such as the lattice potential depth, the lattice geometry and the interaction strength between the particles can be tuned over a wide range, while one is also able to observe the dynamical response of the system [18]. Furthermore, the crucial effect of dimensionality can be investigated and has been at the heart of a series of recent fundamental studies of, e.g., one-dimensional quantum gases [19]. The wavelength of atoms can be orders of magnitude smaller than that of light and so an interferometer based on atoms has the potential to be very sensitive.

Atoms interact quite differently with their environment as compared to photons. For example, atoms couple directly to the gravitational field and so can be a sensitive measure of gravity. Gravity has been intensively studied on large length scales, but the situation at short length scales, below about a millimeter, is comparatively unknown. Atomic interferometers hold out the possibility of making exquisitely sensitive measurements of

the gravitational field at very small distances from an object. Such measurements might have far-reaching consequences since string theory, the current most fundamental but as yet untested theory of 'everything', predicts extra dimensions which can soak up gravitons and thus weaken gravity on small scales [20].

Ultracold atoms can be used to understand some astrophysical phenomena too, for example, stellar superfluidity. Based on the observed cooling rate of the star Cassiopeia A in the Cassiopeia constellation, astrophysicists believe that the neutrons in its core to be in a superfluid state. Neutron stars are the compact remnants of certain supernova explosions. They are born from the catastrophic gravitational collapse of the iron core of massive stars at the end point of their evolution. Their masses are $\sim$ 1 to 2 times mass of the Sun but constrained in a radius of $\sim$ 10 km. The average density of a neutron star is thus $\sim 10^{17}$ kg/m^3 at the core, which is comparable to the density of atomic nuclei. Nucleons are fermions, and due to the Pauli exclusion principle, they generally tend to avoid themselves. This individualistic behavior of nucleons, together with the strong repulsive nucleon-nucleon interaction at short distance, provide the necessary pressure to counterbalance the huge gravitational pull in a neutron star, thereby preventing it from collapsing. However, at low enough temperatures ($\sim 10^9$ K), nucleons may form pairs. These pairs are bosons that can behave coherently on a very large scale and the nucleon condensate can flow without any viscosity, analogous to a superfluid. Neutron matter and ultracold atomic gases are separated by 17 orders of magnitude in temperature: however, in terms of their corresponding Fermi temperatures, their critical temperatures are very large, essentially of comparable magnitude. This is the reason both these systems can be viewed as "high-temperature superfluids" [21].

Ultracold atoms in optical lattices can help us design better superconductors, which are materials that conduct electricity with little or no resistance. Currently superconductivity is achievable only at very low temperatures (< 100K or -173°C). High-temperature superconductors are desirable for a range of applications, from transferring electricity in a

city, to medical applications, etc. Ultracold atoms in optical lattices are very clean systems and can be easily manipulated. It is possible to make a lattice loaded with ultracold atoms so that it has the same structure as that of a high-temperature superconductor. Then we can move and deform that pattern in such a way that we can see which patterns are suitable for superconductivity. This way it is possible to design better high-temperature superconductors.

In addition to the fascinating physics of strongly correlated quantum matter, ultracold atoms in optical lattices also offer many new possibilities for quantum information processing, especially due to the large size of the quantum registers that can be realized. At National Institute of Standards and Technology (NIST, Colarado, U.S.) Rey et al have figured out how a Sr-based quantum computer could store qubits and have come up with a plan for communicating with individual atoms. They have also worked out a scheme for selecting a single atom, moving it to another location in an optical lattice to interact with another qubit, and then moving it back, all under coherent control. These solutions required two specially engineered optical lattices that specifically address the interactions of the Sr atoms with the trapping laser light. The computer's optical lattices would be created from two separate wavelengths of red light. One wavelength (689.2 nm) has no net effect on Sr atoms in their ground state, while the other (627 nm) has no net effect on Sr atoms in their electronically excited, but metastable, state. The 689.2 nm lattice would be the qubit "transport" lattice, and the 627 nm lattice would be the qubit "storage" lattice. The storage lattice would hold the qubits in their ground state. When a specific qubit (i.e., atom) needs to be transported, it could be excited with laser light into its metastable state and loaded into the 689.2 nm transport lattice, where its motion could be precisely controlled (again with laser light) [22, 23].

Coherent matter-wave optics based on BECs (where all the atomic de Broglie waves are in phase) is just starting out, but is rapidly becoming a very active research area.

1.3 Laser cooling

Atoms can be slowed down by shining a laser on them. The idea of laser cooling seems very counterintuitive because lasers are source of high intensity, heat and a lot of energy. But then we can control light so well with lasers, both its frequency and intensity, that we can direct the light to slow atoms down. Normally, atoms don't interact with light. But if the lasers are calibrated to just the right wavelength, the photons and atoms interact. The photons carry momentum and if we can bounce the 'right' photons off of an atom then we can make the atom recoil and slow down. This is equivalent to cooling it. This allows us to cool atoms down to some millionths of a degree above absolute zero, they can then be held in atom traps made from electromagnetic fields and/or 'optical lattices' made from the interference of two or more laser beams. The complete process can be summarized in the steps given below:

1. A stationary atom sees the laser neither red- nor blue-shifted and does not absorb the photon.

2. An atom moving away from the laser sees it red- shifted and does not absorb the photon.

3. An atom moving towards the laser sees it blue- shifted and absorbs the photon, slowing the atom. The photon excites the atom, moving an electron to a higher quantum state.

4. The above atom re-emits a photon in a random direction. Because of this randomness there is no net change in momentum over many absorption-emission cycles. But the final momentum of atom now reduces in the direction opposite to the laser beam.

1.4 Optical lattices

Optical lattices are potential wells created by the interference patterns of counter propagating laser beams. These potential wells can trap neutral atoms, creating a system that resembles a crystal, with the atoms in optical lattices being analogous to electrons in solid-state crystals. Unlike naturally occurring crystals, however, these "artificial light crystals" are completely regular, without flaws. As such, they are an ideal quantum system where all parameters can be manipulated experimentally. They can be used to study effects that are difficult to observe in real crystals or other condensed matter systems. Optical lattices each contain a single large ultracold atom or molecule, with spacing between lattice sites of the order of 500–1000 nm.

Neutral atoms interact with a light field in both a dissipative and a conservative way. The dissipative component of the interaction arises due to the absorption of photons followed by subsequent spontaneous emission. It results in a dissipative force on the atoms caused by the momentum transfer of the absorbed and spontaneously emitted photons. This light force is widely used for laser cooling and magneto-optical traps [24]. The atom–light interaction arises due to the interaction of the light field with the light-induced dipole moment of the atom. This interaction causes a shift in the potential energy, called the ac-Stark shift. For large detuning of the light versus the atomic resonances, spontaneous emission processes can be neglected and the energy shift can be used to create a conservative trapping potential for neutral atoms. By shining a spatially modulated light field onto a cloud of atoms an energy landscape can be formed, where the local potential energy is proportional to the local light intensity [25].

When an atom is placed into a laser light field, the electric field $\mathbf{E}$, oscillating with the complex amplitude E at a frequency $\omega = 2\pi\nu$, induces an oscillating atomic dipole moment $\mathbf{d}$. The dipole moment oscillates at the same frequency with the complex amplitude d given by $d = \alpha(\omega)E$. Here, $\alpha(\omega)$ is the complex polarizability which depends on the laser frequency ω. The resulting dipole potential is determined by time averaging

over **d.E**,

$$V_{dip}(r) = -\frac{1}{2} < dE(r) >= -\frac{1}{2\epsilon_0 c} Re(\alpha) I(r), \tag{1.5}$$

with the laser field intensity given by

$$I = \frac{1}{2}\epsilon_0 c |E|^2. \tag{1.6}$$

Relating the dipole moment to the decay rate Γ of the excited state in a two-level system, one then finds for the optical dipole potential:

$$V_{dip}(r) \approx \frac{3\pi c^2}{2{\omega_0}^3} \frac{\Gamma}{\Delta} I(r) \tag{1.7}$$

where $\Delta = \omega - \omega_0$ denotes the detuning of the laser light relative to the atomic transition frequency ω_0. For a blue detuning $\omega > \omega_0$, a repulsive potential is created; whereas for a red detuning $\omega < \omega_0$ an attractive potential is realized.

By interfering two counter propagating laser beams a periodic potential of the form $V(x) = V_0 sin^2(kx)$ can be created. Here, $k = 2\pi/\lambda$ with λ being the wavelength of the laser light used and V_0 denotes the potential depth of the lattice. This lattice depth is usually expressed in natural units of the recoil energy $E_r = \hbar^2 k^2 / 2m$.

For a one-dimensional standing wave the atoms are confined in pancake-like discs. If two such standing waves are overlapped, one can create an array of tightly confining potential tubes and for the case of three overlapping standing waves one creates a three-dimensional simple cubic lattice potential. The Gaussian beam profile of the laser beams typically leads to an additional harmonic confinement, resulting in a total optical potential of the form:

$$V_{lat}(x,y,z) \approx V_x sin^2(kx) + V_y sin^2(ky) + V_z sin^2(kz) + \frac{1}{2} m({\omega_x}^2 x^2 + {\omega_y}^2 y^2 + {\omega_z}^2 z^2). \tag{1.8}$$

A one-dimensional and a two-dimensional optical lattice sketches are shown in Fig. 1.1 and Fig. 1.2, respectively.

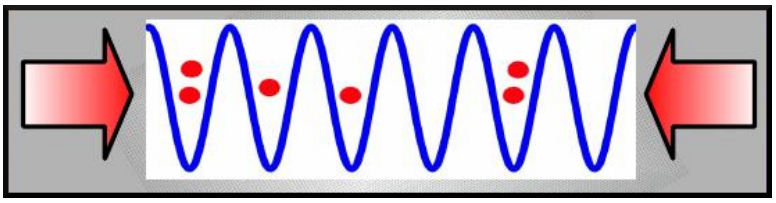

Figure 1.1: A one dimensional optical lattice. Arrows represent laser beams, blue lines represent trapping potential and red dots represent trapped atoms.

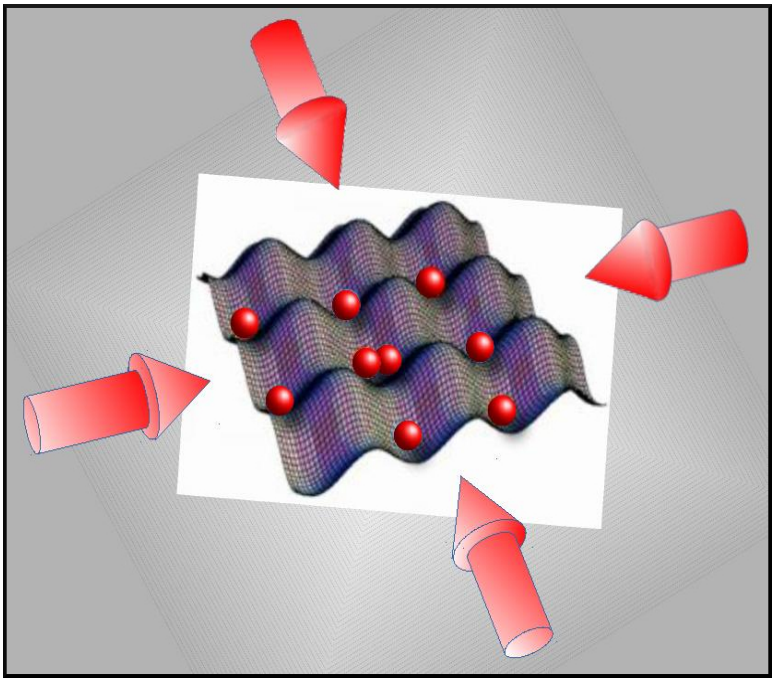

Figure 1.2: A two dimensional optical lattice. Red spheres represent the trapped atoms.

In an optical lattice the atoms are analogous to electrons in a crystal lattice like those found in a metal, but with some differences:

1. Atoms in traps and lattices are extremely idealized systems with almost no imperfections or impurities and minimal interactions with the environment. They are therefore simple to describe theoretically and maintain their quantum coherence for long times in comparison to the relevant timescales of the dynamics.

2. In atomic systems almost all of the parameters are under our control. For example, the dimension and symmetry of the lattice, the strength and even the sign of the inter-atomic interactions, can be chosen at will.

3. The measurement schemes are radically different from traditional condensed matter schemes, e.g. single atoms can now be non-destructively imaged, allowing us to track (and address) individual atoms in real time.

Therefore, ultracold atoms in optical lattices can used to investigate single- and many-particle quantum mechanics in a system that can be stripped down to the bare essentials. They can provide important insights into a wide variety of physical phenomena which cannot be easily dealt with in conventional condensed matter systems. By suitably controlling the laser intensity, it is possible to manipulate different parameters of a system. It is this feature which makes ultracold atoms in optical lattices ideal for the study of quantum phase transitions. For example, the superfluid to Mott insulator transition was observed in atoms in an optical lattice in 2002 [3].

Optical lattices have allowed us to go beyond the physics of a weakly interacting Bose gas and in fact bring the system into a regime where several intriguing phenomena of strongly correlated systems of condensed matter physics can be observed. Such strongly correlated systems lie at the forefront of research in modern condensed matter physics.

1.5 Optical superlattices

An optical superlattice is formed by the superposition of two optical lattices with different wavelengths and a relative phase shift with respect to each other. We consider an optical superlattice made up of two optical lattices with a periodicity of two sites. The relative shift in energy between any two consecutive sites resulting from the superposition is denoted by λ (superlattice potential). Any two consecutive sites are together treated as a single unit cell. Such a system can be studied by extending the simple optical lattice model. The added features in an optical superlattice being periodicity of unit cells (not single sites) and the relative energy shifts of the potential minima. One such superlattice is shown in the figure below. For a periodic optical superlattice as shown in Fig. 1.3 two neighboring sites constitute the unit cell.

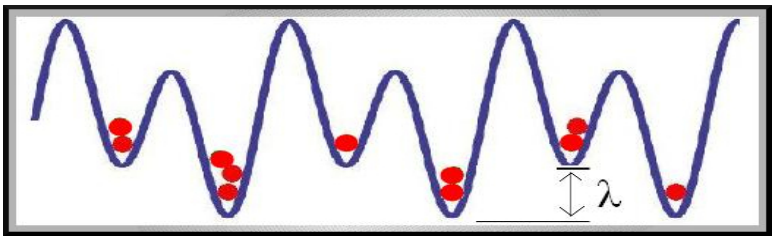

Figure 1.3: A one-dimensional optical superlattice. Red dots represent the trapped atoms and λ denotes the superlattice potential.

1.6 Quantum Phase Transitions

Phase transitions are ubiquitous in nature. Examples are the conversion of water to steam, melting of ice to water, transition from a normal to a superconducting solid, transition from a metal to an insulator etc. The above mentioned phase transitions occur due to changes in temperature (e.g. the long range crystalline order is lost due to thermal fluctuations etc). However, there is a special class of phase transitions which occur even

in the absence of temperature. They are known as quantum phase transitions (QPTs) [2, 7]. Quantum phase transitions are rather rare as they occur at the absolute zero temperature. Non-thermal parameters such as pressure, magnetic field, Coulomb and van der Waals interactions play a crucial role in bringing about these phase transitions which are characterized by a Heisenberg like uncertainty principle. The quantum fluctuations associated with these phase transitions determine the quantum critical points (QCPs). At a particular ratio between the lattice depth and the interaction strength the atoms undergo an abrupt change from being in a superfluid state, with the atoms delocalized across the lattice, to suddenly having exactly one atom (at density 1) per site with highly suppressed fluctuations. This is an example of a so-called quantum phase transition between different ground states of a many-particle system, in this case between a coherent state, where each atom is in a superposition of being on many different sites, and a Fock state of exactly one per site.

1.6.1 Superfluid to Mott-insulator transition

As the intensity of the laser beams is increased, the peak height of the standing waves increases. Eventually, the atoms do not have enough energy to overcome those energy barriers and are trapped in their position. This situation is identical to a similar situation for electrons in a crystal. If the barrier for electrons to jump from one position in the crystal to another is too high, they cannot move. Consequently, no electrical current flows. In condensed matter physics, this state is known as a Mott insulator [28]. In the MI phase, since the atoms are localized to the individual lattice sites, the number fluctuation is zero and hence the number of atoms on each site is a fixed number and can be exactly determined.

A Mott insulator provides an ideal environment for quantum information processing. When the relevant parameters such as density and the external harmonic confinement are tuned to the right values, a large region of the Mott insulator in the optical lattice can

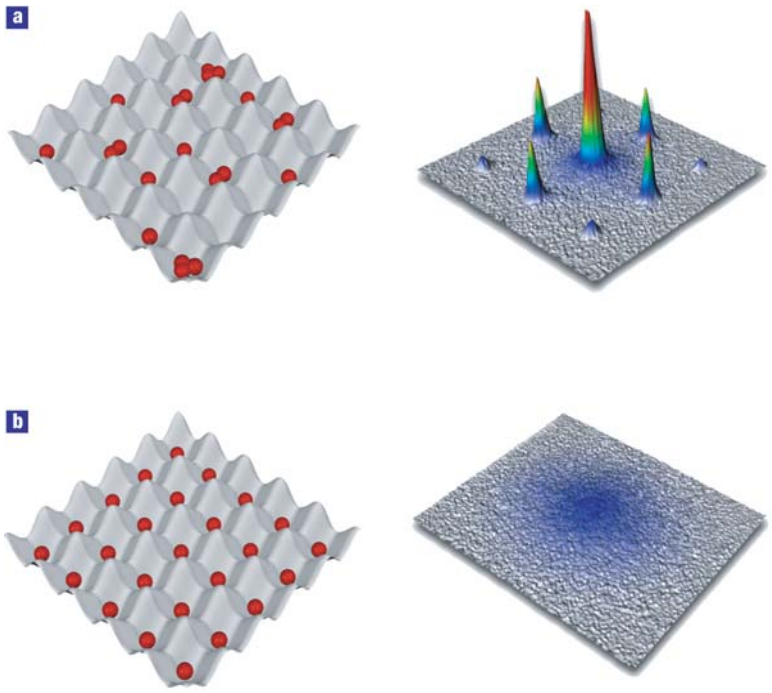

Figure 1.4: The superfluid-to-Mott insulator experiment by Greiner et al, Nature 415, 39 (2002). a) In the superfluid state the atoms are free to hop around the lattice. There is thus coherence between sites and upon release and expansion of the atomic cloud an atomic matter-wave interference pattern is observed. b) In the Mott insulator state there is exactly one atom per site (Fock state) with no coherence between wells so that upon release and expansion no interference is observed.

be filled with exactly one atom per lattice site. The Mott transition can therefore be employed to initialize a quantum register, where each qubit is formed by a single neutral atom on a lattice site with up to a hundred thousand sites being occupied. Condensates and superfluids are inextricably linked, yet many questions surround their relationship. The main difference between atomic gas condensates and superfluid helium lies in the strength of the particle interactions, which are much weaker in the former system. This simplifying feature of ultracold atoms makes them extremely attractive for theoretical studies. A source of coherent atoms also provides a wonderful practical tool. Just as the

development of the laser revolutionized optics, so the ability to generate coherent matter waves opens exciting research possibilities.

Bibliography

[1] T. Müller, B. Zimmermann, J. Meineke, J.-Philippe Brantut, T. Esslinger, and H. Moritz, Phys. Rev. Lett. **105**, 040401 (2010).

[2] E. Haller, J. Hudson, A. Kelly, Dylan A. Cotta, B. Peaudecerf, Graham D. Bruce, S. Kuhr, arXiv:1503.02005

[3] M. Greiner, O. Mandel, T. Esslinger, T. W. Hänsch and I. Bloch, Nature **415**, 39 (2002).

[4] W. Ketterle et al, Phys. Rev. Lett. **78**, 582 (1997).

[5] A. G. Manning, S. S. Hodgman, R. G. Dall, M. T. Johnsson, and A. G. Truscott, Optics Express, Vol. **18** (18), 18712 (2010).

[6] A. Einstein, Sitzungsberichte der Preussichen Akademie der Wissenschaften Physikalisch—Mathematische Klasse, 261 (1924).

[7] M.H. Anderson, J.R. Ensher, M.R. Matthews, C.E. Wieman, and E.A. Cornell, Science **269**, 198 (1995).

[8] C. Cohen-Tannoudji, Phys. Rep. **219**, 153 (1992).

[9] K. B. Davis, M.-O.Mewes, M. A. Joffe, M. R. Andrews, and W. Ketterle, Phys. Rev. Lett., **74**, 5202 (1995).

[10] F. Dalfovo, S. Giorgini, L. P. Pitaevskii, and S. Stringari, Rev. Mod. Phys. **71**, 463 (1999).

[11] T. Kohler, K. Goral and P. S. Julienne, Rev. Mod. Phys. **78**, 1311 (2006).

[12] C. Chin, R. Grimm, P. Julienne and E Tiesinga, Rev. Mod. Phys. **82**, 1225 (2010).

[13] S. L. Cornish, N. R. Claussen, J. L. Roberts, E. A. Cornell, and C. E. Wieman, Phys. Rev. Lett. **85**, 1795 (2000).

[14] E. A. Donley, N. R. Claussen, S. L. Cornish, Jacob L. Roberts, Eric A. Cornell, Carl E. Wieman, Nature **412**, 295 (2001).

[15] A. J. Leggett, Rev. Mod. Phys. **73**, 307 (2001).

[16] C. J. Pethick and H. Smith, Bose-Einstein condensation in Dilute Gases, Cambridge University Press (2002).

[17] P. O. Fedichev, M. W. Reynolds, and G. V. Shlyapnikov, Phys. Rev. Lett. **77**, 2921 (1996).

[18] S. Sachdev, Quantum Phase Transitions, Cambridge University Press (2000).

[19] Stöferle et al 2004, Tolra et al 2004, Paredes et al 2004, Kinoshita et al 2004.

[20] Lisa Randall, Warped Passages: Unraveling The Mysteries Of The Universe's Hidden Dimensions, ECCO, New York (2005).

[21] A. Gezerlis and J. Carlson, arXiv:1109.4946v1

[22] G. Pupillo, Ana Maria Rey, G. Brennen, Carl J. Williams, Charles W. Clark, J. Mod. Opt. **51**, 2395 (2004).

[23] https://jila.colorado.edu/research/quantum-information/quantum-computing.

[24] H. Metcalf and P. van der Straten, Laser Cooling and Trapping, Springer Verlag, New York (1999).

[25] R. Grimm, M. Weidenmuller, and Y. Ovchinnikov, Advances in Atomic, Molecular, Optical Physics **42**, 95 (2000).

[26] M. P. A. Fisher et al., Phys. Rev. B **40**, 546 (1989).

[27] D. Jaksch, Phys. Rev. Lett. **81**, 3108 (1998).

[28] J. Sherson, C. Weitenberg, M. Endres, M. Cheneau, I. Bloch, and S. Kuhr, Nature **467**, 68 (2010).

Chapter 2

Theoretical methods for the determination of Quantum Phase Transitions

2.1 Introduction

This chapter gives a description of all the numerical methods that have been used in this research work. The methods used are:

1. Mean-field (MFT),
2. Cluster mean-field (CMFT),
3. Density Matrix Renormalization Group (DMRG), and,
4. Matrix Product States method.

The details of each method are given in the following sections.

All the research problems taken up for this thesis work are well described by the Bose-Hubbard model (BHM) on optical lattices with some suitable modifications and extensions. Each of the methods mentioned above is aimed towards obtaining the ground state energy and the wave function of a system. To obtain the ground state wave-function and energy, the Hamiltonian matrix is constructed for the model under consideration and diagonalized to obtain the smallest eigen-value and the corresponding eigen-vector. These quantities are the ground state energy and wave-function respectively. Once these quantities are obtained, the signatures of quantum phases and other interesting features of a system can easily be extracted. It turns out that the occupation number $\hat{n}$, is a good quantum number as it commutes with the Bose-Hubbard Hamiltonian and its extensions we have considered. Therefore we work in the occupation number basis or Fock space to construct the Hamiltonian matrices and the wave-functions.

2.2 Mean-field Theory

The system of bosons in a general optical lattice can be best described by the Bose-Hubbard model as follows:-

$$H = -t \sum_{\langle i,j \rangle} (\hat{a}_i^\dagger \hat{a}_j + h.c) + \frac{U}{2} \sum_i \hat{n}_i(\hat{n}_i - 1) - \sum_i \mu_i \hat{n}_i \tag{2.1}$$

In the above equation, $\langle i, j \rangle$ denotes pair of nearest neighbor sites i and j. t denotes the hopping amplitude between adjacent sites and is responsible for the kinetic energy, U represents the on-site inter-atomic interaction or the potential energy term, $\hat{a}_i^\dagger(\hat{a}_i)$ is the creation (annihilation) operator which creates (destroys) an atom at site i and $\hat{n}_i = \hat{a}_i^\dagger \hat{a}_i$ is the number operator. μ_i represents the on-site chemical potential. We can change the number of particles in a system by varying μ and it is similar to working in the grand-canonical ensemble.

In the mean-field theory we treat the complete system at a single site level by decoupling the multi-site terms like $\hat{a}_i^\dagger \hat{a}_j$ under certain approximations. We also assume that the system is homogeneous and the sites are identical. We can make the following substitution in the Eq.(2.1):

$$a_i = \phi_i + \tilde{a}_i; \quad a_i^\dagger = \phi_i^* + \tilde{a}_i^\dagger \tag{2.2}$$

Here $\phi_i = \langle a_i \rangle$ is the mean value and $\tilde{a}$ is the small fluctuation over the mean value. Further ϕ_i is termed as the superfluid (SF) order parameter and is used as a signature of the SF phase. We assume ϕ_i to be real, hence, $\phi_i = \phi_i^* \ \forall \ i$. After some simplifications and rearrangements the kinetic energy term of the Eq.(2.1) can be rewritten as,

$$\begin{aligned} -t \sum_{\langle i,j \rangle} (a_i^\dagger a_j + H.c.) &= -t \sum_{\langle i,j \rangle} (\tilde{a}_i^\dagger \tilde{a}_j + \tilde{a}_i \tilde{a}_j^\dagger) \\ &= -t \sum_{\langle i,j \rangle} (\tilde{a}_i^\dagger \phi_j + \tilde{a}_j \phi_i + \tilde{a}_i \phi_j + \tilde{a}_j \phi_i + 2\phi_i \phi_j) \end{aligned} \tag{2.3}$$

Neglecting the first term, since it is second order in the fluctuations, and defining $\bar{\phi}_i = \frac{1}{z} \sum_\delta \phi_{i+\delta}$, δ is summed over z. Also, $z(=2d)$ is the co-ordination number of a site where, $d(=1, 2, \dots)$ is the dimensionality of the system. On simplifying further we get the following mean-field Hamiltonian,

$$H^{MF} = -tz \sum_i [\bar{\phi}_i (\tilde{a}_i^\dagger + \tilde{a}_i) - \bar{\phi}_i \phi_i] + \frac{U}{2} \sum_i n_i (n_i - 1) - \sum_i \mu_i n_i \tag{2.4}$$

Once again, using the relation $\tilde{a}_i = a_i - \phi_i$, we get the following mean-field Hamiltonian,

$$H^{MF} = -tz \sum_i [\bar{\phi}_i (a_i^\dagger + a_i) + \bar{\phi}_i \phi_i] + \frac{U}{2} \sum_i n_i (n_i - 1) - \sum_i \mu_i n_i \tag{2.5}$$

This Hamiltonian can be expressed as a sum of the single-site Hamiltonians,

$$H^{MF} = \sum_i H_i^{MF}$$

where,

$$H_i^{MF} = -\bar{\phi}_i (a_i^\dagger + a_i) + \bar{\phi}_i \phi_i + \frac{U'}{2} n_i (n_i - 1) - \mu_i' n_i. \tag{2.6}$$

Here, $U' = U/zt$ and $\mu' = \mu_i/zt$ indicate a scaling by zt to make the Hamiltonian and other terms dimensionless.

Then the Hamiltonian H_i^{MF} can be diagonalized in the following manner. Assuming an initial superfluid order parameter ϕ, first construct the matrix elements of the mean-field Hamiltonian in the number occupation basis $\mid n \rangle$, where $n = 0, 1, 2, \ldots, n_{max}$ where n_{max} is the maximum number of bosons allowed per site. The Hamiltonian matrix is then diagonalized to obtain the lowest eigenstate and obtain the new value for the ϕ. Using this new value of ϕ, the calculation is repeated till the convergence is reached that is to say $|\phi_{old} - \phi_{new}|$ becomes sufficiently small and meets our accuracy criteria.

2.3 Cluster Mean-field Theory

As the name suggest this method employs the idea of building up of clusters and solve the problem using mean-field theory. A big system consisting of hundreds of lattice sites can be divided into small clusters each containing a few sites. The bonds between the sites within a cluster are treated exactly but the bonds between any two adjacent sites belonging to different clusters are decoupled via decoupling approximation as mentioned in the previous section. The Hamiltonian then changes accordingly. CMFT has its own advantages over the MFT and other exact numerical methods. Unlike the MFT, (i) it can account for non-local effects and correlations (ii) the number of decoupled bonds (and hence approximations) reduces with increase in the size of the cluster and compared to exact numerical methods it is computationally less expensive yet giving reasonably good results.

The CMFT for a homogeneous one-dimensional chain with nearest-neighbour hopping can be easily formulated. In the first step we divide a system of N-lattice sites into n-clusters of L-sites each as shown in Fig.2.1. Therefore,

$$N = nL. \tag{2.7}$$

Figure 2.1: A one-dimensional clusters of length L. The system is divided into n such clusters. The notations $\ldots\ L-1'\ \ L'$ and $1''\ \ 2''\ \ldots$ represent the sites of the adjacent clusters.

Therefore, the hopping part of the Hamiltonian for the complete system can be written as,

$$H_{hop} = -t\sum_{j=0}^{n-1}\sum_{l=1}^{L-1}(a^{\dagger}_{Lj+l}a_{Lj+l+1} + H.c.) - t\sum_{j=0}^{n-1}(a^{\dagger}_{Lj+L}a_{Lj+L+1} + H.c.) \tag{2.8}$$

where we have isolated the terms which have contribution from $l = L^{th}$ sites, in the second sum. This term will be denoted by H_d as it contains the contribution from the sites which have to be decoupled. We assume periodic boundary conditions so that $a_{Ln+1} \equiv a_1$.

The bonds between the end sites can be decoupled like discussed in previous section. In general we can assume the existence of a homogeneous superfluid order parameter, $\phi = \langle a_i \rangle$ and make the substitution as in Eq.(2.2) in H_d, followed by the back substitution $\tilde{a}_i = a_i - \phi_i$. On simplifying and rearranging the terms we get,

$$H_d \simeq -t\sum_{j=0}^{n-1}\left[(a^{\dagger}_{Lj+L} + a^{\dagger}_{L(j+1)+1})\phi + \left(a_{Lj+L} + a_{L(j+1)+1}\right)\phi^*\right] + 2tn|\phi|^2 \tag{2.9}$$

We thus arrive at the cluster-decoupled Hamiltonian

$$H_{cd} = \sum_{j=0}^{n-1} H_j^{MF}, \tag{2.10}$$

where H_j^{MF} only depends on the site operators within the j-th cluster. Taking $j = 0$, we have

$$H_0^{MF} = H_L^0 + K_L^{MF}, \tag{2.11}$$

where

$$H_L^0 = -t\sum_{l=1}^{L-1}(a_l^\dagger a_{l+1} + a_{l+1}^\dagger a_l) + \frac{U}{2}\sum_{l=1}^{L} n_l(n_l-1) - \mu\sum_{l=1}^{L} n_l \tag{2.12}$$

and

$$K_L^{MF} = -t\left[\phi(\hat{a}_1^\dagger + a_L^\dagger) + \phi^*(a_1 + a_L)\right] + 2t|\phi|^2. \tag{2.13}$$

The ϕ-independent operator H_L^0 is the Hamiltonian of a one-dimensional chain of length L with open ends. The different clusters are independent physical systems but are effectively coupled by means of the order parameter appearing in the mean-field perturbation K_L^{MF}.

Following the same procedure we can derive the effective CMFT equations for systems in higher dimensions.

2.4 Density Matrix Renormalization Group Theory

The Density Matrix Renormalization Group (DMRG) is a very powerful numerical method to study many-body systems. It's predecessor, the Numerical Renormalization Group theory, suffered from improper treatment of boundary conditions and made it very difficult to obtain accurate results for most of the problems. To overcome this, the DMRG theory was developed in 1992 by Steven R. White which made it possible to study quantum lattice many-body systems such as the Hubbard model with a very high accuracy.

The complete information about a system can be extracted from the wave function describing it. As stated earlier, we use Fock space as the basis to represent the wave function for the systems we have considered. Ideally we can put any number of bosons at a given site in an optical lattice but then it will be impossible to handle such a system. So, in general we fix the single-site multiplicity to small number ~ 5. Now, as the size of the system increases the Hilbert space also expands. But because of it's tensor nature, the size of the Hilbert space increases exponentially with the number of sites. For a moderate system of 100-sites, with single-site multiplicity as 4, the size of the Hilbert space will be $4 \times 4 \times \cdots \times 4\ (100 - times) = 4^{100}$. Therefore, even for a small multiplicity and a

limited number of sites the Hilbert space is extremely large. DMRG method allows us to truncate the size of such a Hilbert space systematically and iteratively, yet giving us numerical results with accuracies of the order of 10^{-10}. This is done by keeping only the most probable states (limited in number) describing a wave-function (e.g. the ground state) and discarding states with small probabilities in each iteration.

We start with a *system* of small size, say l sites (typically = 4 or 6) with a basis size M_s, represented by $|\mu_s\rangle$. Let the basis size for a single site be m_s, represented by $|\nu_s\rangle$. Adding a site to our *system* of l sites increases the basis size to $M_s m_s$ and the states are then given as $|\mu_s\ \nu_s\rangle = |\mu_s\rangle \otimes |\nu_s\rangle$. Similarly for the *environment* basis size is given by $M_e m_e$ and the states by $|\mu_e\ \nu_e\rangle = |\mu_e\rangle \otimes |\nu_e\rangle$. The key idea behind this is to embed the system into the environment so that it can mimic a larger system. We can now join the two blocks to form a superblock which will then have $2l + 2$ sites. In general, the ground state of the superblock can be represented as,

$$|\Psi\rangle = \sum_{\mu_s=1}^{M_s} \sum_{\nu_s=1}^{m_s} \sum_{\nu_e=1}^{m_e} \sum_{\mu_e=1}^{M_e} \psi_{\mu_s\nu_s\mu_e\nu_e} |\mu_s\nu_s\rangle\ |\mu_e\nu_e\rangle$$
$$= \sum_{i,j=1}^{N_s,N_e} \psi_{i,j} |i\rangle \otimes |j\rangle. \tag{2.14}$$

In the following section, subscripts s and e are used for *system* and *environment*, respectively. Index *i,i'* are used for the *system* and j for the *environment*. We now want to obtain another wave-function $|\psi_0\rangle$ which matches $|\Psi\rangle$ very closely and has been constructed using a truncated basis for the *system*. This truncated basis consists of highest weights only. Let the size of this truncated basis be t and is represented by $|\tau\rangle$. Now in the truncated Hilbert space $|\psi_0\rangle$ can be written as,

$$|\psi_0\rangle = \sum_{\tau=1}^{t} \sum_{j=1}^{N_e} a_{\tau j} |\tau\rangle |j\rangle. \tag{2.15}$$

For $|\psi_0\rangle$ to be close to $|\Psi\rangle$ we need to minimize,

$$\Big| |\Psi\rangle - |\psi_0\rangle \Big|^2 \tag{2.16}$$

with respect to $a_{\tau j}$.

On taking partial trace (over the *environment*),

$$Tr_e|\Psi\rangle\langle\Psi| = \sum_j \langle ij|\Psi\rangle\langle\Psi|i'j\rangle. \tag{2.17}$$

The reduced density matrix of *system* is defined as,

$$Tr_e|\Psi\rangle\langle\Psi| = (\rho_s)_{ii'} \tag{2.18}$$

Hence,

$$(\rho_s)_{ii'} = \sum_j \psi_{ij}\psi^*_{i'j} \tag{2.19}$$

The eigenvectors of the reduced density matrix are $|\tau\rangle$ with the eigen values ω_τ.

Substituting Eq.(2.14) and Eq.(2.15) in Eq.(2.16) we get,

$$\Big||\Psi\rangle - |\psi_0\rangle\Big|^2 = 1 + \sum_{\tau j} a^2_{\tau j} - 2\sum_{ij\tau} \psi_{ij}a_{\tau j}u_{\tau i}. \tag{2.20}$$

Minimizing this with respect to $a_{\tau j}$ we get the condition,

$$a_{\tau j} = \sum_i \psi_{ij}u_{\tau i} \tag{2.21}$$

On substituting this back in Eq.(2.20) gives,

$$\begin{aligned}
\Big||\Psi\rangle - |\psi_0\rangle\Big|^2 &= 1 - 2\sum_{\tau ij} \psi_{ij}\Big(\sum_{i'} \psi_{i'j}u_{\tau i'}\Big)u_{\tau i} + \sum_{\tau,j}\Big(\sum_i \psi_{ij}u_{\tau i}\Big)^2 \\
&= 1 - \sum_{\tau ii'j} u_{\tau i}\psi_{ij}\psi_{i'j}u_{\tau i'} \\
&= 1 - \sum_{\tau ii'} u_{\tau i}(\rho_s)_{ii'}u_{\tau i'} \\
&= 1 - \sum_{\tau=1}^{t} \omega_\tau.
\end{aligned} \tag{2.22}$$

Therefore we can choose ω_τ(s) such that $(1-\sum \omega_\tau)$ is minimized and meets our truncation error criteria. The eigenvectors corresponding to these ω_τ are kept and used as the new basis for next iteration.

2.4.1 Infinite DMRG algorithm:

Under this scheme the size of the system is virtually infinite but in practice the size of the system is limited by the availability of the computational resources and desired accuracy. The procedure of constructing a system in DMRG method is outlined in Fig.(2.2).

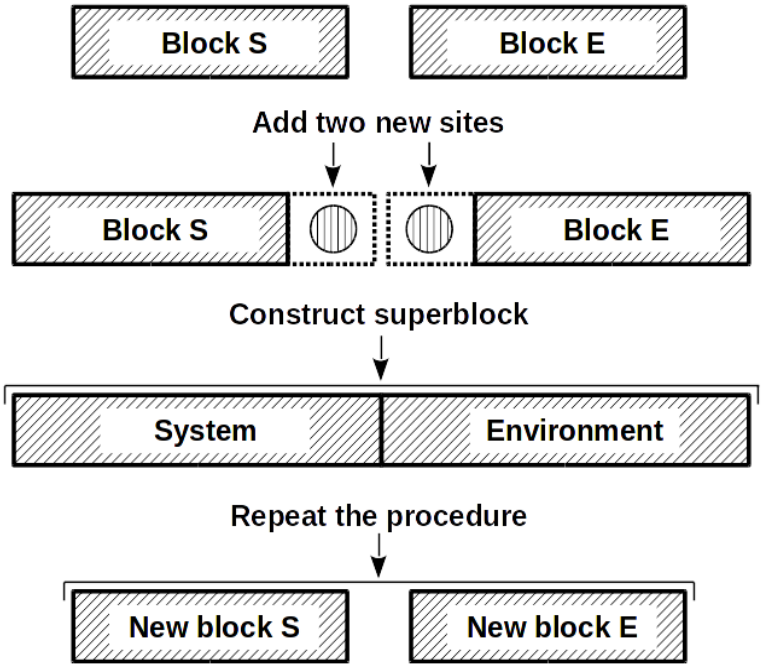

Figure 2.2: Procedure to construct a system in DMRG.

The main steps involved in the DMRG method are outlined below:

1. Construct two blocks, say *block S* and *block E*, of length (sites) l each (in general lengths of the two blocks can be different). Let the basis size of these blocks be $M_S(= m)$ and $M_E(= m)$ respectively. Now add two sites between these blocks and let the basis size of each site be $m_s(= n)$. *Block S* and *Block E* with two added sites constitute what we call as *superblock*.

2. The total size of the *superblock* is $(2l+2)$ and of the Hilbert space is $(mn)^2$. Let the Hamiltonian for the superblock be labelled as H_{SE}.

3. Diagonalize H_{SE} to obtain the ground state Ψ (or any other required target state) using a suitable eigenvalue solver like Jacobi-Davidson or Lanczos method.

4. Obtain the density matrix for the *system* block using this wave-function $|\Psi\rangle$,

$$(\rho_s)_{ii'} = \sum_j \psi_{ij}\psi_{i'j}$$

and diagonalize it. The basis is now truncated and the eigenstates corresponding to the $"t"$ highest eigenvalues only are retained. The limit on t is fixed using Eq.(2.22) to meet our accuracy criteria.

5. We now construct a transformation matrix O using these $"t"$ states and transform all the operators including the Hamiltonian into this new basis.

6. Steps (4) and (5) are repeated for the *environment* block also.

7. By following the steps (1)-(6) we have increased the size of our system from $2l$ to $2l+2$ sites. We repeat these steps for the newly formed block thereby adding 2 sites in each iteration. Once the desired length is achieved iteration is stopped and we can calculate the physical quantities of interest.

2.4.2 Finite DMRG algorithm:

The accuracy of Infinite DMRG is limited by the fact that the initial truncations are carried out even for the small superblocks. These truncations may not result in a very good approximation as the case would have been when the small blocks are embedded in the final system of length L. The other problem with infinite DMRG algorithm is that it can not account properly for the effects of impurities or randomness in the system. The reason being obvious that the total Hamiltonian is not known at the intermediate

steps. As we will see, Finite DMRG algorithm allows us to take care of these problems and reduces the errors due to truncations, etc.

1. After reaching the critical length L which was pre-decided in the Infinite DMRG, we start increasing the sites in the *system* block at the cost of sites in the *environment* block, one at a time.

2. At each step or with each increase(decrease) of a site in the *system*(*environment*) block, we do a basis transformation on the *system* (growing) block. For the *environment* (shrinking) block we can use previously stored basis.

3. The process stops when the sizes of the *system* and *environment* blocks become $L-2$ and 2, respectively.

4. The process starts again, but now with the role of the *system* and *environment* blocks interchanged. The *environment* block starts growing and the *system* block starts shrinking.

5. This process is called *sweeping* and a *sweep* is said to be complete when the both the blocks return to their original size for the first time after each of them has grown and shrunk once. This is illustrated in Fig.(2.3).

6. Sweeping process is continued till the desired convergence is achieved.

2.5 Matrix Product States method

The Matrix Product States (MPS) method is a relatively new method for determining the wave-function and hence properties of a system. Although new, we can see it connected to the DMRG method.

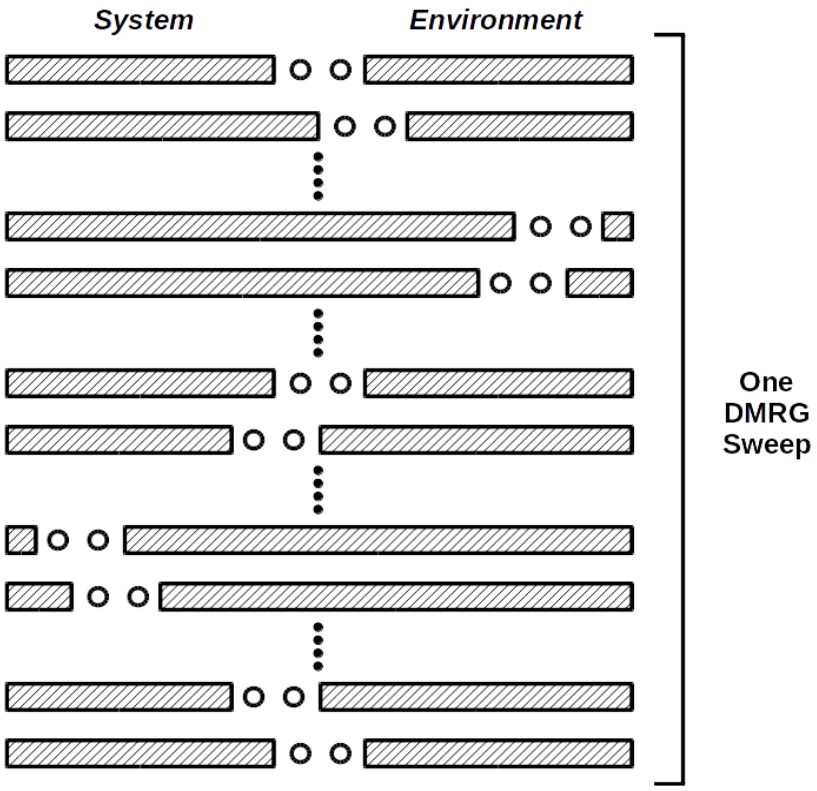

Figure 2.3: One sweeping cycle for Finite size DMRG.

Expressing the wave-functions in MPS form

Consider a system of L lattice sites in which each site is spanned by a local Hilbert space of size d and denoted by $\{\sigma_i\}$, where $i = 1, 2, ...L$. Any state for such a lattice can be expressed as

$$|\psi\rangle = \sum_{\sigma_1,...\sigma_L} c_{\sigma_1,...\sigma_L} |\sigma_1, ...\sigma_L\rangle. \tag{2.23}$$

Like in DMRG, here again the size of total Hilbert space (and coefficients $c_{\sigma_1,...\sigma_L}$) will be extremely large, d^L. To handle this we first try to write the wave-function in a more compact form and express the d^L coefficients in the form of a matrix of dimensions $d \times d^{L-1}$,

with the components related as :

$$\Psi_{\sigma_1,(\sigma_2\ldots\sigma_L)} = c_{\sigma_1\ldots\sigma_L}. \tag{2.24}$$

We can now use Singular Value Decomposition (SVD) on the matrix Ψ to express it in terms of the local site bases but still keeping non-local information of the system as well. SVD allows us to decompose Ψ and write it as,

$$\begin{aligned} c_{\sigma_1,\ldots\sigma_L} = \Psi_{\sigma_1,(\sigma_2\ldots\sigma_L)} &= \sum_{a_1,b_1}^{r_1} U_{\sigma_1,a_1} S_{a_1,b_1} (V^\dagger)_{b_1,(\sigma_2\ldots\sigma_L)} \\ &= \sum_{a_1}^{r_1} U_{\sigma_1,a_1} c_{a_1\sigma_2\ldots\sigma_L} \end{aligned} \tag{2.25}$$

S and $V^\dagger$ have been multiplied and the resulting matrix has been reshaped into a vector. The rank $r_1 \leq d$. Further we decompose the matrix U into d a collection of row vectors, A^{σ_1}, where $A^{\sigma_1}_{a_1} = U_{\sigma_1,a_1}$. We also reshape the vector $c_{a_1\sigma_2\ldots\sigma_L}$ to represent it in a matrix form as $\Psi_{(a_1\sigma_2),(\sigma_3\ldots\sigma_L)}$ of dimension $r_1 d \times d^{L-2}$ as follows :

$$c_{\sigma_1\sigma_2\ldots\sigma_L} = \sum_{a_1}^{r_1} A^{\sigma_1}_{a_1} \Psi_{(a_1\sigma_2),(\sigma_3\ldots\sigma_L)} \tag{2.26}$$

Once again we use SVD on Ψ and decompose it as shown below:

$$\Psi_{(a_1\sigma_2),(\sigma_3\ldots\sigma_L)} = \sum_{a_2,b_2}^{r_2} U_{(a_1\sigma_2),a_2} S_{a_2,b_2} V^\dagger_{b_2,(\sigma_3\ldots\sigma_L)} \tag{2.27}$$

Like before, S and V are multiplied, and reshaped back into a row vector, $c_{a_2\sigma_3\ldots\sigma_L}$, such that

$$c_{\sigma_1\sigma_2\ldots\sigma_L} = \sum_{a_1,a_2}^{r_1,r_2} A^{\sigma_1}_{a_1} U_{(a_1\sigma_2),a_2} c_{a_2\sigma_3\ldots\sigma_L} \tag{2.28}$$

but now we replace U by a set of 'd' matrices, $A^{\sigma_2}_{a_1,a_2}$ of dimensions $r_1 \times r_2$, given by

$$A^{\sigma_2}_{a_1,a_2} = U_{(a_1\sigma_2),a_2} \tag{2.29}$$

Therefore we get,

$$c_{\sigma_1\sigma_2...\sigma_L} = \sum_{a_1,a_2}^{r_1,r_2} A^{\sigma_1}_{a_1} A^{\sigma_2}_{a_1,a_2} c_{a_2,(\sigma_3...\sigma_L)} \tag{2.30}$$

We repeat the above procedure till we reach the L-th site. At the last site, we replace U_{a_{L-1},σ_L} by a set of column vectors $A_{a^{\sigma_L}_{L-1}}$. Thus we have arrived to a stage where we can write the coefficients as a product of matrices :

$$c_{\sigma_1...\sigma_L} = \sum_{a_1,a_2,...a_{L-1}}^{r_1,r_2...} A^{\sigma_1}_{a_1} A^{\sigma_2}_{a_1,a_2} ... A^{\sigma_{L-1}}_{a_{L-2},a_{L-1}} A^{\sigma_L}_{a_{L-1}} \tag{2.31}$$

Hence we can now write the general wave-function of the system in the MPS form as :

$$|\psi\rangle = \sum_{\substack{a_1,a_2,...a_{L-1} \\ \sigma_1,\sigma_2...\sigma_L}} A^{\sigma_1}_{a_1} A^{\sigma_2}_{a_1,a_2} ... A^{\sigma_{L-1}}_{a_{L-2},a_{L-1}} A^{\sigma_L}_{a_{L-1}} |\sigma_1\sigma_2...\sigma_L\rangle \tag{2.32}$$

which can be more compactly written as

$$|\psi\rangle = \sum_{\sigma_1,\sigma_2...\sigma_L} A^{\sigma_1} A^{\sigma_2} ... A^{\sigma_{L-1}} A^{\sigma_L} |\sigma_1\sigma_2...\sigma_L\rangle \tag{2.33}$$

2.5.1 Comparison between DMRG and MPS representations

As seen earlier (in DMRG section), the size of the Hilbert space expands exponentially with the number of lattice sites and to keep it manageable we truncate our basis at several steps. Now, consider one such truncation where the system of $L-1$-sites can be represented by a small basis $|\beta\rangle_{L-1}$ of size m, with $m \leq d^{L-1}$. Adding a single site to the chain will increase the system size to L and basis size to $d \times m$, where d is the single-site basis. The basis states are then given as, $\{|s_L\rangle \otimes |\beta\rangle_{L-1}\}$, where $|s_L\rangle$ represents the basis for newly added site. Like before, we would like to truncate our basis to keep it within manageable limit, say m, with the highest weights. To do this we use a projection operator A_L. The basis of $L-1$ and L sites are related by a recursion relation of the following form :

$$|\alpha_L\rangle = \sum_{\beta,s_L} A_L^{\alpha,(\beta,s_L)} |s_L\rangle \otimes |\beta\rangle_{L-1} \tag{2.34}$$

It is assumed that the initial state, $|\beta\rangle_0$ is already known. The matrices A_L are the variational parameters of MPS method which we need to determine, similar to what we saw in the MPS section. In DMRG method this is done by by keeping the largest eigenvalues of the density matrix.

We now perform a simple change in notation $A_L^{\alpha,\beta}[s_L] \equiv A_L^{\alpha,(\beta,s_L)}$ and write the $m \times (md)$ matrix as a set of d $m \times m$ matrices. We repeat the renormalisation procedure to obtain the following state of the chain of L sites,

$$|\alpha_L\rangle = \sum_{s_L,\ldots,s_1} (A[s_L]A[s_{L-1}]...A[s_1])^{\alpha,\beta} |s_L s_{L-1}...s_1\rangle \otimes |\beta\rangle_0 \tag{2.35}$$

Thus obtaining a wave-function in the matrix-product form.

Bibliography

[1] D. van Oosten, P. van der Straten, and H. T. C. Stoof, Phys. Rev. A **63**, 053601 (2001).

[2] S. R. White, Phys. Rev. Lett. **69**, 2863 (1992).

[3] S. R. White, Phys. Rev. B **48**, 10345 (1993).

[4] U. Schollwöck, Rev. Mod. Phys. **77**, 259 (2005).

[5] K. Hallberg, Theoretical Methods for Strongly Correlated Electrons, CRM Series in Mathematical Physics, Springer, New York, 2003, arXiv:cond-mat/0303557v1.

[6] A. L. Malvezzi, Brazilian Journal of Phys. vol. **33**, no. 1, March, 2003.

[7] G. De Chiara, M. Rizzi, D. Rossini, S. Montangero, arXiv:cond-mat/0603842v2

[8] G. Chan, J. Dorando, D. Ghosh, J. Hachmann, E. Neuscamman, H. Wang, T. Yanai, arXiv:0711.1398v1 [cond-mat.str-el]

[9] S. Östlund and S. Rommer, Phys. Rev. Lett. **75**, 3537 (1995).

[10] U. Schollwöck, Annals of Physics **326**, 96 (2011).

[11] D. Rossini, V. Giovannetti, R. Fazio, J. Stat. Mech. (2011) P05021.

[12] F. Verstraete, J. I. Cirac, V. Murg, Adv. Phys. **57**, 143 (2008).

[13] J. Eisert, M. Cramer and M. B. Plenio, Rev. Mod. Phys. **82**, 277 (2010).

[14] Hamed Saberi, *Matrix-product states for strongly correlated systems and quantum information processing*, Ph.D.. Thesis (München, 2008).

Chapter 3

Study of Quantum Phase Transitions in optical lattices and superlattices using Mean-field Theory

3.1 Introduction

In this chapter we present our study of quantum phase transitions (QPTs) in optical lattices and superlattices using Mean-field theory (MFT) method. In the first part we discuss the QPTs in an optical lattice within the frame work of Bose-Hubbard model using MFT. We first obtain the phase diagram for this model using the numerical technique and then compare our results by using perturbation theory as an analytical method. In the second part of this chapter we extend our study of QPTs in optical lattices to QPTs in optical superlattices using the MFT.

3.2 Model and method

3.2.1 QPTs in an Optical Lattice (MF theory)

As discussed in Section 2.1, a system of bosons in a general optical lattice can be best described by the Bose-Hubbard model as follows:

$$H = -t \sum_{\langle i,j \rangle} (\hat{a}_i^\dagger \hat{a}_j + h.c) + \frac{U}{2} \sum_i \hat{n}_i(\hat{n}_i - 1) - \sum_i \mu_i \hat{n}_i \tag{3.1}$$

which, in decoupling approximation reduces to,

$$H_i^{MF} = -\bar{\phi}_i(a_i^\dagger + a_i) + \bar{\phi}_i\phi_i + \frac{U'}{2} n_i(n_i - 1) - \mu_i' n_i. \tag{3.2}$$

Here, $U' = U/zt$ and $\mu' = \mu_i/zt$ indicate a scaling by zt to make the Hamiltonian and other terms dimensionless. $z = 2d$ where d is the dimensionality of the system. As described earlier, we construct the Hamiltonian matrix for the above in the occupation number basis and diagonalize it self-consistently to obtain the ground state energy and wave function of the system. Once the ground state wave-function is obtained we can calculate various expectation values to get more information of the system.

The occupation number density ρ, is given by the expectation value of the number operator $\hat{n}$ and is defined as,

$$\rho = \langle \hat{n} \rangle = \langle \psi_0 | \hat{a}^\dagger \hat{a} | \psi_0 \rangle \tag{3.3}$$

Similarly, the superfluid density ρ_s is given by the square of the superfluid order parameter ϕ, which is the expectation value of annihilation ($\hat{a}$) or creation ($\hat{a}^\dagger$) operator. It is defined as,

$$\rho_s = \phi^2 = \langle \psi_0 | \hat{a} | \psi_0 \rangle^2 = \langle \psi_0 | \hat{a} | \psi_0 \rangle^2. \tag{3.4}$$

$|\psi_0\rangle$ is the ground state of the system obtained after diagonalizing the H-matrix self-consistently. Below we present our results for the superfluid to Mott-insulator transition obtained using the MFT. First we obtain the ρ, ρ_s vs. μ plots for several values of the

on-site interaction U. One such plot for $U = 15.0$ is shown in the Fig.(3.1). In this plot

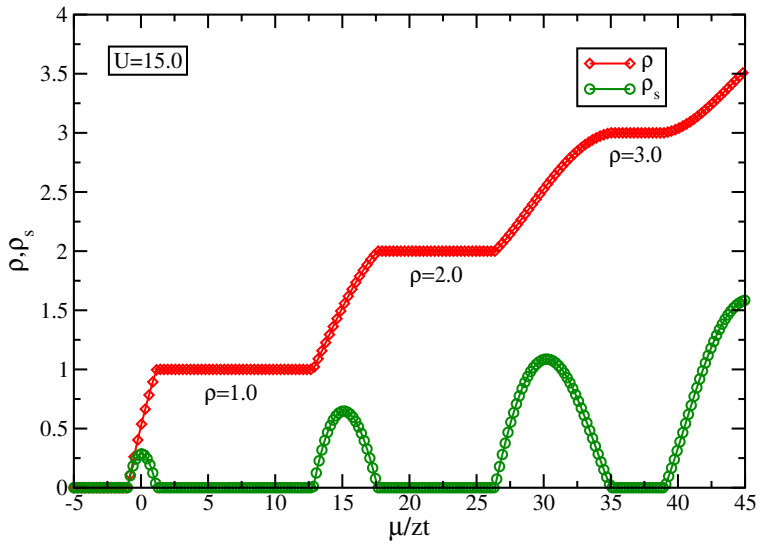

Figure 3.1: ρ, ρ_s vs. μ plot for an optical lattice obtained using the MFT at $U = 15.0$

we can see the plateaus corresponding to the integer densities $\rho = 1.0, 2.0$ and 3.0. At these plateaus the value of ρ_s is simultaneously 0. This is an indicator of the insulator or gapped phase. In between the constant density (ρ) plateaus, we can see that ρ increases in a continuous manner as μ is increased. From these $\rho - \mu$ plots for different values of U, we extract the beginning and the end points of each plateau in the units of μ/zt. These values are then plotted in the $U/zt - \mu/zt$ plane to obtain the phase diagram as shown in the Fig.(3.2). The area inside the lobes represents the constant density parameter space. The superfluid density ρ_s is 0 in this region. These lobes are known as Mott-lobes and the density of each Mott-lobe is represented by the corresponding ρ value. The area outside the lobes lies in the superfluid region. In this region $\rho_s \neq 0$ and $\rho \neq 0$ simultaneously.

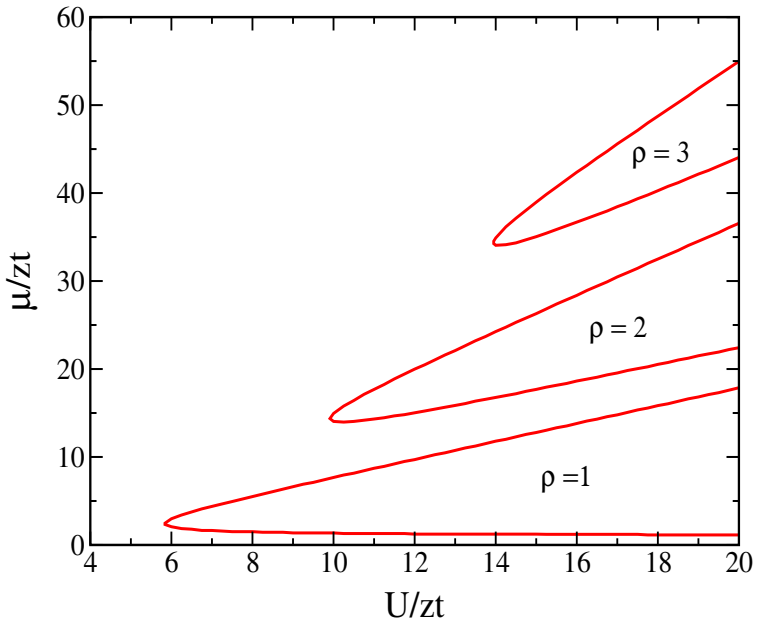

Figure 3.2: Phase diagram for an optical lattice obtained using the MFT (numerical results)

3.2.2 QPTs in an Optical lattice (Perturbation theory)

For a Mott-insulator ground state, the on-site interaction U is much larger than the hopping term t. Therefore in this limit the hopping term can be treated as a perturbation. The hopping term is given by:

$$H_{hop} = -t \sum_{\langle i,j \rangle} (\hat{a}_i^\dagger \hat{a}_j + h.c). \tag{3.5}$$

After applying the standard decoupling approximation reduces to,

$$H_{hop} = \sum_i (H_{hop})_i \approx -zt \sum_i [\phi({a_i}^\dagger + a_i) - \phi^2]. \tag{3.6}$$

Here i is the site index and z is the co-ordination number. We start by looking at a single-site. Let us denote the unperturbed state with n-atoms by $|n\rangle$ and ground state with $|g\rangle$ having n_0-atoms. For zeroth-order the contribution is just,

$$E_g^{(0)} = -zt\phi^2. \tag{3.7}$$

The contribution to the energy from the first-order corrections is zero because the average of an annihilation or creation operator between $|n\rangle$ and $|g\rangle$ is zero. The second-order correction to the energy is given by the expression:

$$E_g^{(2)} = \sum_{n \neq g} \frac{|\langle g|H_{hop}|n\rangle|^2}{E_g^{(0)} - E_n^{(0)}}. \tag{3.8}$$

Therefore,

$$E_g^{(2)} = z^2 t^2 \phi^2 \left[\frac{|\langle n^0| - [\phi(a^\dagger + a)]|n\rangle|^2}{\frac{U}{2}[n_0(n_0-1) - n(n-1)] - \mu(n_0 - n)} \right] \tag{3.9}$$

$$E_g^{(2)} = z^2 t^2 \phi^2 \left[\frac{(n+1)\delta_{n_0,n+1} + n\delta_{n_0,n-1}}{\frac{U}{2}[n_0(n_0-1) - n(n-1)] - \mu(n_0 - n)} \right] \tag{3.10}$$

$$E_g^{(2)} = z^2 t^2 \phi^2 \left[\frac{n_0}{\frac{U}{2}[n_0(n_0-1) - (n_0-1)(n_0-2)] - \mu} + \frac{n_0+1}{\frac{U}{2}[n_0(n_0-1) - (n_0+1)n_0] + \mu} \right] \tag{3.11}$$

$$E_g^{(2)} = z^2 t^2 \phi^2 \left[\frac{n_0}{U(n_0-1) - \mu} + \frac{n_0+1}{-Un_0 + \mu} \right] \tag{3.12}$$

In the Mott-state the hopping process should not contribute towards the free-energy. Therefore the contributions from energy corrections are zero. Using this condition we can determine the phase boundary as follows:

$$E_g^{(0)} + E_g^{(2)} = z^2 t^2 \phi^2 \left[\frac{n_0}{U(n_0-1) - \mu} + \frac{n_0+1}{-Un_0 + \mu} \right] + tz\phi^2 = 0 \tag{3.13}$$

$$1 + tz \left[\frac{n_0}{U(n_0-1) - \mu} + \frac{n_0+1}{-Un_0 + \mu} \right] = 0 \tag{3.14}$$

This equation is quadratic in μ the roots of which come out to be,

$$\mu^{\pm} = \frac{1}{2} \left[U(2n_0 - 1) - tz \pm \{U^2 - 2Utz(2n_0+1) + (tz)^2\}^{\frac{1}{2}} \right] = 0 \tag{3.15}$$

The critical point for SF-Mott insulator transition occurs when $\mu^+ = \mu^-$. On equating μ^+ and μ^- we obtain,

$$U^2 - 2Utz(2n_0 + 1) + (tz)^2 = 0. \tag{3.16}$$

On solving further we obtain,

$$\overline{U} = (2n_0 + 1) + 2\sqrt{n_0(n_0 + 1)} \tag{3.17}$$

where $\overline{U} = U/zt$.

For MI phase at $\rho = 1.0$, $n_0 = 1$. On substituting $n_0 = 1$ in the above equation we get $\overline{U} = 5.83 = U_c$. This value is in very good agreement with our numerical results. Similarly we can find the critical points for $\rho = 2.0$ and higher densities. For $\rho = 2.0$ and 3.0, $U_c = 9.89$ and 13.93 which are also in a good agreement with the numerical results.

3.2.3 QPTs in an Optical superlattice (MF theory)

For an optical superlattices we need to make some modifications to the original Hamiltonian as following. We start with the general Bose-Hubbard model,

$$H = -t \sum_{\langle i,j \rangle} (\hat{a}_i^\dagger \hat{a}_j + h.c) + \frac{U}{2} \sum_i \hat{n}_i(\hat{n}_i - 1) - \sum_i \mu_i \hat{n}_i \tag{3.18}$$

but then while decoupling we take into account the explicit dependence of μ_i on the lattice site i which in turn depends on the structure of the superlattice. An optical superlattice is formed by the superposition of two optical lattices with different wavelengths and a relative phase shift with respect to each other. We consider a superlattice with a periodicity of two sites, thus each unit cell consists of 2^d sites with alternate sites having an energy shift λ_i. We take into account this relative energy shift in the Bose-Hubbard Hamiltonian while using the decoupling approximation. This energy shifts the potential energy minima such that $\mu_i = \mu - \lambda_i$. For such a system, our unit cell consists of two sites, unlike the previous case where we had periodicity at the single site level and unit cell consisted of one-site.

We consider the system to be homogeneous in all the directions and label the sites in our unit cell by 1 and 2. The mean-field Hamiltonian for such a unit cell can be written as

$$\begin{aligned} H_{uc}^{MF} &= -\bar{\phi}_2(a_1^\dagger + a_1) - \bar{\phi}_1(a_2^\dagger + a_2) + 2\bar{\phi}_1\phi_2 \\ &\quad + \frac{\tilde{U}}{2}[n_1(n_1-1) + n_2(n_2-1)] \\ &\quad - \tilde{\mu}[n_1 + n_2] + \tilde{\lambda}_1 n_1 + \tilde{\lambda}_2 n_2 \end{aligned} \tag{3.19}$$

We can label the quantity $|\lambda_1 - \lambda_2|$ as the superlattice potential λ. Rest of the procedure remains the same and we obtain the ground state energy and wave function as before. As in this case we have two sites per unit cell, ρ, ρ_s represent the average density and superfluid density of the unit cell i.e. $\rho = (\rho_1 + \rho_2)/2$, $\rho_s = (\phi_1^2 + \phi_2^2)/2$.

3.3 Results and discussions

Without any loss of generalisation, we can assume $\lambda_1 = 0$ and $\lambda_2 = \lambda$ for a unit cell and then vary λ to see how it affects the phases.

In this case also we can plot the ρ, ρ_s vs. μ and later on obtain a phase diagram using these plots. But in this case we need to plot the average ρ, ρ_s in a unit cell which we label them as $\rho_{avg}, \rho_{s\ avg}$. One such $\rho, \rho_{s\ avg}$ vs. μ plot is shown in the Fig.(3.3).

It can be seen in Fig.(3.3) that we obtain plateaus not only at integer densities but also at half-integer densities $0.5, 1.5$, etc. Also, the average superfluid density is simultaneously 0 in these plateau regions. Like before this a signature of gapped / insulating phase. But this insulator phase is different from the standard Mott insulator phase arising due to the on-site interaction. The reason for the formation of an insulator phase here is due to the superlattice potential which breaks the translational symmetry of the system. To distinguish this insulator from the regular Mott insulator phase, we call it as superlattice induced Mott insulator (SLMI) [58]. Now if we look at density 0.5 plateau, it implies that there is 1 atom per unit cell. In such a scenario, the individual site number

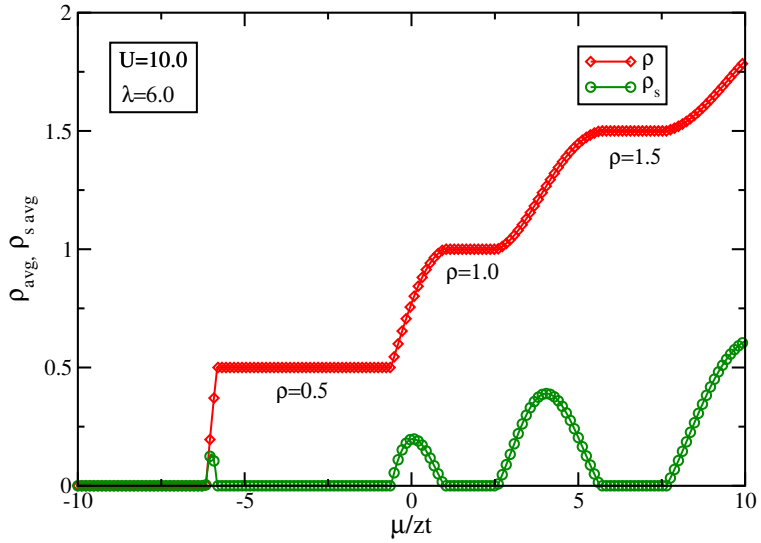

Figure 3.3: Variation of average densities ($\rho_{avg}, \rho_{s\ avg}$) as a function of the chemical potential μ for U=10, at the superlattice potential $\lambda = 6$.

densities are $\rho_1 = 1,\ \rho_2 = 0$ and the superfluid densities are $\rho_{s1} = 0,\ \rho_{s2} = 0$. Therefore within a unit cell one site is occupied and the other site is empty. The distribution of bosons on the lattice then follows a pattern [1 0 1 0 1 0 $\cdots$]. Similarly for the density 1.5 plateau there are 3 atoms in each unit cell. The arrangement of atoms then can be [2 1 2 1 2 1 $\cdots$] or [3 0 3 0 3 0 $\cdots$], depending on the value of on-site interaction strength and the superlattice potential as we will see later.

To obtain the phase diagram in this case we start with a relatively small value of $U(= 2.0)$ and plot the average density ρ and the superfluid density ρ_s as a function of the chemical potential μ, as shown in the Figs. 3.4 and 3.5. We vary λ starting from 0.5 to 5.5 at an interval of 1.0. At low values of the on-site interaction is not strong enough to drive the system into an insulating phase. Therefore at $U = 2.0$, $\lambda = 0$, the system is in the superfluid phase. We keep U fixed and vary λ. The system remains in the superfluid phase as long as λ remains less than a critical value $\lambda_c(\sim 4.5)$. Beyond this value we observe a plateau at $\rho = 1/2$ for a certain range of μ. This plateau(s) can be seen in

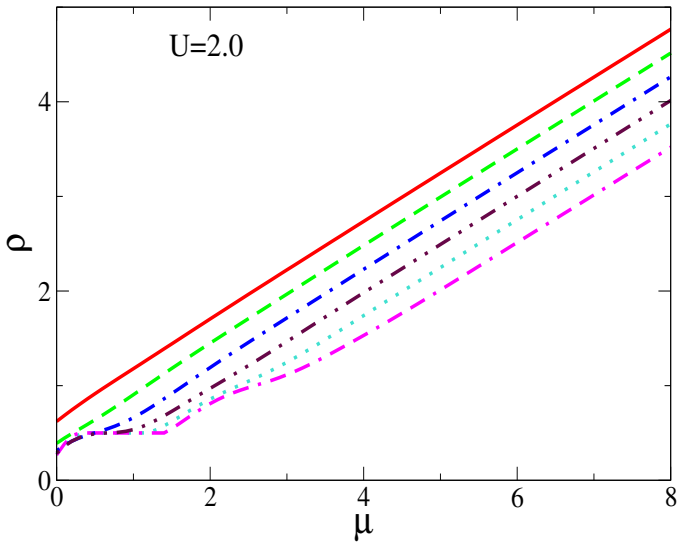

Figure 3.4: ρ_{avg} vs. μ plot for U=2, for different values of λ starting from 0.5 (red solid curve) to 5.5 (magenta double dash dot curve) at the intervals of 1.0.

Fig. 3.4 at $\lambda = 5.5$. We also plot the ρ_s vs. μ plot for the same set of parameters. It was seen that the superfluid density goes to 0 in the same μ range for which $\rho = 1/2$ plateau is obtained, see Fig. 3.5. This is the signature of a gapped phase. For all other densities the superfluid density remains finite.

Therefore, at $U = 2.0$ and $\lambda > \lambda_c$, the system is in the SLMI phase only at $\rho = 1/2$ and a range of μ values. As the value of U in increased to 5.0, we obtain the ρ, ρ_s vs. μ plots which are qualitatively same as for the case of $U = 2.0$. In Figs. 3.6 and 3.7 we can see such plots. Here again the system remains in the superfluid phase for low values of λ at any commensurate densities. But for $\lambda \geq \lambda_c(\ 2.6)$ a plateau appears in the ρ vs. μ plot at $\rho = 1/2$ with the superfluid density being simultaneously 0 for the same range of μ, see Fig.3.7. The system thus enters a gapped phase. The region of this gapped phase increases as the λ is increased. However, the system still remains in the SF phase at $\rho = 1$.

We further increase the value of U and fix it to 10.0. For an optical lattice without

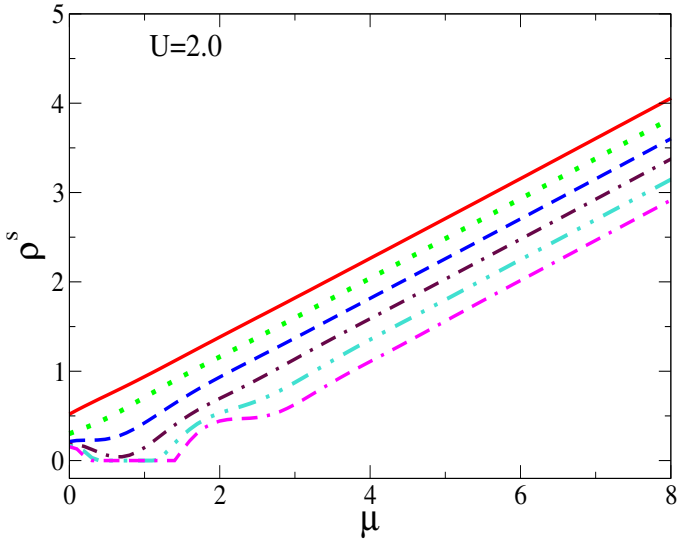

Figure 3.5: $\rho_{s\ avg}$ vs. μ plot for U=2. λ varies from 0.5 (red solid curve) to 5.5 (magenta double dash dot curve) at the intervals of 1.0.

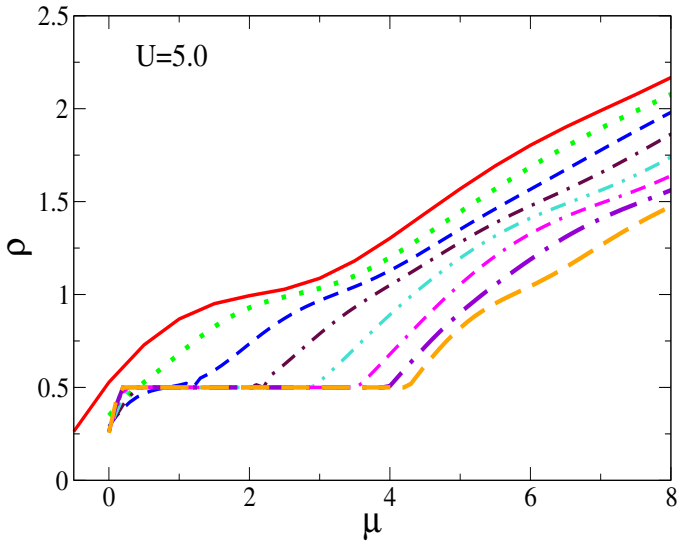

Figure 3.6: ρ_{avg} vs. μ plot for U=5, but for different values of λ starting from 0.2 (red solid curve) to 7.2 (orange dashed curve) at intervals of 1.0.

a superlattice potential the critical value of SF-MI transition at $\rho = 1$, has been predicted to be $U_c \sim 5.8$ [54]. Therefore, our system is already in the $\rho = 1$ Mott insulator phase

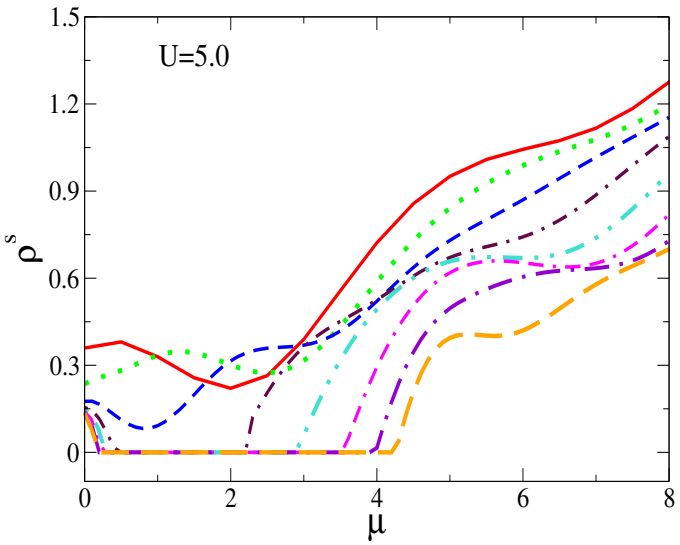

Figure 3.7: $\rho_{s\ avg}$ vs. μ plot for U=5. λ varies from 0.2 (red solid curve) to 7.2 (orange dashed curve) in the intervals of 1.0.

at $U = 10.0$. The ρ vs. μ, ρ_s vs. μ for this case are given in the Figs. 3.8 and 3.9 respectively. It can be seen that these plots are very different from those obtained for $U = 2.0$ and 5.0. We observe that in this case the system remains in the MI phase for small values of λ. But as the value of λ becomes sufficiently high, $\rho = 1$ plateau shrinks and disappears signifying the destruction of the MI phase. On further increase in λ, $\rho = 1$ plateau reappears along with two new plateaus at $\rho = 0.5$ and 1.5. From the number density calculations for the individual sites in the unit cell it is found that these densities correspond to [0 1 0 1 $\cdots$], [0 2 0 2 $\cdots$], and [2 1 2 1 $\cdots$] configuration for densities $\rho = 0.5, 1.0$, and 1.5, respectively. Once again, the SF density is 0 in these plateau regions. Therefore we obtain the SLMI phases with an increase in λ while keeping U fixed at 10.0.

We present another test case by fixing $U = 15.0$ and varying λ. The results are given in the Figs. 3.10 and 3.11. From the plots we can see that the results are not very different form $U = 10$ case. It can be seen that, with an increase in λ the extent of various insulating phases also increases.

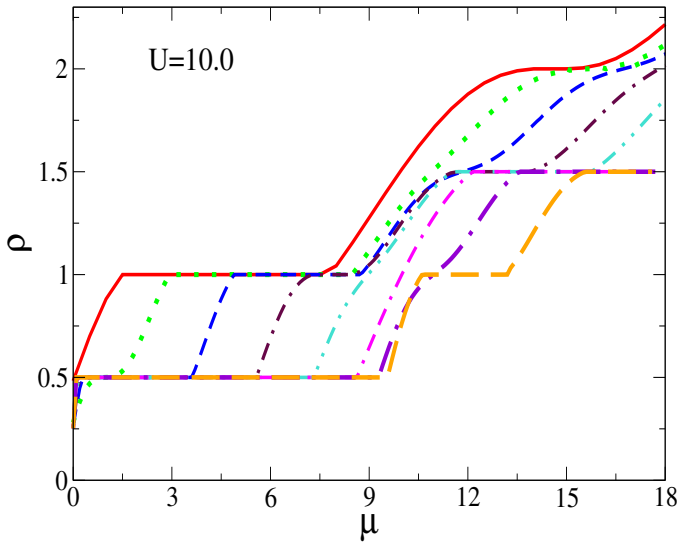

Figure 3.8: ρ_{avg} vs. μ plot for U=10, but for different values of λ, varying from 0.2 (red solid curve) to 14.2 (orange large dashed curve) at intervals of 2.0.

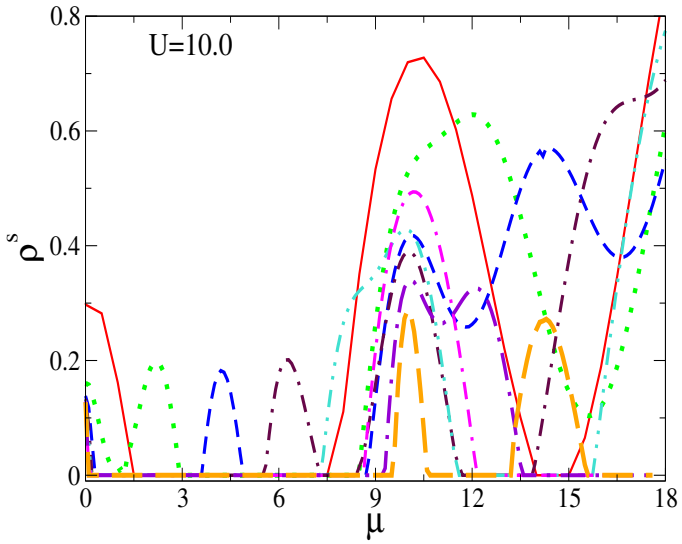

Figure 3.9: $\rho_{s\ avg}$ vs. μ plot for the same set of parameters as in Fig. 3.8 and for the same range of λ.

3.4 Conclusions

We now summarize our results of our work for optical lattice and superlattice. We found that the phase diagram obtained for the BH model using our numerical technique of

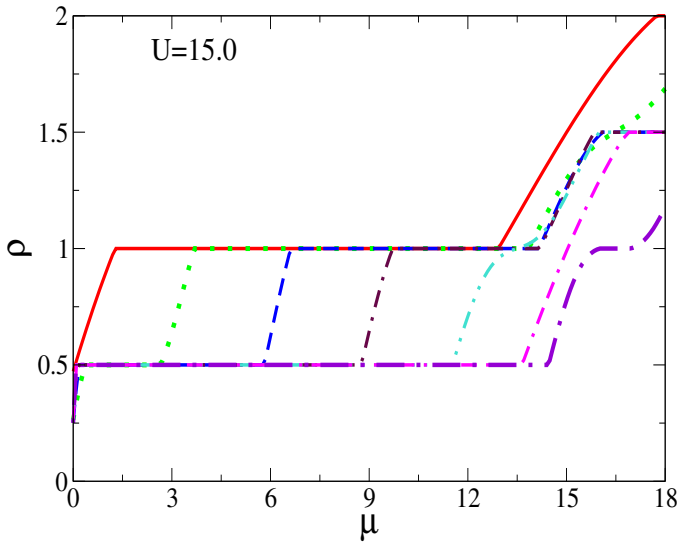

Figure 3.10: ρ_{avg} vs. μ plot for U=15, but for different values of λ, varying from 0.2 (red solid curve) to 18.2 (violet large dot dashed curve) at intervals of 3.0.

self-consistent MFT are in a very good agreement with that found from the analytical

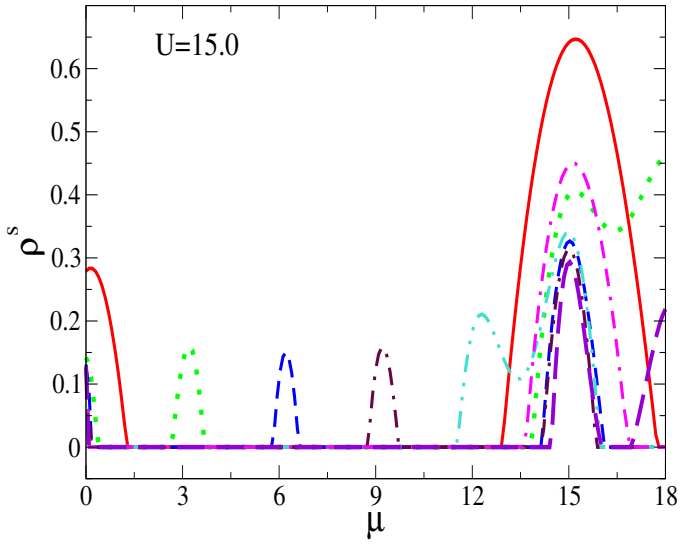

Figure 3.11: $\rho_{s\ avg}$ vs. μ plot for the same set of parameters as in Fig. 3.10 and for the same range of λ.

method. At relatively low values of U and (or) at incommensurate densities there is no Mott-insulating phase. As U increases, the system undergoes a phase transition from the SF to MI phase at integer densities. The SF-MI transition critical points found from our calculations are as follows: (i) at $\rho = 1.0$, $\overline{U}$ 5.8, (ii) at $\rho = 2.0$, $\overline{U}$ 9.9, (iii) at $\rho = 3.0$, $\overline{U}$ 14.0, and (iv) at $\rho = 4.0$, $\overline{U}$ 18.1.

Introducing a superlattice potential in the lattice system breaks the translational symmetry which results in the SLMI phases. These phases, like MI phases are gapped but arise not because of any change in the interaction between the atoms but because of change in the geometry of the potential wells. Moreover these phases arise at half-integer densities and can be seen below U_c for the SF-MI transition. The regular MI phases are also affected by the superlattice potential λ. For small values of λ the system remains unaffected but for sufficiently high λ the regular MI phase (e.g. $\rho = 1$, [...1 1 1 1...]) undergoes a transition to a SLMI phase ($\rho = 1$, [...0 2 0 2...]) via a SF phase at $\lambda \approx U$.

Bibliography

[1] V. G. Rousseau, D. P. Arovas, M. Rigol, F. Hebert, G. G. Batrouni, and R. T. Scalettar, Phys. Rev. B **73**, 174516 (2006).

[2] R. Roth and K. Burnett, Phys. Rev. A **68**, 023604 (2003).

[3] F. Schmitt, M. Hild, and R. Roth, Phys. Rev. A **80**, 023621 (2009).

[4] B.-L. Chen, S.-P. Kou, Y. Zhang, and S. Chen, Phys. Rev. A **81**, 053608 (2010).

[5] F. Schmitt, M. Hild, and R. Roth, eprint arXiv:1005.3129v1 [cond-mat.quant-gas].

[6] G. Roux, T. Barthel, I. P. McCulloch, C. Kollath, U. Schollwöck, and T. Giamarchi, Phys. Rev. A **78**, 023628 (2008).

[7] S. Piel, J. V. Porto, B. Laburthe Tolra, J. M. Obrecht, B. E. King, M. Subbotin, S. L. Rolston, and W. D. Phillips, Phys. Rev. A **67**, 051603 (R) (2003).

[8] J. Sebby-Strabley, M. Anderlini, P. S. Jessen, and J. V. Porto, Phys. Rev. A **73**, 033605 (2006).

[9] P. Cheinet, S. Trotzky, M. Feld, U. Schnorrberger, M. Moreno-Cardoner, S. Fölling, and I. Bloch, Phys. Rev. Lett. **101**, 090404 (2008).

[10] K. Sheshadri, H. R. Krishnamurthy, R. Pandit, and T. V. Ramakrishnan, Europhys. Lett. **22**, 257 (1993).

[11] D. Jaksch, C. Bruder, J. I. Cirac, C. W. Gardiner, and P. Zoller, Phys. Rev. Lett. **81**, 3108 (1998).

[12] D. van Oosten, P. van der Straten, and H. T. C. Stoof, Phys. Rev. A **63**, 053601 (2001).

[13] W. Krauth, M. Caffarel, and J. P. Bouchaud, Phys. Rev. B **45**, 3137 (1992).

[14] D. S. Rokhsar and B. G. Kotliar, Phys. Rev. B **44**, 10328 (1991).

[15] R. V. Pai, K. Seshadri, and R. Pandit, in *Current Topics in Atomic, Molecular and Optical Physics*, edited by C. Sinha and S. Bhattacharyya (World Scientific, Singapore, 2007), p. 105.

[16] T. Mishra, R. V. Pai, S. Ramanan, M. S. Luthra, and B. P. Das, Phys. Rev. A **79**, 013625 (2009).

[17] S. R. White, Phys. Rev. Lett. **69**, 2863 (1992); Phys. Rev. B **48**, 10345 (1993).

[18] U. Schollwöck, Rev. Mod. Phys. **77**, 259 (2005).

[19] T. D. Kuhner, S. R. White, and H. Monien, Phys. Rev. B **61**, 12474 (2000).

[20] R. V. Pai and R. Pandit, Phys. Rev. B **71**, 104508 (2005).

[21] T. D. Kuhner, S. R. White, and H. Monien, Phys. Rev. B **61**, 12474 (2000).

[22] L. Urba *et al.*, J. Phys. B **39**, 5187 (2006).

[23] Bo-lun Chen, Xiao-bin Huang, Su-Peng Kou, and Yunbo Zhang, Phys. Rev. A **78**, 043603 (2008).

[24] P. R. Johnson, E. Tiesinga, J. V. Porto, and C. J. Williams, New J. Phys. **11**, 093022 (2009).

[25] Kezhao Zhou, Zhaoxin Liang, and Zhidong Zhang, Phys. Rev. A **82**, 013634 (2010).

[26] Sebastian Will, Thorsten Best, Ulrich Schneider, Lucia Hackermüller, Dirk-Sören Lühmann, and I. Bloch, Nature **465**, 197 (2010).

[27] M. J. Mark, E. Haller, K. Lauber, J. G. Danzl, A. J. Daley, and H.-C. Nägerl, Phys. Rev. Lett. **107**, 175301 (2011).

[28] R. Ma, M. E. Tai, P. M. Preiss, W. S. Bakr, J. Simon, and M. Greiner, Phys. Rev. Lett. **107**, 095301 (2010).

[29] M. Greiner, O. Mandel, T. Esslinger, T. W. Hänsch and I. Bloch, Nature **415**, 39 (2002).

Chapter 4

Mean-field study of ultracold bosonic atoms in an optical lattice and superlattice with the three body on-site interaction

4.1 Introduction

In Chapter 3 we discussed the superfluid to Mott insulator transition of the ultracold bosonic atoms in an optical lattice and superlattice using the MFT approach. In that case we considered only the two-body on-site interaction. In this chapter we extend our study of ultracold bosonic atoms in optical lattices and superlattices by including the on-site three-body interaction as well.

The extension of the insulating lobes in the presence of the on-site three-body interactions has been studied earlier, using the decoupling mean-field theory [16]. The generation of effective three- and higher-body interactions by two-body collisions of atoms

confined in the lowest vibrational states of a three-dimensional optical lattice has been reported by Johnson *et al.* [10]. The effect of three-body interactions on the insulating lobes in an optical lattice has been considered using the mean-field and functional integral approaches in the Bose-Hubbard approximation for optical lattices [7, 11].

Will *et al.* [14] have detected and precisely measured the on-site three and higher body interaction strengths experimentally by observing the collapse and revival of the superfluid matter waves in a deep optical lattice. Nägerl et al [15] have been able to precisely determine the on-site interaction energies including multi-body interaction shifts. In another work, Greiner *et al.* [16] have determined the three-body interaction strengths by using occupation- sensitive photon-assisted tunnelling.

In this chapter we first discuss the effect of the three body on-site interaction on ultracold atoms in an optical lattice and then we see how it affects the phases in an optical superlattice also.

4.2 Model and method

The system of bosons in an optical superlattice with three-body interaction can be described by the modified Bose-Hubbard model as follows:-

$$H = -t\sum_{\langle i,j\rangle}(\hat{a}_i^\dagger \hat{a}_j + \text{H.c}) + \frac{U}{2}\sum_i \hat{n}_i(\hat{n}_i - 1)$$
$$+\frac{W}{6}\sum_i \hat{n}_i(\hat{n}_i - 1)(\hat{n}_i - 2) - \mu\sum_i \hat{n}_i + \sum_i \lambda_i \hat{n}_i \tag{4.1}$$

Here W represents the on-site inter-atomic three-body interaction and λ is the superlattice potential. We consider a bipartite lattice with sub-lattices $\mathcal{A}$ and $\mathcal{B}$ with a periodicity of two sites. We apply standard decoupling approximation [54, 66, 13] to the hopping term

in Eq. (7.1) to obtain the mean-field Hamiltonian given by

$$\begin{aligned}\frac{H_i^{MF}}{zt} &= -\phi_i(\hat{a}_i^\dagger + \hat{a}_i) + \phi_i\psi_i + \frac{\overline{U}}{2}\hat{n}_i(\hat{n}_i - 1) \\ &\quad + \frac{\overline{W}}{6}\hat{n}_i(\hat{n}_i - 1)(\hat{n}_i - 2) - \overline{\mu}\hat{n}_i + \overline{\lambda}_i\hat{n}_i \end{aligned} \tag{4.2}$$

where the superfluid order parameter $\psi_i =< \hat{a}_i >$ is taken to be real [54], $\phi_i = \frac{1}{z}\sum_\delta \psi_{i+\delta}$, the summation over δ is taken over z nearest neighbouring sites, $\overline{U} = U/zt$, $\overline{W} = W/zt$, $\overline{\mu} = \mu/zt$ and $\overline{\lambda}_i = \lambda_i/zt$ are dimensionless parameters. For an optical lattice, $\lambda_i = 0$ for all i, thus $\psi_i = \psi$. For our optical superlattice, $\lambda_i = 0$ for sub-lattice $\mathcal{A}$ and $\lambda_i = \lambda$ for sub-lattice $\mathcal{B}$, thus $\psi_i = \psi_A(\psi_B)$ if i belongs to sub-lattice $\mathcal{A}$ ($\mathcal{B}$). The mean-field eigen value equation is solved self-consistently to obtain the local superfluid density $\rho_i^s = \psi_i^2$ and density $\rho_i = \langle\hat{n}_i\rangle$ of the ground state of the system.

4.3 Results and discussion

To study the effect of $\overline{W}$ on MI phases in an optical lattice, we first present the mean-field phase diagram for an optical lattice (Fig. 4.1), in the $\overline{U}$ - $\overline{\mu}$ plane obtained from the density ρ and the superfluid density ρ^s, for various values of $\overline{W}$. Figure 4.2 shows the $\overline{\mu}$ - ρ, ρ^s plot for different $\overline{W}$.

For an optical superlattice we show the effect of $\overline{W}$ on MI and SLMI phases in the phase diagram plotted in the $\overline{\mu}$ - $\overline{\lambda}$ plane (Figs. 4.3 and 4.4). In Fig. 4.3 we present the phase diagram for $\overline{U} = 10$ and $\overline{W} = 0.0$. Fig. 4.4 is the phase diagram for $\overline{U} = 10$ and $\overline{W} = 5.0$. Lobes Lρ represent the MI phase with density ρ. Lobes R1 to R6 represent SLMI phases with density in sub-lattices $\mathcal{A}$ ($\mathcal{B}$) respectively given by 1(0), 2(0), 2(1), 3(1), 3(2) and 4(2).

From the mean field results (Figs. 4.1 and 4.2) for the optical lattice, we find that the $\rho = 1$ MI lobe remains unaltered in the presence of $\overline{W}$. However, for higher densities, the critical value $\overline{U}_C(\overline{W})$ for SF-MI transition decreases as $\overline{W}$ increases (e.g. $\overline{U}_C$ for

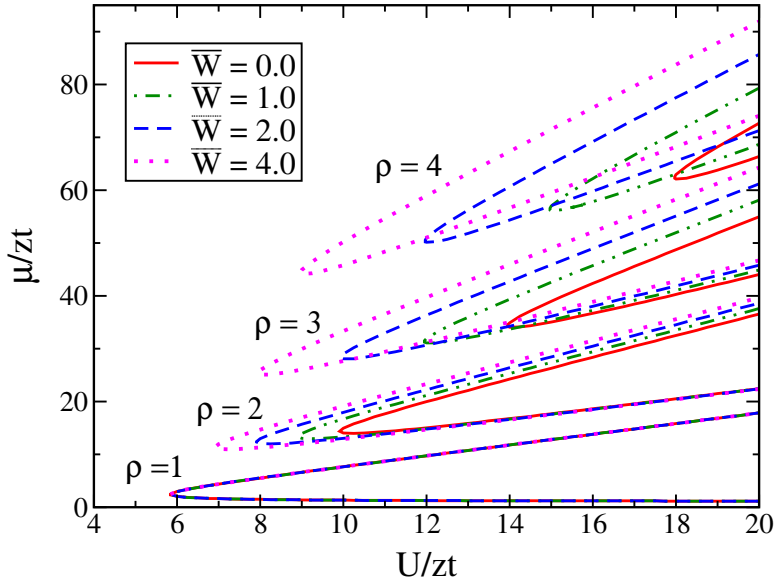

Figure 4.1: Phase diagram of Eq. (7.2) for different $\overline{W}$ for optical lattice. The lobes represent Mott insulator phases for densities $\rho = 1, 2, 3, 4$.

$\rho = 2$ lobe decreases from ~ 10 to ~ 7 when $\overline{W}$ increases from 0.0 to 4.0) and this is more prominent as the density increases, as shown in Fig. 4.1. Also, the MI lobes get enlarged as the $\overline{W}$ increases.

The reason for this behaviour at higher densities is that there is a greater probability of having three or more atoms at a site, which enhances the three-body interaction and suppresses atom hopping from one site to another.

From the mean field results for the optical superlattice (Figs. 4.3 and 4.4), we see that the lobes L1, R1 and R2 remain unaffected in the presence of a finite $\overline{W}$. This is expected because in such configurations, no two adjacent sites have more than two atoms, and for an atom to hop two sites is a second order process, which is of much less probability. However, the SLMI phase R3, which has sub-lattice atomic densities $\rho_A = 2$ and $\rho_B = 1$ (and thus has average density $\rho = 3/2$) gets enlarged in the presence of $\overline{W}$. This is understood from the following reason. When $\overline{W} = 0.0$ and as we increase $\overline{\lambda}$,

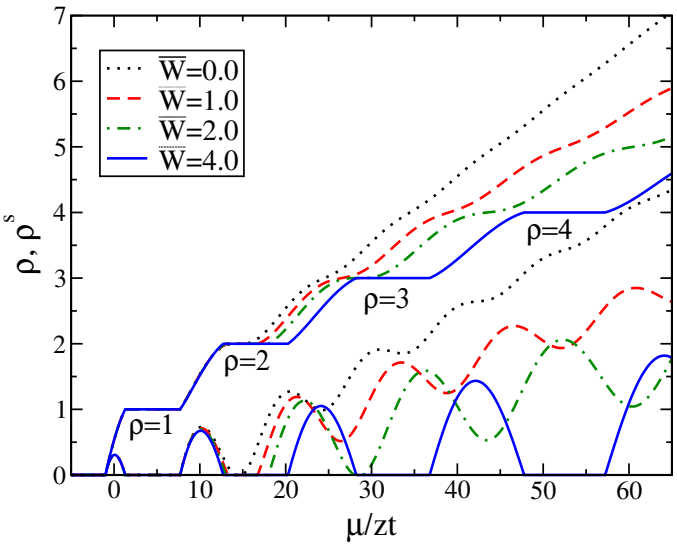

Figure 4.2: Variation of density ρ and superfluid density ρ^s with $\overline{\mu}$ for $\overline{U} = 10$, for optical lattice. Top to bottom, the first four curves represent density ρ and the next four curves represent superfluid density ρ^s. The plateaus in the ρ plots represent MI phases with vanishing ρ^s.

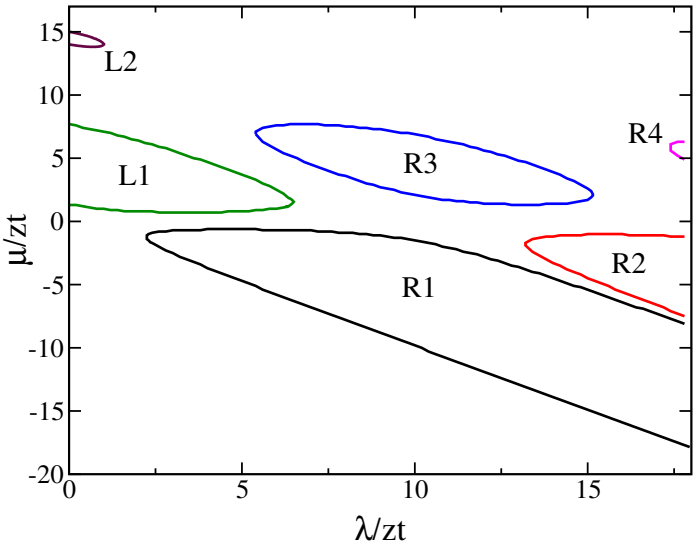

Figure 4.3: $\overline{\lambda}$ - $\overline{\mu}$ phase diagram for $\overline{U} = 10$, $\overline{W} = 0.0$, for optical superlattice.

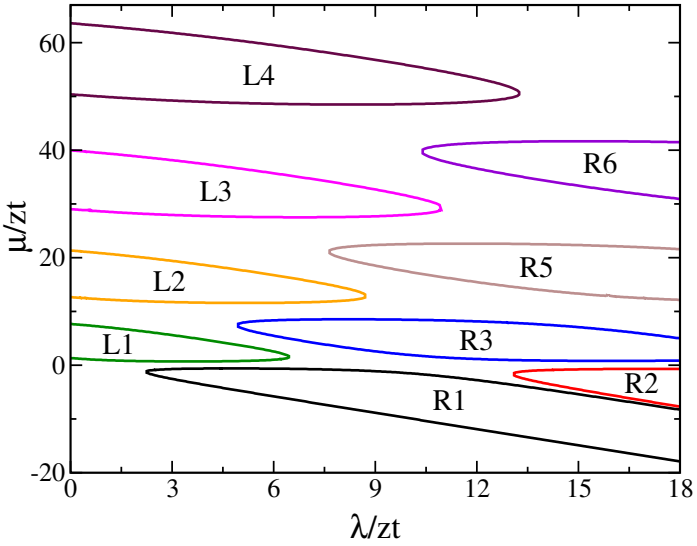

Figure 4.4: $\overline{\lambda}$ - $\overline{\mu}$ phase diagram for $\overline{U} = 10$, $\overline{W} = 5.0$, for optical superlattice

keeping the average density $\rho = 3/2$, the ground state goes from the superfluid to the SLMI phase R3. With a further increase of $\overline{\lambda} > 15$, the ground state is again a superfluid which has $2 < \rho_A < 3$ and $0 < \rho_B < 1$. However, when $\overline{W}$ is finite, the system does not prefer to have sub-lattice densities above 2. Thus SLMI phase R3 has a lower energy than superfluid with sub-lattice densities $2 < \rho_A < 3$ and $0 < \rho_B < 1$.

The phase diagram for the system with a filling factor $\rho = 2$, shows a marked difference in the presence of $\overline{W}$. Comparing Figs. 4.3 and 4.4, we find that the MI lobe L2 becomes large and its tip shifts from $\overline{\lambda} \sim 1$ to $\overline{\lambda} \sim 9$. Also as $\overline{\lambda}$ increases to ~ 17.5 (Fig. 4.3), the MI lobe L2 goes to the SLMI phase R4. However, in the presence of $\overline{W}$ (Fig. 4.4), the tip of the R4 lobe gets shifted to ~ 20.5. As we have considered the maximum value of $\overline{\lambda}$ till 18.0, SLMI phase R4 does not appear in Fig. 4.4.

4.4 Conclusions

The three-body interaction strength scales with the two-body interaction strength as follows: $\overline{W} \propto \ln(C\eta^2)(V_0/E_r)^{3/4}\ e^{-2\sqrt{V_0/E_r}} a_s^2 k^2 \overline{U}^2$ [16, 22, 23, 24]. The typical range of

$a_s^2 k^2$ is 10^{-8} to 10^{-2} which supports the fact that the three-body interaction is weaker than the two-body interaction [25]. Also it can be seen that three-body interaction is tunable and can be adjusted by varying (V_0/E_r). The three-body effects have been experimentally observed before through various methods as mentioned earlier [14, 15, 16]. We propose an alternate method to observe these effects in an optical lattice and superlattice that we have considered in our present work. The effect of W is very small compared to the two-body interaction in the system of bosons in an optical lattice. This is of course true when the filling factor of the system is unity. From Eq(7.1) it is clear that the three-body energy scales as n^3. Therefore, in order to observe the effect of the three-body interaction in the experiment it is important to study the SF-MI transition at higher densities. In the seminal work of Greiner *et al.* [4], the SF-MI transition was observed by probing the excitation spectrum resulting from a particle-hole excitation. Such an excitation was created by applying a potential gradient to the system in the MI phase. By plotting the excitation probability versus an applied vertical potential gradient, two narrow resonance peaks were seen. The first peak was at the potential gradient equal to the single particle excitation gap, and this corresponds to the MI shell at density equal to one. One of the possible reasons for the appearance of the second peak was the particle-hole excitation created in the MI shell at a density equal to two. In the MI shell at a density equal to two, the particle-hole excitation at a given site would populate one of the neighbouring sites with three-atoms. In principle, when there are three or more atoms in a lattice site, the atoms will experience the effect of W along with that of U. In general when there are n (> 1) atoms in each site the system is in the MI phase with a density equal to n, the excitation gap is $\Delta = U + (n-1)W$ for the optical lattice and $\Delta = U + (n-1)W + \lambda$ for the optical superlattice. Therefore, by measuring the values of the potential gradients for the higher order peaks, and taking the difference between them for different densities, it would be possible to determine the value of W.

In the optical lattice, and the superlattice as well, we find that the Mott insulator

lobes get enlarged as the value of W increases. When the density $\rho = 1$, the effect of W is not significant. However, as the density of the system increases the effect of W becomes significantly large which changes the SF-MI critical point drastically. We obtain the phase diagrams for different combinations of densities, strengths of the three-body interaction and the superlattice potential. Finally, we have also suggested a possible experimental scenario by which it may be possible to observe a signature of the three-body interaction.

Bibliography

[1] M.P.A. Fisher, P.B. Weichmann, G. Grinstein and D.S. Fisher, Phys. Rev. B **40**, 546 (1989).

[2] D. Jaksch, C. Bruder, J. I. Cirac, C. W. Gardiner and P. Zoller, Phys. Rev. Lett. **81**, 3108 (1998).

[3] M Greiner, O. Mandel, T. Esslinger, T. W. Hansch and I. Bloch, Nature **415**, 39 (2002).

[4] M. Lewenstein, A. Sanpera, V. Ahufinger, B. Damski, A. Sen De and U. Sen, Advances in Physics, Vol. **56**, 243 (2007).

[5] I. Bloch, J. Dalibard and W. Zwerger, Rev. Mod. Phys. **80**, 885 (2008).

[6] Simon Folling, Artur Widera, Torben Muller, Fabrice Gerbier, and Immanuel Bloch, Phys. Rev. Lett. **97**, 060403 (2006).

[7] G. K. Campbell, J. Mun, M. Boyd, P. Medley, A. E. Leanhardt, L. G. Marcassa, D. E. Pritchard, and W. Ketterle, Science **313**, 649 (2006).

[8] Bo-lun Chen, Xiao-bin Huang, Su-Peng Kou, Yunbo Zhang, Phys. Rev. A **78**, 043603 (2008).

[9] P. R. Johnson, E. Tiesinga, J. V. Porto, C. J. Williams, New Journal of Physics **11**, 093022 (2009).

[10] Kezhao Zhou, Zhaoxin Liang, Zhidong Zhang, Phys. Rev. A **82**, 013634 (2010).

[11] Arya Dhar, Tapan Mishra, R. V. Pai, B. P. Das, Phys. Rev. A **83**, 053621 (2011).

[12] Arya Dhar, Manpreet Singh, R. V. Pai, B. P. Das, Phys. Rev. A **84**, 033631 (2011).

[13] Sebastian Will, Thorsten Best, Ulrich Schneider, Lucia Hackermüller, Dirk-Sören Lühmann and Immanuel Bloch, Nature **465**, 197 (2010).

[14] M. J. Mark, E. Haller, K. Lauber, J. G. Danzl, A. J. Daley, and H.-C. Nägerl, Phys. Rev. Lett. **107**, 175301 (2011).

[15] Ruichao Ma, M. Eric tai, Philipp M. Preiss, Waseem S. Bakr, Jonathan Simon, and Markus Greiner, Phys. Rev. Lett. **107**, 095301 (2011).

[16] D. van Oosten, P. van der Straten, and H. T. C. Stoof, Phys. Rev. A **63**, 053601 (2001).

[17] K. Sheshadri, H. R. Krishnamurthy, R. Pandit, and T. V. Ramakrishnan, Europhys. Lett. **22**, 257 (1993).

[18] J. M. Kosterlitz and D. J. Thouless, J. Phys. C **6**, 1181 (1973).

[19] Thierry Giamarchi, *Quantum Physics in One Dimension* (Clarendon Press, Oxford, 2004).

[20] Tapan Mishra, Juan Carrasquilla, and Marcos Rigol, Phys. Rev. B **84**, 115135 (2011).

[21] Y. Zhang and F. Han, Journal of Low Temperature Physics, **141**, 314 (2005).

[22] Thorsten Köhler, Phys. Rev. Lett. **89**, 210404 (2002).

[23] T. T. Wu, Phys. Rev., **115**, 1390 (1959).

[24] C. J. Pethick and H. Smith, *Bose-Einstein Condensation in Dilute Gases*, (Cambridge University Press, Cambridge, England, 2002).

Chapter 5

Density Matrix Renormalization Group study of the Bose-Hubbard model with on-site 3-body interaction in Optical Lattices and Optical superlattices

5.1 Introduction

In the previous sections we have discussed the superfluid-Mott insulator (SF-MI) transition for the simple Bose-Hubbard model within the framework of the mean-field theory. However, because of the decoupling approximation we loose the contribution made by the higher order terms. Also, because of the small system size in the mean-field theory correlation functions are not taken into account properly. As a result we over-estimate the value of SF-MI transition critical point. DMRG on the other hand is more sophis-

ticated method and gives better results. In this chapter we first discuss the results for the SF-MI transition obtained using the DMRG method in 1D and compare it with those obtained from the MFT. Later on we discuss our findings for the Bose-Hubbard model in the presence of the on-site three-body interaction in an optical lattice and superlattice.

5.2 Model and method

As before, system of bosons in an optical lattice can be described by the following Hamiltonian:

$$H = -t \sum_{\langle i,j \rangle} (\hat{a}_i^\dagger \hat{a}_j + \text{H.c}) + \frac{U}{2} \sum_i \hat{n}_i(\hat{n}_i - 1) - \mu \sum_i \hat{n}_i \tag{5.1}$$

The first DMRG study of this model was done by Monien and Kühner [1]. The infinite-

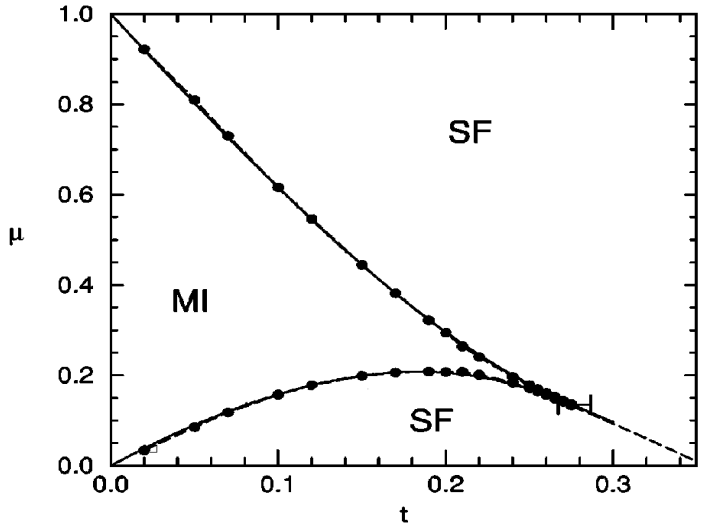

Figure 5.1: Phase diagram for the SF-MI transition obtained using DMRG method [1].

size density-matrix renormalization group method with periodic boundary conditions was used to estimate the SF-MI critical point. Maximum number of particles allowed per site was fixed to 5. The maximum size of the system considered was of 76-sites and the

number of DMRG states in each iteration was 128. The energy gap obtained for various system sizes was then extrapolated to obtain it's actual value in the thermodynamic limit. By repeating the calculations for several values of t phase boundaries were obtained as shown in the Fig. 5.1. Using this method the SF-MI critical point was estimated to be at $t_c \sim 0.277 \pm .01$. The value of U was fixed at 1.0, therefore $(U/t)_c$ for the SF-MI transition in 1D was found to be $\sim$ 3.6. Similar calculations in the recent past with hundreds of sites and higher number of DMRG states estimate this critical point to be close to 3.4. Whereas the single-site mean-field theory in the decoupling approximation estimates SF-MI $(U/t)_c \sim 11.7$ in 1D. Therefore DMRG method is better than the conventional single-site MFT in 1D. MFT results improve as the dimensionality increases. Theoretically MFT gives accurate results in infinite dimensions.

The system of bosons in an optical superlattice with three-body interaction can be described by the modified Bose-Hubbard model as follows:-

$$H = -t \sum_{\langle i,j \rangle} (\hat{a}_i^\dagger \hat{a}_j + \text{H.c}) + \frac{U}{2} \sum_i \hat{n}_i(\hat{n}_i - 1)$$
$$+ \frac{W}{6} \sum_i \hat{n}_i(\hat{n}_i - 1)(\hat{n}_i - 2) - \mu \sum_i \hat{n}_i + \sum_i \lambda_i \hat{n}_i \tag{5.2}$$

Here W represents the on-site inter-atomic three-body interaction and λ is the superlattice potential. We consider a bipartite lattice with sub-lattices $\mathcal{A}$ and $\mathcal{B}$ with a periodicity of two sites.

5.3 Results and discussions

In this section first we present our results for the BHM describing an optical lattice with the three-body on-site interaction which is then followed by the results for an optical superlattice with three-body on-site interaction. We use finite size-DMRG method to perform calculations and obtain phase diagram for both the cases. For the calculations using the FS-DMRG method, we fix the hopping matrix element $t = 1$ to fix the energy

scale (so all the quantities plotted, are in units of t) and to estimate the critical points U_C, we perform finite-size scaling of the single particle gap G_L (defined by the difference between the energies needed to add an atom and remove an atom from the system). The plots of LG_L for different system sizes L (see Fig.(5.2)), assuming that the SF to MI transitions belong to the Berezinskii-Kosterlitz-Thouless (BKT) type [19, 20], coalesce in the superfluid phase below the U_C. The value of U_C is then estimated within an error bar of 0.1 if the values of LG_L, say for $L = 140$ and 200, differ by less than 4 %. At the BKT transition the gap closes satisfying the relation, $G_L \sim \exp[-a/|U - U_C|^{1/2}]$, where a is a constant. The correlation length ξ, is finite in the gapped phase and diverges at the critical point as $(1/G_L) = exp\ [a/|U - U_C|^{1/2}]$. Near U_C, the finite-size-scaling relation $LG_L[1 + \{1/(2\ ln\ L + C)\}] = F(\xi/L)$, is used to estimate the transition point as done in Ref. [21].

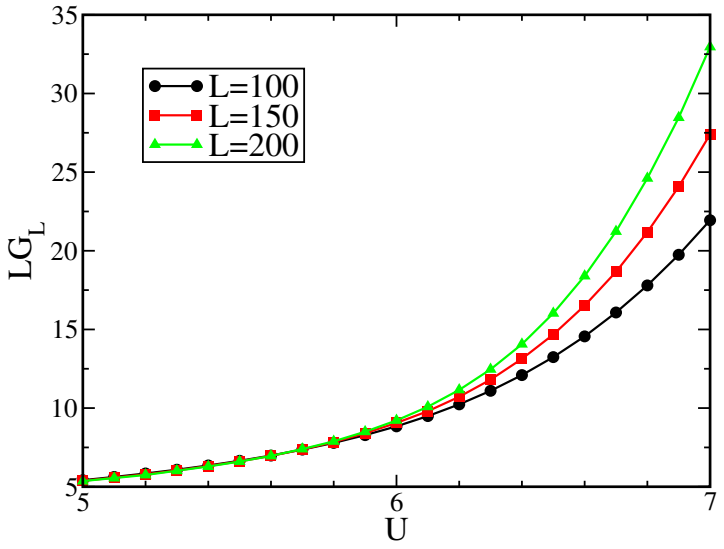

Figure 5.2: Scaling of gap LG_L plotted as function of U for $\rho = 2$ and $W = 0.0$.

Therefore, if we plot $ln(L/\xi)$ vs. $LG_L\,(1 + (1/(2\ ln\ L + C))$ then the curves for different lengths collapse in the vicinity of U_C(scaled) (see Fig.(5.3), main panel). Combining the scaling method described above and DMRG results, we give an approximate

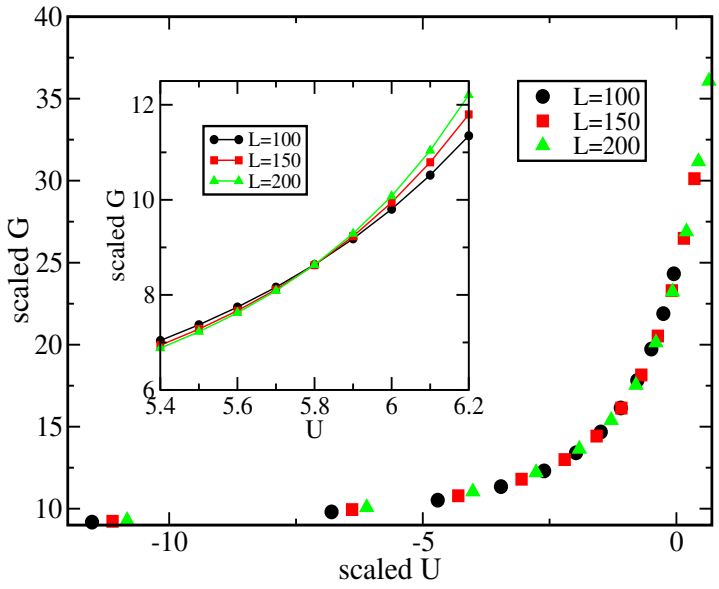

Figure 5.3: Scaled gap G_L plotted as a function of scaled U for $\rho = 2$ and $W = 0.0$. The curves for different lengths collapse in the vicinity of U_C as the correlation length ξ diverges exponentially near U_C. (Inset) Scaled gap G_L plotted as a function of U. The curves for different lengths cross at U_C ($\sim$ 5.8) showing the critical point for SF-MI transition.

value of U_C in various configurations.

The DMRG results obtained for the optical lattice are given in Figs. 5.4 and 5.5, for $\rho = 2$ and 3 respectively. Figures 9(a) and 9(b) are the phase diagrams for the optical superlattice for $\rho = 3/2$ and 2 respectively, with two values of $W(= 0.0, 5.0)$. DMRG results (Fig.5.6(a)) show a trend similar to what is seen in the MF analysis for the same model. When $W = 0.0$, the system undergoes a phase transition from the SF phase to the SLMI phase R3 at a value of $\lambda \sim 0.3$. However, in the presence of a finite W, the transition occurs at a lower $\lambda(\sim 0.15)$, signifying the enlargement of the insulating lobes.

The trend is the same for both the densities, $\rho = 2$ and 3, but the effect of W is more when the density is large. For $\rho = 2$, $U_C(W = 4.0) \approx 1.6$ compared to $U_C(W = 0.0) \approx 5.7$. For $\rho = 3$, U_C decreases steadily as W increases; $U_C(W = 0.0) \approx 8.6$, $U_C(W = 1.0) \approx 6.6$,

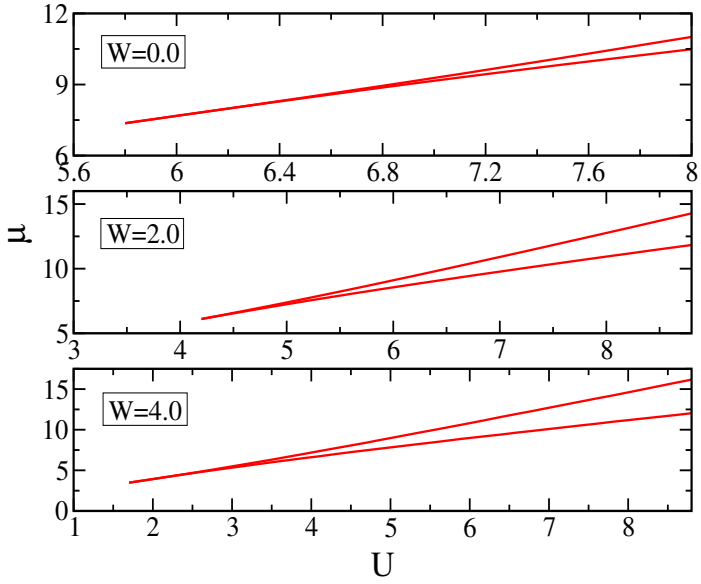

Figure 5.4: Phase diagram for $\rho = 2$ for various values of W, for optical lattice.

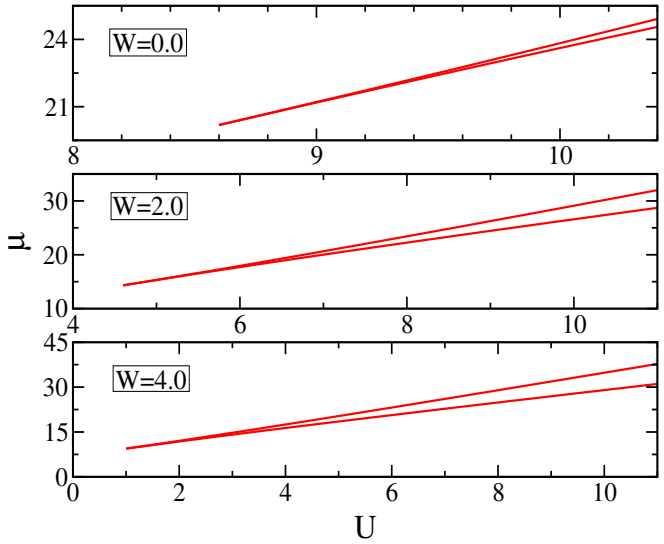

Figure 5.5: Phase diagram for $\rho = 3$ for various values of W, for optical lattice.

$U_C(W = 2.0) \approx 4.6$, for $U_C(W = 3.0) \approx 2.6$ and $U_C(W = 4.0) \approx 0.8$. Similar results are obtained for the superlattice also (Fig.5(b)). For finite $W = 5.0$, the critical superlattice potential λ_C for transition from the MI phase L2 to SF phase shifts from 9.4 to 14.8 and

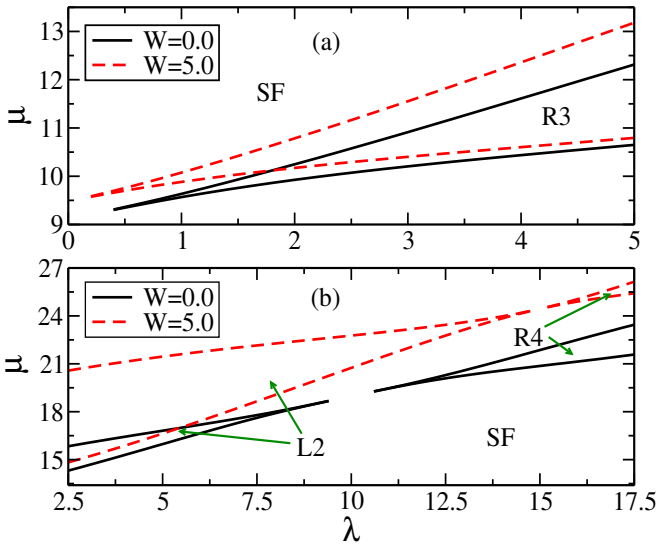

Figure 5.6: (a) Phase diagram for $\rho = 3/2$ and (b) phase diagram for $\rho = 2$, in an optical superlattice with $W = 0.0$ and 5.0.

that for the SF phase to SLMI phase R4 shifts from 10.6 to 15.2. In the absence of W and for lower values of λ, the superlattice initially stays in the MI phase L2, for $U = 10.0$. As λ becomes comparable to U, the system goes from the MI phase to the SF phase at $\lambda \sim 9.4$. As λ is further increased, the system goes from the SF phase to the SLMI phase R4, at a value of $\lambda \sim 10.6$. For $W = 5.0$, the system initially is in the MI phase, L2. Now, due to the presence of W, the SF window is shifted to a λ value which is comparable to $U + W$ as shown in Fig.5.6(b). The MI to SF transition takes place at $\lambda \sim 14.8$, and the second transition from SF to SLMI (R4) takes place at $\lambda \sim 15.2$. The SF window not only shifts for $W = 5.0$ but also shrinks when compared to that of $W = 0.0$. This shifting of the R4 lobe can be understood as follows: in the R4 phase there are three atoms at every alternate site. As W increases, it becomes difficult to confine three or more atoms at a single site. Hence to suppress this effect due to the increase in W, we need to increase λ.

5.4 Conclusions

In conclusion, we have studied the effects of the on-site three-body interactions in a system of neutral bosons in an optical lattice and superlattice. We have used the FS-DMRG method to obtain the phase diagram for these systems. The DMRG results confirm the results obtained using the mean-field theory and are in a good qualitative agreement.

Bibliography

[1] T. D. Kühner and H. Monien, Phys. Rev. B **22**, 58 (1998).

[2] M.P.A. Fisher, P.B. Weichmann, G. Grinstein and D.S. Fisher, Phys. Rev. B **40**, 546 (1989).

[3] D. Jaksch, C. Bruder, J. I. Cirac, C. W. Gardiner and P. Zoller, Phys. Rev. Lett. **81**, 3108 (1998).

[4] M Greiner, O. Mandel, T. Esslinger, T. W. Hansch and I. Bloch, Nature **415**, 39 (2002).

[5] M. Lewenstein, A. Sanpera, V. Ahufinger, B. Damski, A. Sen De and U. Sen, Advances in Physics, Vol. **56**, 243 (2007).

[6] I. Bloch, J. Dalibard and W. Zwerger, Rev. Mod. Phys. **80**, 885 (2008).

[7] Simon Folling, Artur Widera, Torben Muller, Fabrice Gerbier, and Immanuel Bloch, Phys. Rev. Lett. **97**, 060403 (2006).

[8] G. K. Campbell, J. Mun, M. Boyd, P. Medley, A. E. Leanhardt, L. G. Marcassa, D. E. Pritchard, and W. Ketterle, Science **313**, 649 (2006).

[9] Bo-lun Chen, Xiao-bin Huang, Su-Peng Kou, Yunbo Zhang, Phys. Rev. A **78**, 043603 (2008).

[10] P. R. Johnson, E. Tiesinga, J. V. Porto, C. J. Williams, New Journal of Physics **11**, 093022 (2009).

[11] Kezhao Zhou, Zhaoxin Liang, Zhidong Zhang, Phys. Rev. A **82**, 013634 (2010).

[12] Arya Dhar, Tapan Mishra, R. V. Pai, B. P. Das, Phys. Rev. A **83**, 053621 (2011).

[13] Arya Dhar, Manpreet Singh, R. V. Pai, B. P. Das, Phys. Rev. A **84**, 033631 (2011).

[14] Sebastian Will, Thorsten Best, Ulrich Schneider, Lucia Hackermüller, Dirk-Sören Lühmann and Immanuel Bloch, Nature **465**, 197 (2010).

[15] M. J. Mark, E. Haller, K. Lauber, J. G. Danzl, A. J. Daley, and H.-C. Nägerl, Phys. Rev. Lett. **107**, 175301 (2011).

[16] Ruichao Ma, M. Eric tai, Philipp M. Preiss, Waseem S. Bakr, Jonathan Simon, and Markus Greiner, Phys. Rev. Lett. **107**, 095301 (2011).

[17] D. van Oosten, P. van der Straten, and H. T. C. Stoof, Phys. Rev. A **63**, 053601 (2001).

[18] K. Sheshadri, H. R. Krishnamurthy, R. Pandit, and T. V. Ramakrishnan, Europhys. Lett. **22**, 257 (1993).

[19] J. M. Kosterlitz and D. J. Thouless, J. Phys. C **6**, 1181 (1973).

[20] Thierry Giamarchi, *Quantum Physics in One Dimension* (Clarendon Press, Oxford, 2004).

[21] Tapan Mishra, Juan Carrasquilla, and Marcos Rigol, Phys. Rev. B **84**, 115135 (2011).

[22] Y. Zhang and F. Han, Journal of Low Temperature Physics, **141**, 314 (2005).

[23] Thorsten Köhler, Phys. Rev. Lett. **89**, 210404 (2002).

[24] T. T. Wu, Phys. Rev., **115**, 1390 (1959).

[25] C. J. Pethick and H. Smith, *Bose-Einstein Condensation in Dilute Gases*, (Cambridge University Press, Cambridge, England, 2002).

Chapter 6

Quantum phases of attractive bosons on a Bose-Hubbard ladder with three-body constraint

6.1 Introduction

We obtain the complete quantum phase diagram of bosons on a two-leg ladder in the presence of attractive onsite and repulsive interchain nearest-neighbor interactions by imposing the onsite three-body constraint. We find three distinct phases; namely, the atomic superfluid (ASF), dimer superfluid (DSF), and the dimer rung insulator (DRI). In the absence of the interchain nearest-neighbor repulsion, the system exhibits a transition from the ASF to the DSF phase with increasing onsite attraction. However, the presence of the interchain nearest-neighbor repulsion stabilizes a gapped DRI phase, which is flanked by the DSF phase. We also obtain the phase diagram of the system for different values of the interchain nearest-neighbor interaction. By evaluating different order parameters, we obtain the complete phase diagram and the properties of the phase transitions using

the self-consistent cluster mean-field theory.

Low-dimensional systems have been studied widely in the past few decades. In particular $1D$ or quasi-$1D$ systems are of very special interest because interactions play a crucial role in realizing novel phases [21, 20]. Quasi-$1D$ systems such as ladders have been of special interest to understand the phenomenon of high-temperature superconductivity, spin-gapped metallic state [22, 23, 24] etc. The extra coupling between the legs of the ladder makes these systems unique, as a result of which, the quantum phase transitions are influenced substantially even in a simple model like the Bose-Hubbard ladder [25, 26, 27].

Earlier studies have shown that an ultracold bosonic gas in a lattice with attractive interactions undergoes a transition from an atomic superfluid (ASF) to the dimer superfluid (DSF) phase when the atoms are subjected to the onsite three body constraint [7]. This phenomenon was first predicted in the context of an atomic Bose gas in the continuum with Feshbach resonance [45]. This prediction suggests that the bosons can pair up to form the DSF phase when the attraction between them is sufficiently large. This transition was predicted to be Ising like at the commensurate filling and first order at other fillings. Detailed investigations on this model have been made on a square lattice in the recent past [8, 9] to obtain the ground state phase diagram. The effect of nearest neighbor interaction on a square lattice has predicted a dimer checker board solid phase [10]. Bosons with two-body onsite attractive interactions in optical lattices that are subjected to the onsite three- or four-body constraint can form dimer and density wave phases as well [11, 7, 12].

In this chapter, we focus on a system of ultracold bosonic atoms possessing long-range interactions along the rungs of a two leg ladder as shown in Fig. 6.1. This system can be realised by using dipolar bosons and polarizing them at the magic angle ϕ with reference to the plane of the ladder, and perpendicular to the rungs of the ladder. The dipole-dipole interaction energy is proportional too $(1 - 3cos^2\phi)$. Therefore if the angle ϕ is chosen such that the condition $cos^2\phi = 1/3$ is satisfied, the dipole-dipole interaction

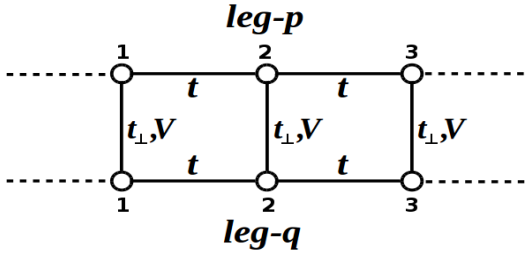

Figure 6.1: A small section of the ladder model is shown and the cluster contains six sites. Dashed lines represent bonds between decoupled sites, circles represent lattice sites.

energy along the leg becomes zero but remains finite along the rungs. Taking the on-site interactions to be attractive for such a system and imposing the three body constraint, we study its ground state phase diagram. In addition, we also study the quantum phases of this model in the case of hard core bosons to validate our predictions. We use the self consistent cluster mean-field theory (CMFT) to determine the various order parameters to obtain the different quantum phase transitions in this model.

The remaining part of this chapter is organized as follows. In Sec. II we give details of the model and the method used in our calculation. Section III is devoted to our results. Sec. IV contains concluding remarks.

6.2 Model and method

The effective many-body lattice model which describes the problem mentioned above is given by

$$\begin{aligned} H = &-t\sum_{\alpha,i}(a^{\dagger}_{\alpha,i}a_{\alpha,i+1} + H.c.) - t_{\perp}\sum_{i}(a^{\dagger}_{p,i}a_{q,i} + H.c.) \\ &+\frac{U}{2}\sum_{\alpha,i} n_{\alpha,i}(n_{\alpha,i}-1) + V\sum_{i} n_{p,i}n_{q,i} - \sum_{i}\mu_{\alpha,i}n_{\alpha,i} \end{aligned} \tag{6.1}$$

where ${a_{\alpha,i}}^{\dagger}(a_{\alpha,i})$ is the bosonic creation (annihilation) operator at the site i of leg - $\alpha(=p,q)$. t is the hopping amplitude between the nearest neighbour sites along the

legs of the ladder and $t_\perp$ is the hopping along the rungs of the ladder. $n_{\alpha,i} = a^\dagger_{\alpha,i} a_{\alpha,i}$ is the number operator at site (α, i). U and V represent the on-site inter-atomic two-body and nearest-neighbour interactions respectively. The chemical potential is represented by μ. In this work we assume the three body constraint, *i.e.* $(a^\dagger)^3|0\rangle = 0$ and the value of U is negative. We also assume that the ladder is arranged in such a way that the nearest neighbour repulsion V is only present along the rungs of the ladder.

The ground state properties of this model can be studied quite accurately by using powerful numerical methods such as the density matrix renormalization group method (DMRG) [51, 52] or the quantum monte carlo (QMC) methods. However, in order to qualitatively understand the quantum phase transitions exhibited in this model, we use the self consistent CMFT method. This method is capable of capturing the relevant physics that arises due to quantum correlations, which was not always possible to achieve in the conventional single site mean-field theory decoupling approximation [53, 54, 55, 6, 57, 58]. The CMFT can account for non-local interaction more accurately by retaining them in the exact form. For the regular SF-MI transition the estimation of the critical point improves when CMFT is used and approaches the value obtained by the methods like QMC and DMRG [60]. In this method a cluster of sites is treated exactly and the mean-field approximation is for the coupling which connects the cluster with rest of the lattice. The accuracy of the calculation depends on the size of the cluster considered. As the cluster size increases, the number of decoupled bond reduces and the Hamiltonian approaches the exact form. In one of its very first applications this method was used to study the phase diagram of a one-dimensional optical superlattice [59]. In recent years it has been used to study various other models where the results are found to be in good agreement with those obtained using exact numerical methods [61, 60, 62, 63].

We consider six sites cluster as shown in Fig. 6.1. Then the model given in Eq. (6.1) can be written as

$$H = \sum_k H_c^k \tag{6.2}$$

where summation over k is over all the clusters and H_c^k is the Hamiltonian for k^{th} cluster which can be written as (dropping k since all the clusters are identical)

$$H_c = H_e + H_d, \tag{6.3}$$

where H_e is the exact Hamiltonian of the cluster and H_d is the decoupled hopping term to the nearest neighbour cluster. Using the mean-field decoupling approximation one can make the following substitution since i and j are adjacent sites in the nearest neighbour clusters,

$$a_i^\dagger a_j \simeq \langle a_i^\dagger \rangle a_j + {a_i}^\dagger \langle a_j \rangle - \langle {a_i}^\dagger \rangle \langle a_j \rangle \tag{6.4}$$

in the hopping term in Eq.(1) and introduce the superfluid order parameter

$$\phi_i \equiv \langle a_i^\dagger \rangle \equiv \langle a_i \rangle \tag{6.5}$$

to obtain the following Hamiltonian for the decoupled part,

$$H_d = -t \sum_{\alpha=\{p,q\}} \sum_{\substack{i,i'=1,3 \\ i\neq i'}} \left[\phi_{\alpha,i} ({a_{\alpha,i'}}^\dagger + a_{\alpha,i'}) + \phi_{\alpha,i}\phi_{\alpha,i'} \right] \tag{6.6}$$

The exact Hamiltonian, H_e is given by

$$\begin{aligned} H_e &= -t \sum_{\substack{\alpha=\{p,q\} \\ i=\{1,2\}}} (a_{\alpha,i}^\dagger a_{\alpha,i+1} + H.c.) \\ &\quad -t_\perp \sum_{i=\{1,2,3\}} (a_{p,i}^\dagger a_{q,i} + H.c.) \\ &\quad + \sum_{\substack{\alpha=\{p,q\} \\ i=\{1,2,3\}}} \left[\frac{U}{2} n_{\alpha,i}(n_{\alpha,i}-1) + V n_{p,i} n_{q,i} - \mu_{\alpha,i} n_{\alpha,i} \right] \end{aligned} \tag{6.7}$$

We set the energy scale by choosing $t = 1$, as a result, all the physical parameters considered are dimensionless. We choose to work in the occupation number basis and

construct the Hamiltonian matrix using the expression given by H_c. This matrix is then diagonalized self-consistently to obtain the ground state of the system. The ground state so obtained can then be used to calculate the necessary expectation values.

6.3 Results and discussion

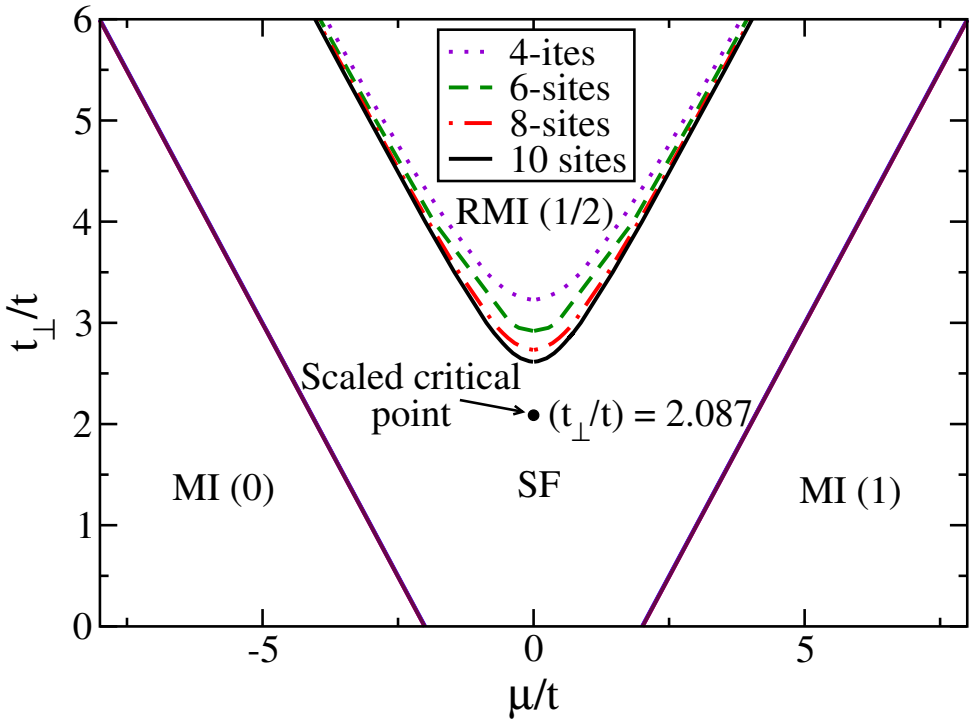

Figure 6.2: Phase diagram for hard-core bosons in absence of V for different cluster sizes. The cluster sizes are indicated in the legend. The scaled critical point for RMI(1/2)-SF transition is represented by a black dot.

In this section we report our findings and analyse the results of our work. Before presenting the main results, we validate our method; i.e. the CMFT by studying an already known phase diagram using other exact methods. It has been predicted that in the case of hardcore bosons ($U = \infty$) on a ladder, the system exhibits a rung Mott

insulator (RMI) phase due to the competition between the intra-chain and inter-chain couplings, t and $t_\perp$ respectively [64, 65]. When the value of $t_\perp$ is large compared to t, the atoms can only hop within the rungs of the ladder, which results in the system being gapped. We have investigated this model using our CMFT approach and obtain the phase diagram shown in Fig.6.2. This phase diagram is in a very good qualitative agreement with the results presented in Ref. [65]. We have done the calculations using $4-, 6-, 8-$ and $10-$sites clusters. The RMI(1/2)-SF critical transition point found from each of these calculations are then scaled to the thermodynamic limit. This gives an estimate of $(t_\perp/t)_c \sim 2.087$.

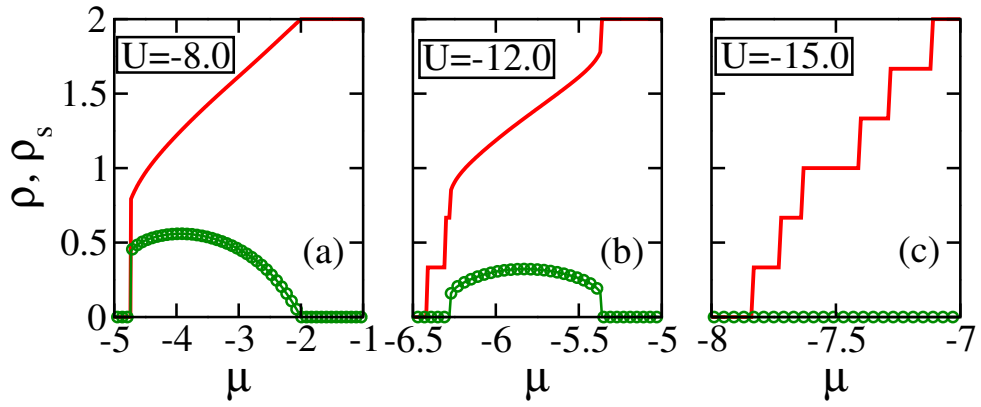

Figure 6.3: $\rho, \rho_s - \mu$ plot for (a)$U = -8.0$, (b)$U = -12.0$ and (c)$U = -15.0$ for $V = 0.0$. Solid (red) curves represent average density ρ and circles (green curves) represent average superfluid density ρ_s in the cluster.

We now turn to the results of our work. Recent numerical and analytical works on the model given in Eq.(6.1), in the absence of the nearest neighbour interactions, have predicted the existence of a transition from the ASF phase to the DSF phase in one and two dimensions [7, 12, 8, 9, 10]. Apart from this, two trivial gapped (insulating) phases, MI(0) at $\rho = 0$ and MI(2) at $\rho = 2$, are also present. It has been predicted for a two dimensional square lattice that (i) the MI to DSF transition is always continuous, (ii) there exists a first order transition from the MI(0) to ASF phase and (iii) there exists

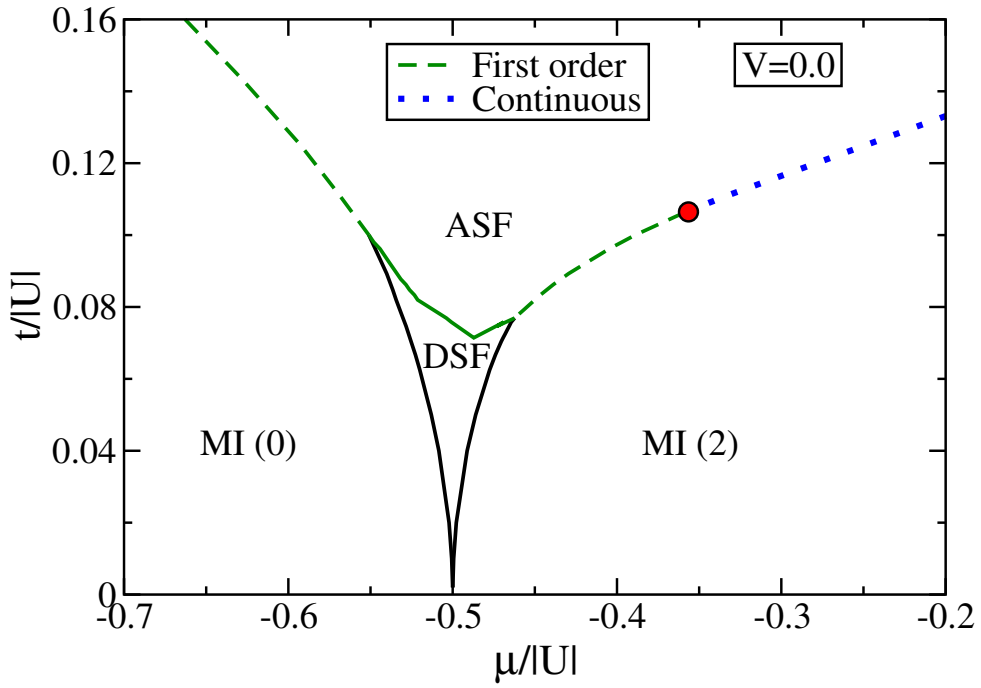

Figure 6.4: Phase diagram for $U < 0$ and $V = 0.0$. Green (dashed) line and blue (dotted) line indicate first and second-order transitions, respectively. The first- to second-order change on the phase boundary is marked by a red circle.

a tricritical point along the ASF-MI(2) transition boundary [8]. In the presence of the nearest neighbour interaction V, the region of the first order phase boundary shrinks as V is increased. A dimer checker board solid (DCS) appears when $V \neq 0$ [10].

As stated earlier, the system we consider here is a two leg ladder and the nearest neighbour interaction is allowed only along the rungs of the ladder. We have considered three different cases: $V = 0.0,\ 0.5$ and 1.0 to demonstrate the salient features of phase diagrams for these three cases. When $V = 0.0$, the system exhibits a phase diagram qualitatively similar to that obtained for the square lattice case as shown in Fig.6.4. This phase diagram consists of four phases, the MI(0), MI(2), ASF and DSF phases. To obtain this in our CMFT approach, we use the superfluid order parameter ϕ and the density ρ as the order parameters. In the ASF phase, the atomic superfluid density $\rho_s = \phi^2 = \langle (a^\dagger) \rangle^2$

is finite and is zero for the MI phases. In other words the ASF phase is gapless and compressible and the MI phases are gapped. In order to obtain the phase boundary between different phases we plot the density ρ (solid line (red curve)) and superfluid density ρ_s (circles (green curve)) as a function of the chemical potential μ for different values of U in Fig.6.3 where it can be seen that the ρ versus μ plot (solid (red) curves) has two plateaus corresponding to the gapped MI(0) and MI(2) phases at $\rho = 0$ and $\rho = 2$ respectively. However, at intermediate densities the ASF and DSF phases appear. When U is small, say -8.0, a region exists where ρ_s is finite, circles(green curve) in Fig.6.3(a) and the value of ρ (solid(red) curves) increases suddenly from zero to some finite value and then increases continuously till it saturates at two. This region in the parameter space is the ASF phase since the superfluid density ρ_s remains finite. The sudden jump in the values of ρ and ρ_s from zero to finite value suggests that the transition from the MI(0) to ASF phase is first order which will be discussed in more detail later. When U becomes more negative and the value of μ is small, the attraction between particles favours dimer formation which hop around to form the DSF phase.

In the framework of our CMFT approach, it is difficult to predict the dimer phases directly from the calculation of the DSF order parameter. However, if on increasing the value of the chemical potential, the system density increases in steps of two atoms, then we conclude that it has entered the DSF phase. This shows that the system consists of only dimers and they behave as single entities. When the chemical potential is increased, for small values of μ as seen in the Fig.6.3(b) for $U = -12.0$, the density of the system increases only if the chemical potential increases to accommodate two bosons or one dimer. However, for higher values of the chemical potential, the density increases in a continuous manner with the chemical potential, because the kinetic energy dominates in this situation and the system behaves like an atomic superfluid. At this value of U, a first order type transition from the ASF to the MI(2) phase takes place, which can be seen from the sharp jump in the density at the chemical potential close to the MI(2) plateau.

When U is highly attractive, say $U = -15.0$, all the particles form dimers and the system is fully in the DSF phase. The particle density then increases in steps of two particles till it reaches the MI(2) state. This behaviour can be seen in the Fig.6.3(c). Since in this calculation we have considered a cluster consisting of 6 sites, we get jumps in the density when it reaches the values 1/3, 2/3, 4/3, 5/3 and 2 *i.e.* when the total number of bosons in the cluster is equal to, respectively, 2, 4, 6, 8, 10 and 12. By locating the transition points from the $\rho - \mu$ curves we obtain various phases and the phase diagram as shown in Fig.6.4. Although the DSF to ASF phase transition shows a first-order type behaviour in the $\rho, \rho_s - \mu$ plots, it is actually predicted to be of Ising type at unit filling in other models in earlier works[7]. In our CMFT approach it is difficult to predict the nature of this transition. The small plateaus we obtain in $\rho - \mu$ curves in the DSF region

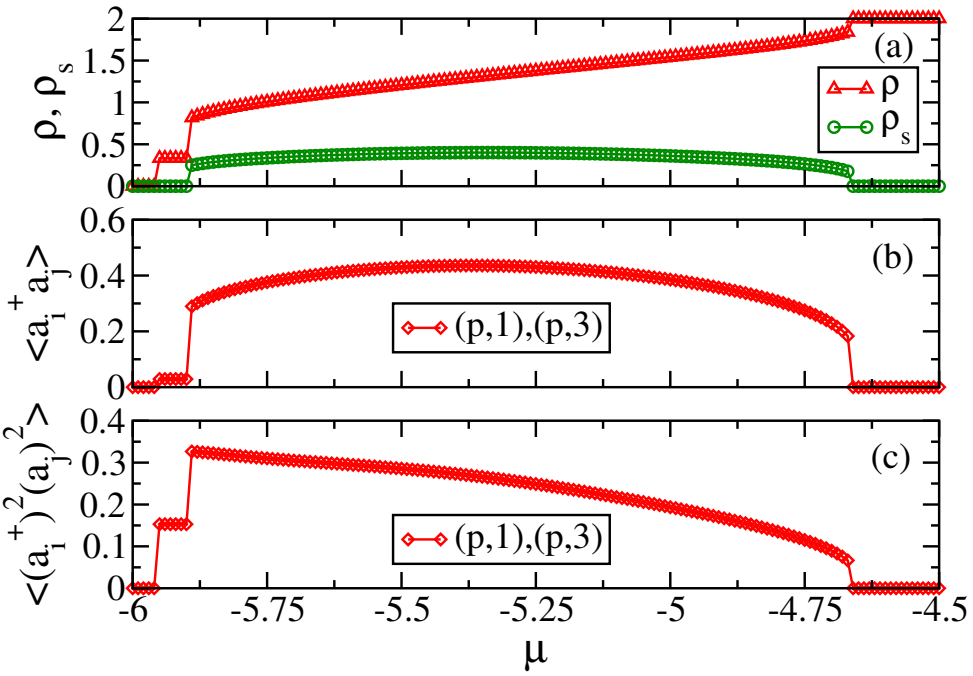

Figure 6.5: $U = -11.0, V = 0.0$. (a)ρ, ρ_s $-$ μ plot (b)single-particle tunnelling and, (c)pair tunnelling amplitude between sites.

are artefacts of the finite size of the system we have used in our work. We expect these

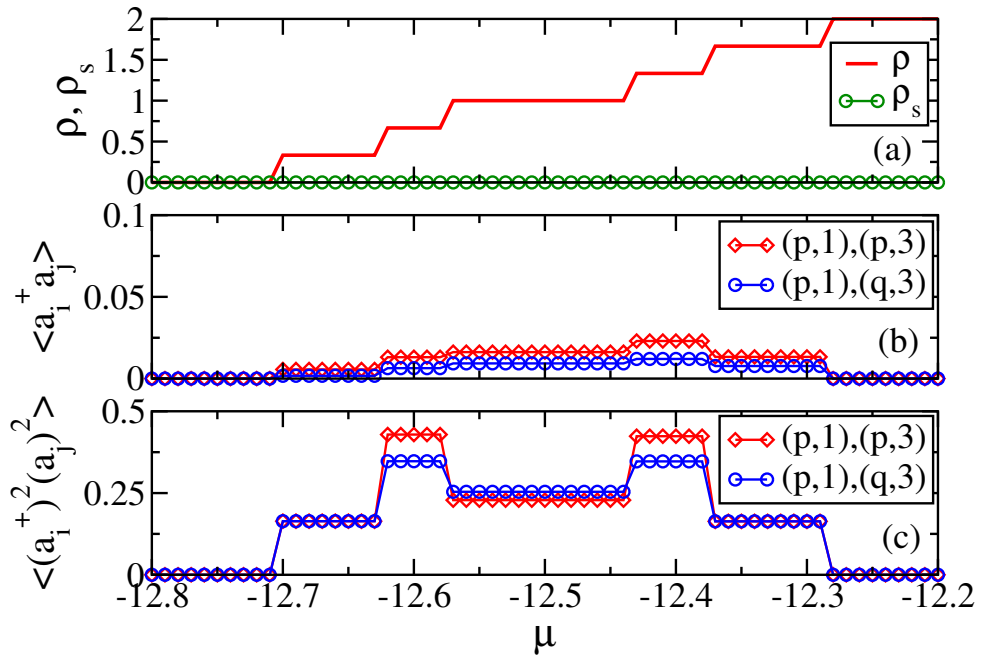

Figure 6.6: $U = -25.0, V = 0.0$. (a)ρ, ρ_s $-$ μ plot (b)single-particle tunnelling and, (c)pair tunnelling amplitude between sites.

plateaus to become smaller and gradually disappear as the system size is increased. In fact, the disappearance of such plateaus has been shown in a comparative study of a system of hard-core bosons using the exact-diagonalization and quantum Monte Carlo methods [44].

Another signature of the dimer formation can be inferred by comparing the single-particle tunnelling and the paired-tunnelling amplitudes. As an example we have plotted the above quantities for $U = -11.0$ and $U = -25.0$ in Fig.6.5 and Fig.6.6 respectively. The quantity $\langle {a_i}^\dagger a_j \rangle$ is the tunnelling amplitude for a single boson and $\langle {a_i}^{\dagger 2} {a_j}^2 \rangle$ is the tunnelling amplitude for a pair of bosons between the sites i and j. The pair of sites i, j between which tunnellings are considered are given in the legends of the respective plots. For $U = -11.0$, DSF exists only for a small region of μ values, around $\mu = -5.9$, while the ASF phase dominates the rest of the region, as shown in Fig.6.5. The paired-tunnelling

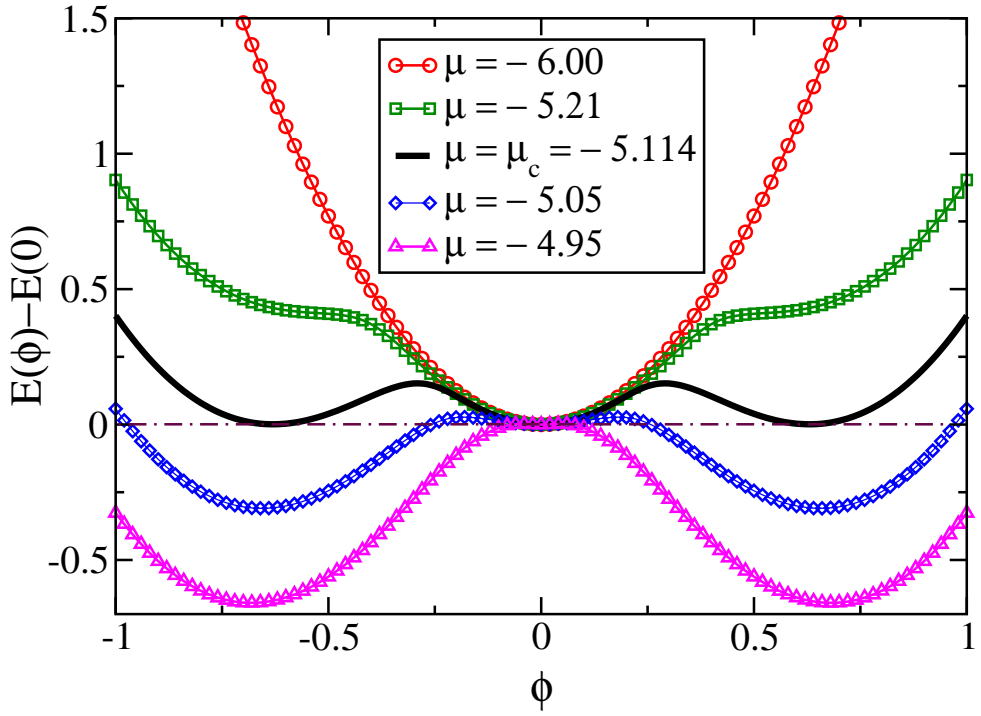

Figure 6.7: (E(ϕ)-E(0) versus order parameter (ϕ) plot for $U = -9.0, V = 0.0$. From top to bottom, $\mu = -6.0, -5.21, -5.114$ (μ_c), -5.05 and -4.95 for MI(0)-ASF transition across the left most boundary in Fig.6.4.

amplitude dominates over the single boson tunnelling in the DSF phase and as expected both have finite values in the ASF phase. When the DSF phase dominates, as in the case for $U = -25.0$, paired-tunnelling amplitude remains constant as $|i - j|$ increases while the single boson tunnelling decreases to zero, as shown in Fig. 6.6. These features confirm our earlier conclusion that we do not have the ASF phase for higher values of $|U|$ as shown in Fig.6.4. The order of the phase transition between MI(0) to ASF and ASF to MI(2) can be obtained by observing the ground state energy of the system around the critical point on the common phase boundary. We plot $E(\phi) - E(\phi = 0)$ as a function of the superfluid order parameter ϕ for the μ values at and around the critical point. One such plot for $U = -9.0, V = 0.0$ is given in Fig.6.7. This point lies on the phase

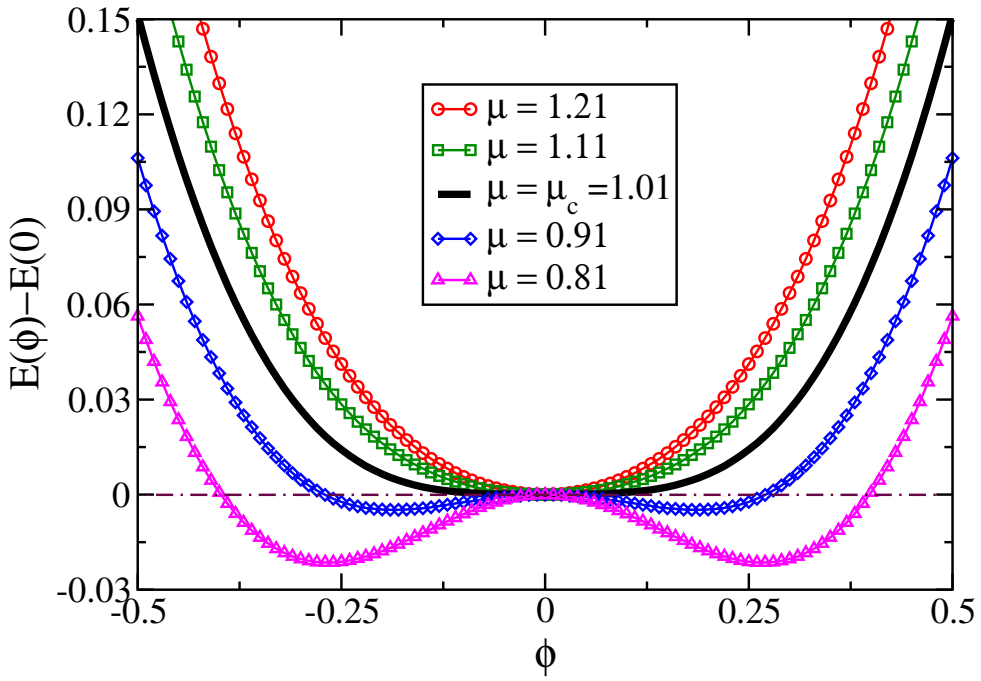

Figure 6.8: E(ϕ)-E(0) vs. order parameter (ϕ) plot for $U = -5.0$. From top to bottom, $\mu = 1.21, 1.11, 1.01(\mu_c), 0.91$ and 0.81 for ASF-MI(2) transition across the right most boundary in Fig.6.4.

boundary between MI(0) and the ASF phases (Fig.6.4). When $\mu < -5.114$ the system is in the MI(0) phase and we obtain a single minimum, but as μ increases and approaches the critical point ($\mu_c = -5.114$), two more minima start appearing. At the exact critical point all the three minima become degenerate. A single minimum indicates a unique solution which corresponds to the MI phase and the three degenerate minima indicate the three of the possible solutions of the infinitely degenerate SF phase. This is an indicator of a first-order transition.

We pick one other point at $U = -5.0, V = 0.0$ on the phase boundary between ASF and MI(2) phases and repeat the above procedure to find out the order of transition. The corresponding plot is shown in Fig.6.8. We can see that there are only two minima merging into a single minimum at this point. Therefore this is a second-order transition.

We repeat these calculations for several values of U around which there are sudden jumps in $\rho,\ \rho_s - \mu$ plots. For $V = 0.0$ we find that the nature of the SF-MI(2) transition changes from first-order to second-order at $U \sim -9.4$. This point is marked by a red circle in Fig.6.4, which is a tricritical point.

Now we discuss our findings by considering the effect of the nearest neighbour interaction V. As mentioned before, we consider the nearest neighbour interaction only along the rungs of the ladder such that the system does not break any translational symmetry by forming a density wave order. In such a situation, the effect of a small value of V is dramatic when U is highly attractive. We investigate the system for two different values of V equal to 0.5 and 1.0. In both the cases we study the phase diagram by increasing the magnitude of U and making it more attractive. When U is slightly negative the system exhibits the ASF phase for densities intermediate between 0 and 2. However, when the value of U is sufficient to form dimers and at $\rho = 1$, the small

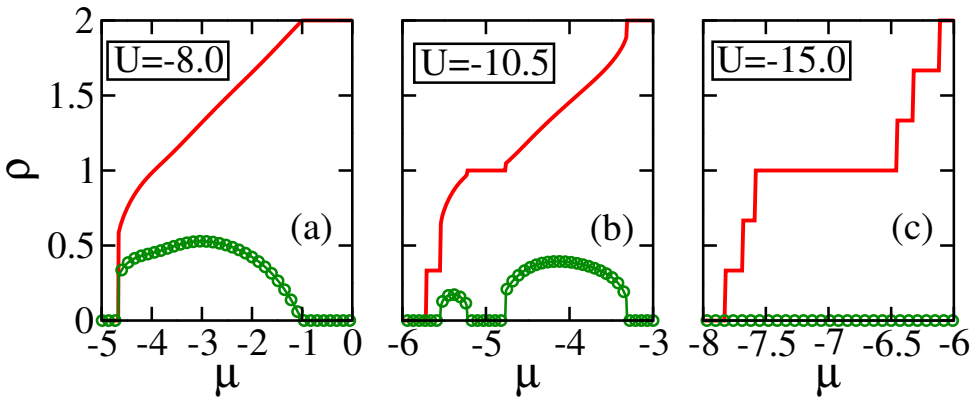

Figure 6.9: $\rho,\ \rho_s - \mu$ plot for (a)$U = -8.0$, (b)$U = -10.5$ and (c)$U = -15.0$ for $V = 0.5$. Solid (red) curves represent average density, solid-circle (green) curves represent average superfluid density in the cluster.

value of V tries to prevent two dimers to sit on a single rung. However, it cannot restrict the dimer to hop within the sites of a rung which is governed by the kinetic term $t_\perp$. Hence the dimers are localized on the rungs of the ladder creating a singlet on

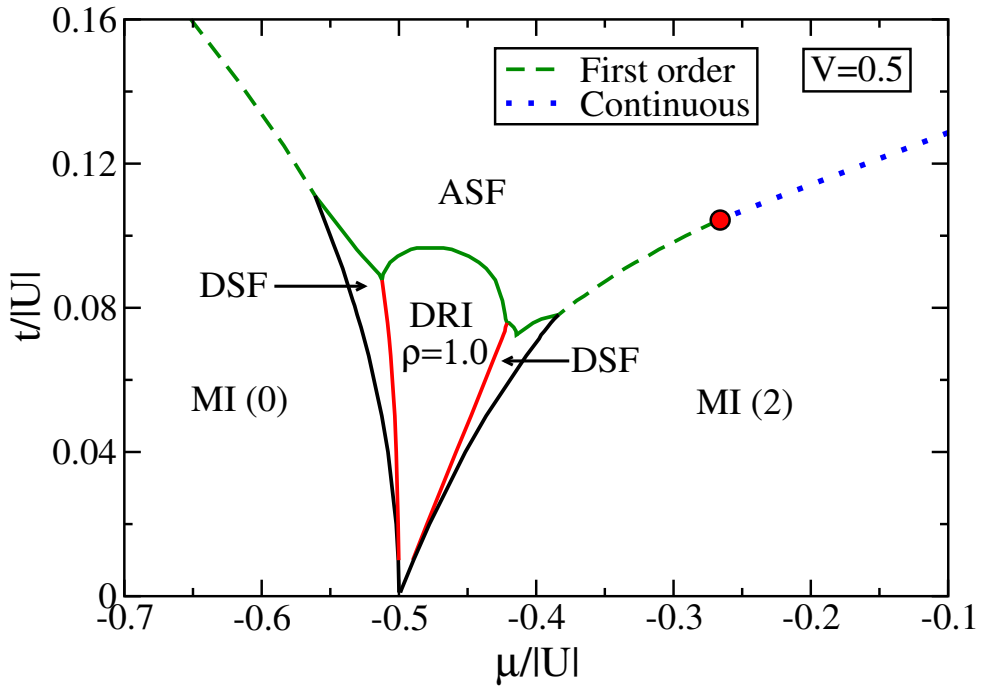

Figure 6.10: Phase diagram for $U < 0$ and $V = 0.5$ showing different phases. Green (dashed) line and blue (dotted) line indicate first and second-order transitions, respectively. The first- to second-order change on the phase boundary is marked by a red dot.

each rung. This phase exhibits a finite single particle gap, and vanishing superfluid order parameter. This phase can be called as the dimer rung insulator (DRI). However, for the density range $0 < \rho < 1$ and $1 < \rho < 2$, the system remains in the DSF phase. In order to obtain the phase diagram we analyse the plots of ρ and ρ_s as a function of μ and is given for $V = 0.5$ in Fig.6.9. It is evident that when $U = -8.0$, the effect of V is not visible as shown in Fig.6.9(a). However, Fig.6.9(b) shows that for $U = -10.5$ there appears a plateau at $\rho = 1/3$ and $\rho = 1$. The length of the $\rho = 1/3$ plateau increases slightly but $\rho = 1$ plateau increases considerably as $|U|$ increases, as shown in Fig.6.9(c). At the $\rho = 1$ plateau region the value of ρ_s is zero which reflects that the DRI phase is gapped. By picking the boundary points from the ρ versus μ curve we obtain the phase diagram as shown in Fig.6.10. When the value of $V = 1.0$, the DRI phase gets enlarged as

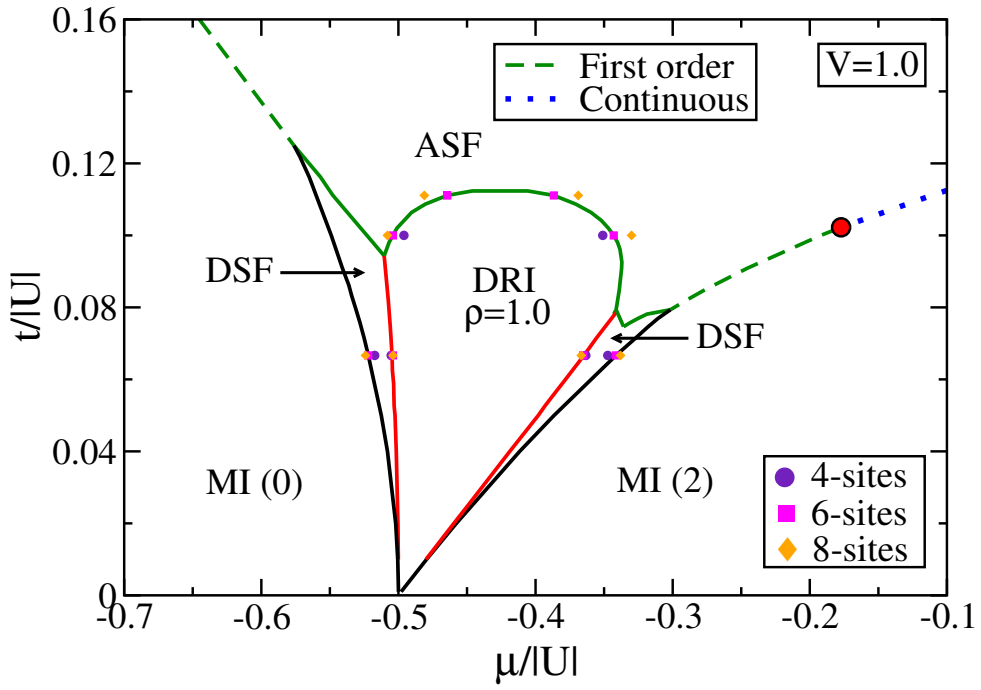

Figure 6.11: Phase diagram for $U < 0$ and $V = 1.0$ showing different phases. Green (dashed) line and blue (dotted) line indicate first and second-order transitions, respectively. The first- to second-order change on the phase boundary is marked by a red dot. The change in phase boundaries with cluster size is also indicated at $U = -9.0, -10.0$ and -15.0. For the 4-sites cluster, the DRI lobe does not extend beyond $U = -9.12$.

shown in Fig.6.11. Changes in the phase boundaries with a change in cluster size are also indicated in Fig.6.11. A scaling of ASF-DRI critical point with 4-,6- and 8-sites clusters gives an estimate of $U_c \sim -7.92$ in the thermodynamic limit. The order of the phase transitions, like before, are also obtained by simultaneously observing the sharp jump in the corresponding $\rho - \mu$ plots and the quantity $E(\phi) - E(0)$. The position of the tricritical point shifts to the higher values of $\mu/|U|$ as the value of V increases. This phenomena was also predicted before in a similar model for a square lattice [10].

The plateau at $\rho = 1$ also appears in the DSF phase. In order to distinguish between the DSF and DRI phases, we plot the single dimer correlation function (paired-tunnelling

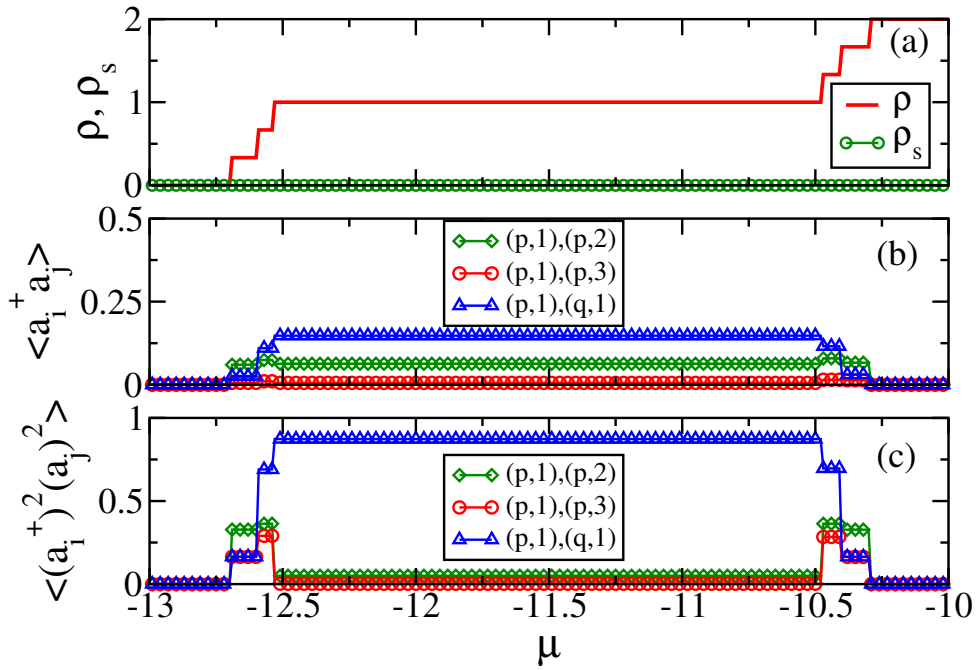

Figure 6.12: $U = -25.0, V = 1.0$. (a)$\rho, \rho_s - \mu$ plot (b)single particle tunnelling amplitude between sites (c)pair tunnelling amplitude between sites.

amplitudes) along the rung and the leg of the ladder. When the system is in the DSF phase, this correlation function is finite both along the rungs and the legs. However, in the DRI phase, it is large on the rungs compared to the legs. As the value of V increases, they tend to zero along the legs whereas they tend to one along the rungs as shown in Fig.6.12. In Fig.6.12(a) we plot the $\rho, \rho_s - \mu$ plot for $U = -25.0$ and $V = 1.0$ for comparison. In Fig.6.12(b) and (c) we plot the single particle and dimer correlations, respectively. At this density each rung has one dimer and is in a superposition of $|0, D\rangle$ and $|D, 0\rangle$ states, where D stands for a dimer. It becomes energetically unfavourable for a dimer to hop from one rung to the another as the presence of V will tend to increase the energy. As a result dimers get confined to their respective rungs. Therefore, we argue that the phase which appears at $\rho = 1$ in the presence of V is the DRI phase. The stability of the DRI phase in the thermodynamic limit is difficult to predict using the CMFT, as it takes

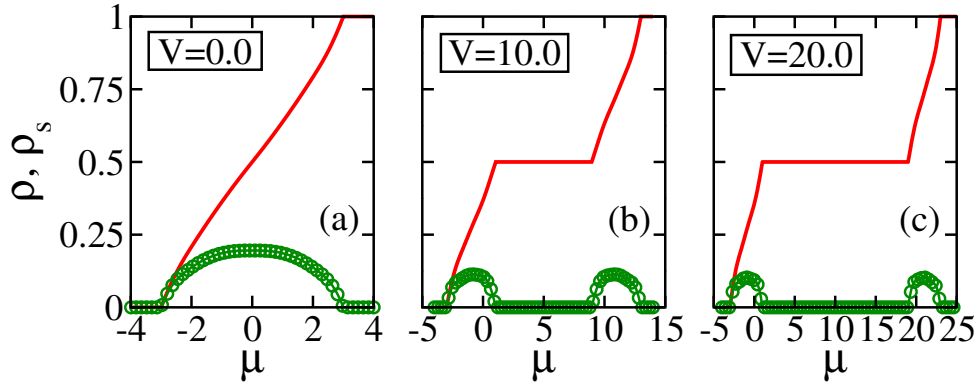

Figure 6.13: $\rho, \rho_s - \mu$ plot for HC bosons for (a)$V = 0.0$ (b)$V = 10.0$ and (c)$V = 20.0$.

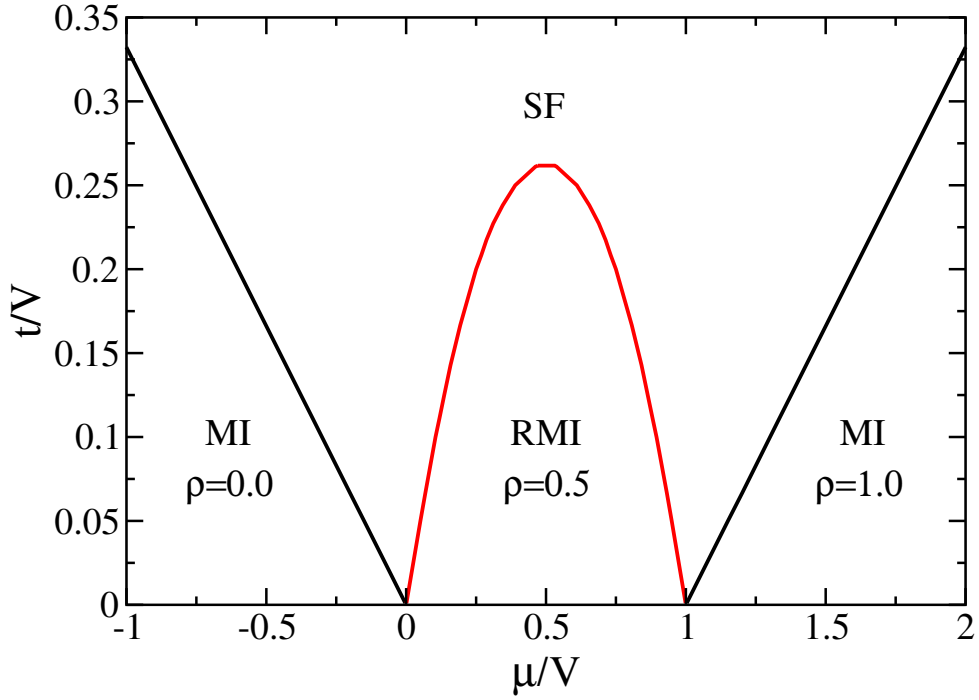

Figure 6.14: Phase diagram for hard-core bosons in the presence of inter-chain nearest neighbour interaction V.

into account only a limited number of sites in a cluster. One needs to perform rigorous numerical calculations to understand this phase in more detail.

In order to further clarify the existence of the DRI phase, we study a model of

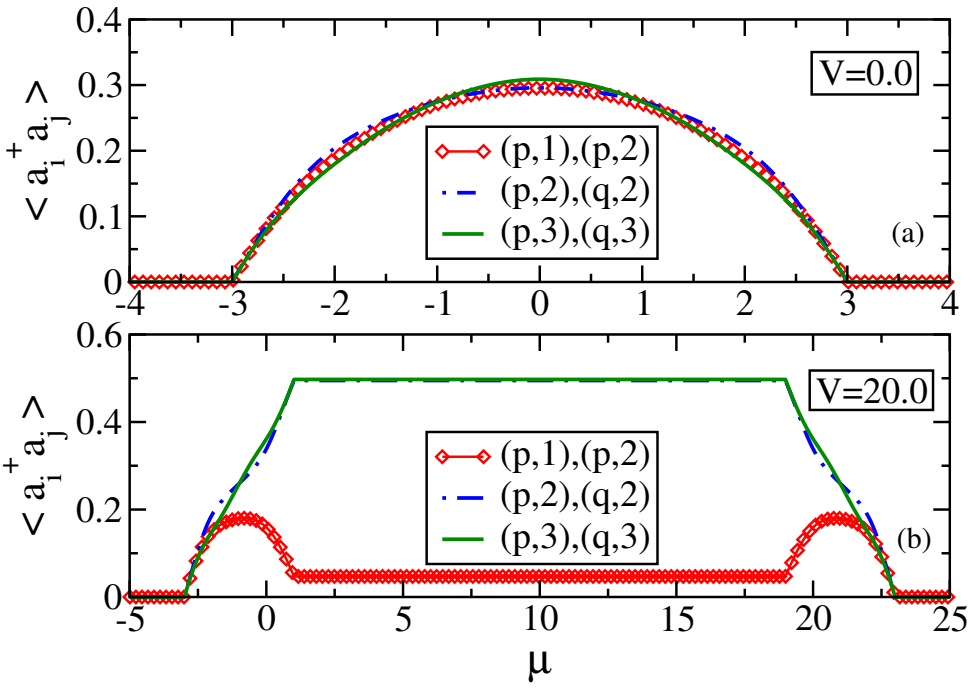

Figure 6.15: Single particle tunnelling amplitudes for hardcore bosons at (a)$V = 0.0$ and, (b)$V = 20.0$.

hardcore bosons on a two leg ladder with the nearest neighbour interactions acting along the rungs. This model at half filling is similar to the model discussed above in the limit of large attractive U at unit filling when all the atoms have formed dimers. In the previous case, because of the three body constraint the dimers behaved like hardcore bosons. Therefore, it is indeed possible to get the rung insulator (RI) phase in a similar model of hardcore bosons. The phase-diagram for hard-core bosons at $V = 0.0$ is trivial and there are only SF and MI phases. For low values of μ the system is in the $\rho = 0.0$ MI phase. As μ is increased, the density of the system increases continuously, it enters the SF phase and finally ends up in the $\rho = 1.0$ MI phase. However, by switching on the value of V, we obtain a plateau at $\rho = 0.5$ which gets enlarged as the value of V increases, as shown in Fig.6.13. The argument here is that, at $\rho = 0.5$ and at finite V the favourable ground state is when each rung of the ladder has only one hardcore boson. In

such a situation a singlet of hardcore bosons is formed along the rungs, which is a rung Mott insulator phase as discussed before. We obtain the phase diagram for this model which is shown in Fig.6.14. The presence of the RI phase can be further confirmed by comparing Fig.6.15(a) and Fig. 6.15(b). We can see that in the former case when $V = 0$, the tunnelling amplitudes between all the sites are almost the same for all values of μ but in the latter cases when $V \neq 0$ they become different. For $V \neq 0$, at $\rho = 0.5$ the tunnelling amplitude of bosons within the same leg decreases and within a rung it increases.

6.4 Conclusions

We have studied the phases and the phase transitions in an attractive Bose-Hubbard model on a two leg ladder in the presence of the three body constraint. We obtain the ground state phase diagram of this model by using the self consistent cluster mean-field theory. By calculating various physical parameters of interest, we find that there exists a transition from the ASF to the DSF phases when the density of the system varies from zero to two. When the density is zero and two we obtain two gapped phases such as MI(0) and MI(2). By introducing nearest neighbour interactions between the particles sitting in the two sites of a rung, we obtain the dimer rung insulator(DRI) phase at unit filling. The DRI phase is gapped in which the particle motion is confined within the rungs of the ladder. This phase appears in the middle of the DSF phase which gets enhanced as the value of the nearest neighbour interaction increases. We also find that the MI(0)-ASF transition boundary is first order. However, the ASF-MI(2) phase boundary is continuous for small values of $|U|$ and becomes first order when $|U|$ is large through a tricritical point. This point shifts towards the smaller values of $|U|$ as the value of V increases. We also complement our prediction of the DRI phase by studying a system of hardcore bosons on a two leg ladder with nearest neighbour repulsions only along the rung. To check the stability of the phases and scaling of the critical points we have done the calculations

using 4, 6, 8 and 10 site clusters for the hardcore bosons. For the soft-core bosons with the three-body constraint we have done calculations up to 8-sites keeping V fixed at 1.0. In the case of hard-core bosons on a ladder we find that phase diagram improves with the increase in cluster size and the RI-SF critical point approaches the value as obtained from DMRG and QMC calculations. In the case of soft-core bosons with the three-body constraint we find that overall the phase diagram remains the same qualitatively and there are only small changes in the phase boundaries with the change in cluster size.

Bibliography

[1] M. Lewenstein, A. Sanpera, V. Ahufinger, Ultracold Atoms in Optical Lattices, (Oxford Univ. Press), (2012).

[2] D. Jaksch, C. Bruder, J. I. Cirac, C. W. Gardiner, and P. Zoller, Phys. Rev. Lett. **81**, 3108 (1998).

[3] M. Greiner, O. Mandel, T. Esslinger, T. W. Hänsch, and I. Bloch, Nature **415**, 39 (2002).

[4] T. Lahaye, C. Menotti, L. Santos, M. Lewenstein, and T. Pfau, Rep. Prog. Phys., **72**, 126401 (2009).

[5] F. Hebert, G. G. Batrouni, R. T. Scalettar, G. Schmid, M. Troyer, and A. Dorneich, Phys. Rev. B **65**, 014513 (2001).

[6] G. G. Batrouni, R. T. Scalettar, G. T. Zimanyi, and A. P. Kampf, Phys. Rev. Lett. **74**, 2527 (1995).

[7] M. Boninsegni and N. V. Prokof'ev, Phys. Rev. Lett. **95**, 237204 (2005).

[8] S. Wessel and M. Troyer, Phys. Rev. Lett. **95**, 127205 (2005).

[9] D. Heidarian and K. Damle, Phys. Rev. Lett. **95**, 127206 (2005).

[10] R. G. Melko, A. Paramekanti, A. A. Burkov, A. Vishwanath, D. N. Sheng, and L. Balents, Phys. Rev. Lett. **95**, 127207 (2005).

[11] G. G. Batrouni, F. Hebert, and R. T. Scalettar, Phys. Rev. Lett. **97**, 087209 (2006).

[12] T. Mishra, R. V. Pai, S. Ramanan, M. S. Luthra, and B. P. Das, Phys. Rev. A **80**, 043614 (2009).

[13] T. Mishra, R. V. Pai, and B. P. Das, Phys. Rev. B **81**, 024503 (2010).

[14] A. Griesmaier, J. Werner, S. Hensler, J. Stuhler, and T. Pfau, Phys. Rev. Lett. **94**, 160401 (2005).

[15] Q. Beaufils, R. Chicireanu, T. Zanon, B. Laburthe-Tolra, E. Marechal, L. Vernac, J. C. Keller, and O. Gorceix, Phys. Rev. A **77**, 061601 (2008).

[16] M. Lu, N. Q. Burdick, S. H. Youn, and B. L. Lev, Phys. Rev. Lett. **107**, 190401 (2011); M. Lu, N. Q. Burdick, and B. L. Lev, ibid. **108**, 215301 (2012).

[17] K. Aikawa, A. Frisch, M. Mark, S. Baier, A. Rietzler, R. Grimm, and F. Ferlaino, Phys. Rev. Lett. **108**, 210401 (2012).

[18] K.-K. Ni et al., Science **322**, 231 (2008); M. H. G. de Miranda et al., Nat. Phys. **7**, 502 (2011); A. Chotia, B. Neyenhuis, S. A. Moses, B. Yan, J. P. Covey, M. Foss-Feig, A. M. Rey, D. S. Jin, and J. Ye, Phys. Rev. Lett. **108**, 080405 (2012).

[19] T. F. Gallagher and P. Pillet, in Advances in Atomic, Molecular, and Optical Physics, edited by E. Arimondo (Academic Press, London, 2008), Vol. **56**, p. 161.

[20] M. A. Cazalilla, R. Citro, T. Giamarchi, E. Orignac, and M. Rigol, Reviews of Modern Physics **83**, 1405 (2011).

[21] T. Giamarchi, Quantum Physics in One Dimension, (Oxford Univ. Press), (2006).

[22] E. Dagotto and T. M. Rice, Science **271**, 618 (1996).

[23] M. Uehara, T. Nagata, J. Akimitsu, H. Takahashi, N. Môri1 and K. Kinoshita, J. Phys. Soc. Jpn. **65**, 2764 (1996).

[24] C. Kim, A. Y. Matsuura, Z.-X. Shen, N. Motoyama, H. Eisaki, S. Uchida, T. Tohyama, and S. Maekawa, Phys. Rev. Lett. **77**, 4054 (1996).

[25] M. A. Cazalilla, A. F. Ho and T. Giamarchi, New J. Phys. **8**, 158 (2006).

[26] P. Donohue and T. Giamarchi, Phys. Rev. B **63**, 180508(R) (2001).

[27] M. S. Luthra, T. Mishra, R. V. Pai, and B. P. Das, Phys. Rev. B **78**, 165104 (2008).

[28] E. Orignac and T. Giamarchi, Phys. Rev. B **64**, 144515 (2001).

[29] A. Dhar, M. Maji, T. Mishra, R. V. Pai, S. Mukerjee, and A. Paramekanti, Phys. Rev. A **85**, 041602(R) (2012).

[30] A. Dhar, T. Mishra, M. Maji, R. V. Pai, S. Mukerjee, and A. Paramekanti, Phys. Rev. B **87**, 174501 (2013).

[31] A. Dhar, T. Mishra, R. V. Pai, S. Mukerjee, and B. P. Das, Phys. Rev. A **88**, 053625 (2013).

[32] T. Mishra, R. V. Pai, and S. Mukerjee, Phys. Rev. A **89**, 013615 (2014).

[33] T. Mishra, R. V. Pai, S. Mukerjee, and Arun Paramekanti, Phys. Rev. B **87**, 174504 (2013).

[34] A. Petrescu and K. Le Hur, Phys. Rev. Lett. **111**, 150601 (2013).

[35] M. P. Zaletel, S. A. Parameswaran, A. Rüegg and E. Altman, arXiv:1308.3237 (2013).

[36] W. S. Cole, S. Zhang, A. Paramekanti, and N. Trivedi, Phys. Rev. Lett. **109**, 085302 (2012).

[37] M. Dalmonte, G. Pupillo, and P. Zoller, Phys. Rev. Lett. **105**, 140401 (2010).

[38] M. Bauer and Meera M. Parish, Phys. Rev. Lett. **108**, 255302 (2012).

[39] I. Danshita, J. E. Williams, C. A. R. Sá de Melo, and C. W. Clark, Phys. Rev. A **76**, 043606 (2007).

[40] I. Danshita, Carlos A. R. Sá de Melo, and Charles W. Clark, Phys. Rev. A **77**, 063609 (2008).

[41] M. Albiez, R. Gati, J. Fölling, S. Hunsmann, M. Cristiani, and M. K. Oberthaler, Phys. Rev. Lett. **95**, 010402 (2005).

[42] M. Atala, M. Aidelsburger, M. Lohse, J. T. Barreiro, B. Paredes, I. Bloch, arXiv:1402.0819

[43] A. J. Daley, J. M. Taylor, S. Diehl, M. Baranov, and P. Zoller, Phys. Rev. Lett. **102**, 040402 (2009).

[44] K. P. Schmidt, J. Dorier, A. Läuchli, and F. Mila, Phys. Rev. B **74**, 174508 (2006).

[45] M. W. J. Romans, R. A. Duine, Subir Sachdev, and H. T. C. Stoof, Phys. Rev. Lett. **93**, 020405 (2004).

[46] L. Bonnes and S. Wessel, Phys. Rev. Lett. **106**, 185302 (2011).

[47] Y.-W. Lee and M.-F. Yang, Phys. Rev. A **81**, 061604(R) (2010).

[48] Y.-C. Chen, K.-K. Ng, and M.-F. Yang, Phys. Rev. B **84**, 092503 (2011).

[49] A. J. Daley and J. Simon, arXiv:1311.1783v1

[50] S. Greschner, L. Santos, and T. Vekua, Phys. Rev. A **87**, 033609 (2013).

[51] S. R. White, Phys. Rev. Lett. **69**, 2863 (1992).

[52] U. Schollwöck, Rev. Mod. Phys. **77**, 259 (2005).

[53] D. van Oosten, P. van der Straten, and H. T. C. Stoof, Phys. Rev. A **63**, 053601 (2001).

[54] K. Sheshadri, H. R. Krishnamurthy, R. Pandit, and T. V. Ramakrishnan, Europhys. Lett. **22**, 257 (1993).

[55] Ramesh V. Pai, K. Sheshadri, and R. Pandit, Phys. Rev. B **77**, 014503 (2008).

[56] R. V. Pai, J. M. Kurdestany, K. Sheshadri, and R. Pandit, Phys. Rev. B **85**, 214524 (2012).

[57] M. Singh, A. Dhar, T. Mishra, R. V. Pai, and B. P. Das, Phys. Rev. A **85**, 051604 (R).

[58] A. Dhar, M. Singh, R. V. Pai, B. P. Das, Phys. Rev. A **84**, 033631 (2011).

[59] P. Buonsante, V. Penna, and A. Vezzani, Laser Physics, **15**, 361 (2005).

[60] T. McIntosh, P. Pisarski, R. J. Gooding, and E. Zaremba, Phys. Rev. A **86**, 013623 (2012).

[61] D. Huerga, J. Dukelsky, and G. E. Scuseria, Phys. Rev. Lett. **111**, 045701 (2013).

[62] D. Yamamoto, A. Masaki, and I. Danshita, Phys. Rev. B **86**, 054516 (2012).

[63] S. R. Hassan and L. de' Medici, Phys. Rev. B **81**, 035106 (2010).

[64] J. Carrasquilla, F. Becca, and M. Fabrizio, Phys. Rev. B **83**, 245101 (2011).

[65] F. Crépin, N. Laflorencie, G. Roux, and P. Simon, Phys. Rev. B **84**, 054517 (2011).

[66] P. Massignan and H. T. C. Stoof, Phys. Rev. A **78**, 030701(R) (2008).

[67] T. Mishra, J. Carrasquilla, and M. Rigol, Phys. Rev. B **84**, 115135 (2011).

[68] T. Stöferle, H. Moritz, C. Schori, M. Köhl, and T. Esslinger, Phys. Rev. Lett. **92**, 130403 (2004).

Chapter 7

Dynamics of ultracold bosonic atoms in optical lattices with nearest-neighbour interaction

7.1 Introduction

Ultracold bosonic atoms in optical lattices with nearest-neighbour interaction can be described well by using the extended Bose-Hubbard model. In this chapter first we give a brief introduction to the Extended Bose-Hubbard EBH) model and it's phase diagram for various boundary conditions. After discussing the EBH model for the static case we focus on it's dynamics.

The Bose-Hubbard (BH) model for ultracold atoms is the simplest model for describing a system of ultracold atoms in optical lattices. For sufficiently large interaction strengths and integer densities the well known superfluid to Mott insulator transition can be observed. However, the Bose-Hubbard model takes into account only the two-body on-site interaction and tunnelling of atoms to the nearest neighbouring sites. But as seen

in Chapter 6, in addition to the on-site (local) interaction, it is possible to have nearest-neighbour (non-local) interactions also which account for the interactions between two particles present in adjacent sites. This situation in which the Bose-Hubbard model is augmented by nearest neighbour two body interactions is referred to as the Extended Bose-Hubbard (EBH) model [1, 2, 3].

During a continuous quantum phase transition a system passes through a critical point located on the boundary separating the phases. The study of the time evolution of the system when it is quenched by the application of a time dependent potential, would enable the study of the behaviour of the excitations produced during this process [4]. There have been studies on the quenching in the BH model from the SF to the MI phase and vice-versa. In these and similar works, time evolution of various quantities such as coherence length, particle number density, etc. has been studied numerically [5-27]. There have been some experimental studies as well [28, 29, 30]. The number of defects generated then exhibits a power-law behaviour with respect to the rate of quench. This phenomenon is analogous to the Kibble-Zurek (KZ) mechanism for defect generation in non-equilibrium classical phase transitions. This mechanism was first proposed in the context of early-universe where the phase transitions took place because of the thermal fluctuations [4, 5, 6] but recently the quantum analogue has also been demonstrated [31, 32]. It was shown that the number of excitations generated in a quench scales with the adiabaticity parameter as a power related to the critical exponents characterizing the phase transition. The KZ mechanism divides and approximates a phase transition in three regimes: (i) adiabatic (far from the critical region, before crossing the critical point), (ii) impulse (very close to the critical point), and (iii) adiabatic (far from the critical region, after crossing the critical point). Near the critical point the system does not respond to the change in the external parameters sharply. If the critical region is gapless it results in a finite correlation length (ξ) in the final state. The correlation length is then given by $\xi \sim \tau_Q^{[\frac{\nu}{1+\nu z}]}$, where τ_Q is the characteristic time for the adiabatic transition and ν, z are the critcal exponents.

The density of excitations is proportional to τ_Q^{-k}, where $|k| > 0$ [33].

Although the system can be quenched in a number of ways we have considered only a linear quench. The KZ mechanism then predicts that the density of the defects and the quench velocity are connected via a power law behaviour. As stated earlier, here also the power law exponent is given in the terms of the critical exponents of the transition. We chose the EBH model for our work because the phase diagram for this model at equlibirum is well known and the phase diagram is rich enough to study quenches for different types of phase transitions.

7.2 Model and method

7.2.1 EBH model

We have discussed the simple Bose-Hubbard model in the previous chapters and shown that it exhibits only the superfluid-Mott insulator transition for integer densities. Also in Chapter 6 we show that apart from the usual on-site interaction if the nearest-neighbour interaction is introduced it can give rise to new phases. Here we consider a system of bosons in a 1D optical lattice with on-site and nearest-neighbour interactions. Such a system can be described by the following Hamiltonian:

$$H = -t \sum_{\langle i,j \rangle} (\hat{a}_i^\dagger \hat{a}_j + \text{H.c}) + \frac{U}{2} \sum_i \hat{n}_i(\hat{n}_i - 1) + V \sum_{\langle i,j \rangle} \hat{n}_i \hat{n}_j \tag{7.1}$$

Here, $\hat{a}_i^\dagger(\hat{a}_i)$ is the creation (annihilation) operator which creates (destroys) an atom at site i, $\hat{n}_i = \hat{a}_i^\dagger \hat{a}_i$ is the number operator, t is the hopping amplitude between the adjacent sites $\langle i, j \rangle$, U represents the on-site inter-atomic two-body interaction and V is the non-local nearest-neighbour interaction. We use time adaptive DMRG in MPS formalism to obtain the time evolved wave-function and energy.

The EBH model given in Eq. 7.1 has been studied earlier using different methods [2, 3, 34, 35] including DMRG [4, 6, 37, 38] and MPS [5] methods. The inclusion of the

nearest-neighbour interactions gives rise to the density wave (DW) phase apart from the regular superfluid and MI phases. Also, depending on the different boundary conditions (BCs), the position of the various phase boundaries may shift giving rise to a different phase diagram. The phase diagram for the EBH model for different boundary conditions is given in Fig. 7.1.

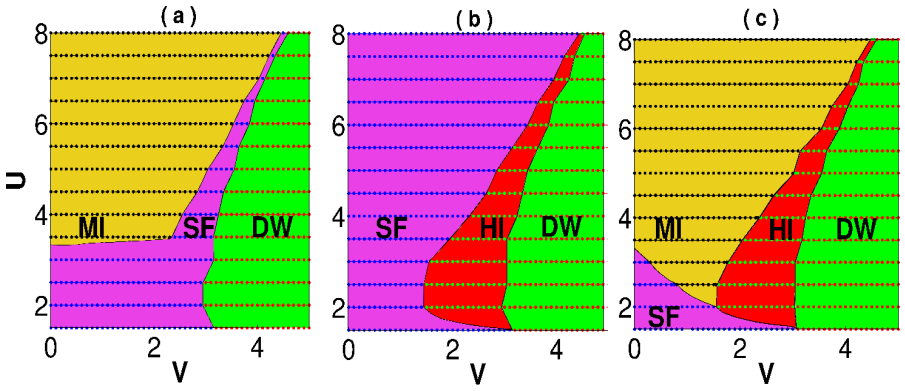

Figure 7.1: Phase diagrams in the (U, V) plane for the 1D EBHM with the following constraints (a) BC1 (N = L), (b) BC2 (N = L + 1), and (c) BC3 (N = L) and $\mu_r = -\mu_l = 2$ showing Mott-insulator (MI ochre), superfluid (SF purple), Haldane-insulator (HI red), and density wave (DW green) phases and the phase boundaries between them; in this range of U and V all transitions are continuous; at larger values of U and V the MI-DW and HI-DW transitions become first-order. N and L are no. of bosons and lattice sites respectively [6].

The appearance of the different phases can be summarized as follows: in an optical lattice if $V = 0$ and U is sufficiently larger than t then we get the Mott insulator (MI) phase at integer densities but if U and t are comparable, then we get the superfluid (SF) phase at all densities. When $V \neq 0$ and is sufficiently large then we have a density wave phase at commensurate densities. This phase is characterized by integer filling of alternate lattice sites. So, if the system has a density of 1/2 then we have [$\cdots$ 1 0 1 0 $\cdots$] type of arrangement and for density 1 we have [$\cdots$ 2 0 2 0 $\cdots$] type of arrangement of bosons

in the lattice. When U and V are comparable and BC2 (or BC3) is satisfied, we obtain the Haldane insulator (HI) phase. This phase is characterized by an underlying hidden order, that is a non-trivial ordering of the fluctuations which appear in alternating order separated by strings of equally populated sites of arbitrary length. For our work we make use of the phase diagram given in Fig. 7.1(a),(c).

7.2.2 Dynamics of ultracold atoms in the EBH model

The quantum phase transitions of ultracold atoms in optical lattices in Extended Bose-Hubbard model with nearest neighbour interaction have been studied extensively using different methods [4, 5, 40, 41, 42, 43]. However, these studies have been performed for the equilibrium case, where all the parameters are fixed with respect to time. In this work we study the effects of time varying on-site (U) and nearest neighbour interaction (V) in a one-dimensional optical lattice. The system is linearly quenched across the different phase boundaries thereby crossing a single quantum critical point. Quenching the system from one phase to another generates excitations (defects). We intent to explore whether the number of defects generated has a power law dependence on the rate of quench. In our present work we use a time dependent MPS formalism to numerically investigate how well this power law behaviour matches with the well known Kibble-Zurek scaling relation for defect generation in different scenarios for the quenching in EBH model. To do so, we vary U (or V) with time while keeping all the other parameters fixed. To study the dynamics of the system we make the following choices:
for superfluid to Mott insulator transition $U \to U(\tau)$,

$$H(\tau) = -t \sum_{\langle i,j \rangle} (\hat{a}_i^\dagger \hat{a}_j + \text{H.c}) + \frac{U(\tau)}{2} \sum_i \hat{n}_i(\hat{n}_i - 1) + V \sum_{\langle i,j \rangle} \hat{n}_i \hat{n}_j \tag{7.2}$$

and for superfluid to density wave, Mott insulator to density wave transitions $V \to V(t)$,

$$H(\tau) = -t \sum_{\langle i,j \rangle} (\hat{a}_i^\dagger \hat{a}_j + \text{H.c}) + \frac{U}{2} \sum_i \hat{n}_i(\hat{n}_i - 1) + V(\tau) \sum_{\langle i,j \rangle} \hat{n}_i \hat{n}_j \tag{7.3}$$

The time-evolved wave function $|\Psi(t)\rangle$ is given by the solution of Schrödinger equation for the time-dependent Hamiltonian $\hat{H}(t')$ as

$$|\Psi(t)\rangle = exp(-i\int_0^t \hat{H}(t')dt')|\Psi(0)\rangle \tag{7.4}$$

where $|\Psi(0)\rangle$ is the ground state wave function at $t = 0$, and in our case it can be the wave-function corresponding to the superfluid or the Mott insulator phase depending on the regime under study. As mentioned earlier, during a quench excitations are generated. As a result the final state of the system at the end of quench is not a perfect ground state corresponding to any particular phase as it would have been if there were no quenching. The final state so obtained has the contribution from higher excited states also. If E_0 be the ground state for a particular set of parameters and E_f be the energy at the end of quench for the same set of parameters, then we define 'residual energy' as $E_{res} = E_f - E_0$. We can find an expression for residual energy and explicitly show that it is equal to the weighted sum of the various excitation energies by the following argument. The normalized wave-function $|\Psi\rangle$ can be written as,

$$|\Psi\rangle = \sum_n c_n|\psi_n\rangle \tag{7.5}$$

where $|\psi_n\rangle$ are the eigen states or eigen vectors of form the orthonormal basis for $|\Psi\rangle$. Therefore, residual energy,

$$E_{res} = \langle\Psi_f|H(\tau_f)|\Psi_f\rangle - \langle\psi_f^g|H(\tau_f)|\psi_f^g\rangle \tag{7.6}$$

where τ_f is the time elapsed during the quench, $|\Psi_f\rangle$ is the time evolved wave-function and $|\psi_f^g\rangle$ is time independent wave-function, superscript g denotes the ground state. Substituting Eq.(7.5) in Eq.(7.6) gives,

$$\begin{aligned} E_{res} &= \sum_m\sum_n c_m^* c_n \langle\psi_f^m|H(\tau_f)|\psi_f^n\rangle - \langle\psi_f^g|H(\tau_f)|\psi_f^g\rangle \\ &= \sum_m\sum_n c_m^* c_n E_n \langle\psi_f^m|\psi_f^n\rangle - E_0 \\ &= \sum_n c_n^* c_n E_n - E_0. \end{aligned} \tag{7.7}$$

Here E_0 is the ground state energy corresponding to $|\psi_f^g\rangle$ and E_n is the energy of n^{th} excited state. Also,

$$\begin{aligned}
\langle\psi_f|\psi_f\rangle &= 1 \\
L.H.S. &= \sum_m \sum_n c_m^* c_n \langle\psi_f^m|\psi_f^n\rangle \\
&= \sum_n c_n^* c_n \delta_{mn} \\
&= \sum_{n\neq 0} c_n^* c_n + c_0^* c_0 = 1. \qquad (7.8)
\end{aligned}$$

Rearranging Eq.(7.8) and substituting in Eq.(7.7) gives,

$$\begin{aligned}
E_{res} &= \sum_{n\neq 0} c_n^* c_n E_n + (c_0^* c_0 - 1)E_0 \\
&= \sum_{n\neq 0} c_n^* c_n E_n - \sum_{n\neq 0} c_n^* c_n E_0 \\
&= \sum_{n\neq 0} c_n^* c_n (E_n - E_0). \qquad (7.9)
\end{aligned}$$

We study the dynamics for the three cases: (i)SF-MI, (ii)SF-DW and (iii)MI-DW transition. For the SF-MI transition U is varied with respect to time at different rates $\alpha(\propto (1/\tau))$, keeping V fixed. We repeat the calculations for four different values of V. For each value of V, the starting value of U is chosen such that the system is in the SF phase and the end value of U is such that the system is in the MI phase. Both the U values are symmetrically located about the phase boundary. The points on the phase boundary (about which U values are symmetrically located) are taken from the Fig. 7.1. Corresponding to each α, we obtain the residual energy and plot $log\ (1/\tau)$ $vs.$ $log\ E_{res}$ on X- and Y-axis respectively. Theory predicts the relationship between E_{res} and τ as:

$$log\ E_{res} = -k\ log(\tau) + const. \quad (k > 0) \qquad (7.10)$$

We perform the best linear fit to the points obtained for each V value and find the slope, k. The negative of the slope of the line gives the KZ coefficient. For the SF-DW (and

MI-DW) dynamics the procedure is same as above except the fact that in these two cases we vary V at different rates α while keeping U fixed. We repeat the calculations for four different values of U. The starting and the ending values of V are symmetrically located about the phase boundaries. The points on the phase boundaries are found as mentioned in the previous sections.

7.3 Results and discussion

We have done systematic studies of quenching by dividing the EBH phase diagram into three regions covering three different types of phase transitions:
(i) Superfluid to Mott-insulator transition,
(ii) Superfluid to Density wave transition, and
(iii) Mott-insulator to Density wave transition.
In all the three cases we choose four sets of quantum critical points on each of the three phase boundaries. We quench our system by keeping V fixed and varying U with time in the first case and for the last two cases we keep U fixed and vary V with time.

7.3.1 Quenching from the superfluid to Mott-insulator phase

For the quench from the SF to MI phase, the range of parameters for U and V is given in Table 7.1. U_i is the initial value of the on-site interaction strength U, at the beginning of the quench and U_f if the final value, at the end of quench. The nearest-neighbour interaction remains unchanged, therefore $V_i = V_f$.

No.	U_i	U_f	V_i	V_f
1	2.00	4.00	0.25	0.25
2	1.80	3.80	0.50	0.50
3	1.50	3.50	0.75	0.75
4	1.30	3.30	1.00	1.00

Table 7.1: Table summarizing the values of the interaction parameters for the superfluid to Mott-insulator phase quench.

The values of interaction parameters are chosen such that the system starts from the superfluid phase, far from the superfluid-Mott insulator phase boundary and ends up in the Mott-insulator phase. The interval between U_i and U_f is 2 units.

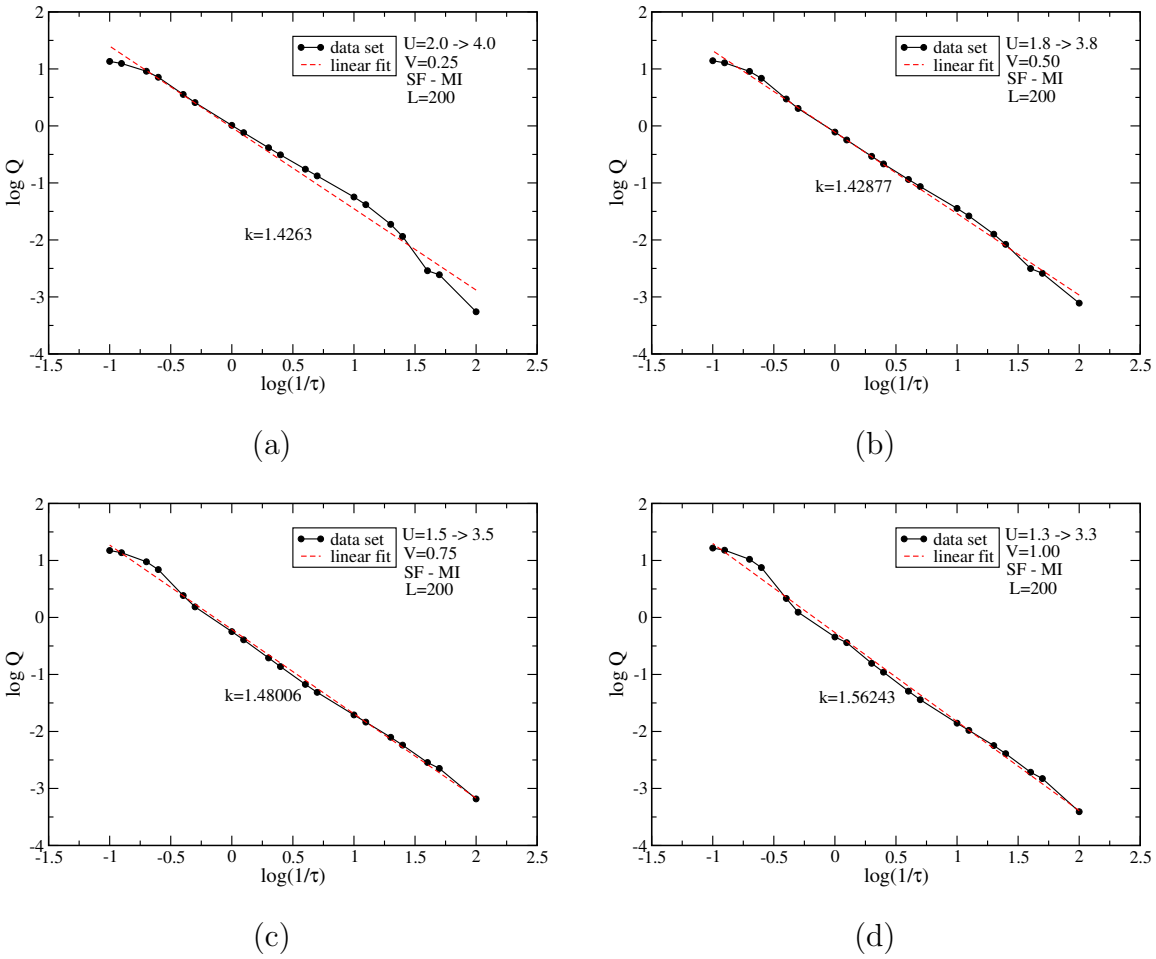

Figure 7.2: Quenching from SF to MI phase for different values of U and V, as indicated in each of the plots. Black dots indicate the data obtained from our numerical calculations and red-dashed line indicates the linear fit for these data points.

The results for the superfluid-Mott insulator quench are presented in Fig. 7.2. The value of the Kibble-Zurek coefficient found for the superfluid to Mott-insulator quench ranges from 1.42630 to 1.56243 in our calculations.

7.3.2 Quenching from the superfluid to density wave phase

For the quench from the superfluid to the density wave phase, the range of parameters for U and V is given in Table 7.2. The on-site interaction remains unchanged for this quench and therefore the initial and final values of the on-site interaction strength U, that is U_i and U_f, are the same. The nearest-neighbour interaction changes from V_i to V_f.

No.	U_i	U_f	V_i	V_f
1	1.50	1.50	0.10	6.10
2	2.00	2.00	0.70	6.70
3	2.50	2.50	0.70	6.70
4	3.00	3.00	0.00	6.00

Table 7.2: Table summarizing the values of the interaction parameters for the superfluid to density-wave phase quench.

The values of the interaction parameters are chosen such that the system starts from the superfluid phase, far from the superfluid-density wave phase boundary, and ends up in the density wave phase. The interval between V_i and V_f is 6 units. The results for the superfluid-density wave phase quench are presented in Fig. 7.3. It can be seen in this figure that all the data points can not be fitted with a single linear fit. Therefore, we divide the quench region into three parts: (i) slow, (ii) intermediate and (iii) fast quench. We present our results for these regions accordingly.

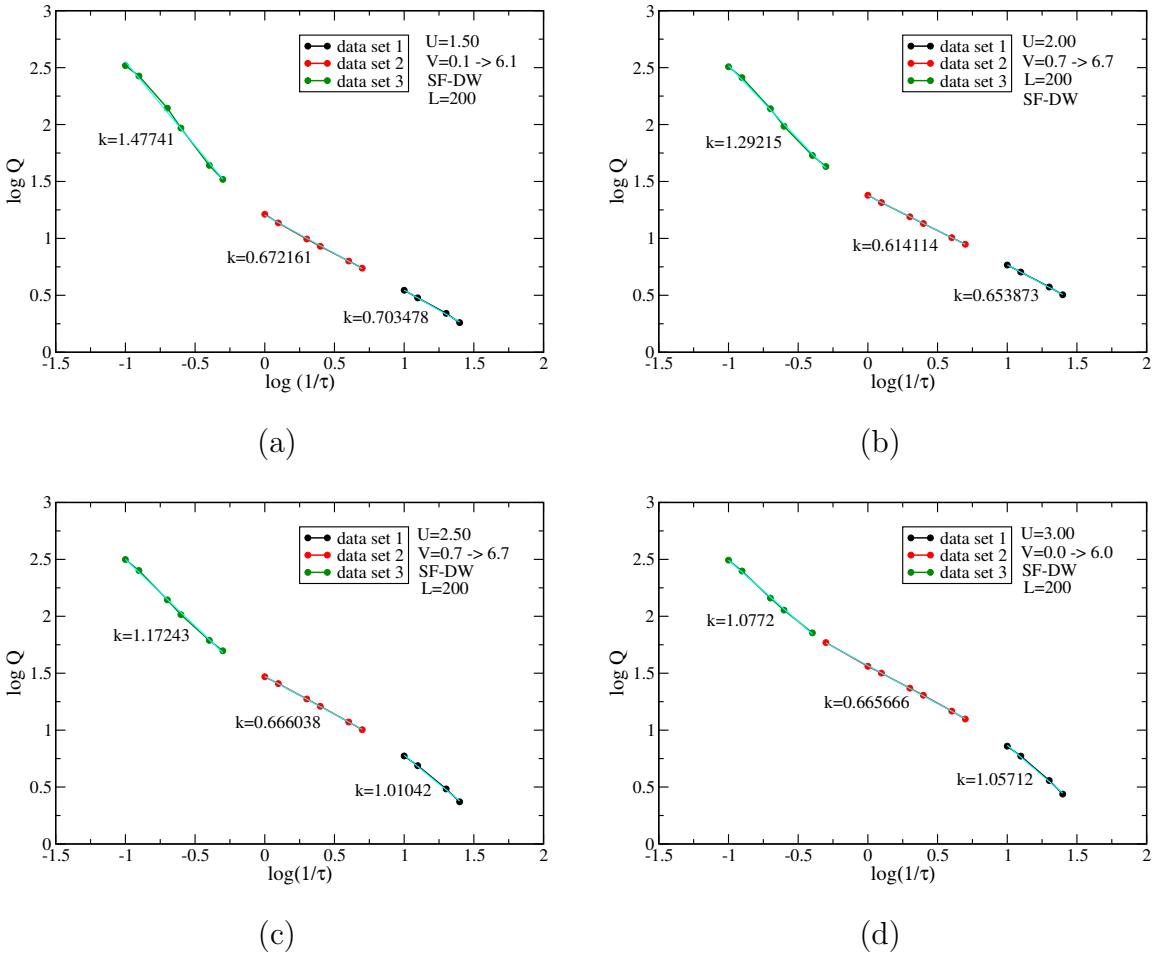

Figure 7.3: Quenching from the SF to the DW phase for different values of U and V, as indicated in each of the plots. Dots indicate the data obtained from our numerical calculations and solid lines indicates the linear fits for these data points.

The values of the Kibble-Zurek coefficients found for the superfluid to density wave quench range from 0.653873 to 1.05712 for the slow quench. For the intermediate quench rates the Kibble-Zurek coefficients vary from 0.614114 to 0.672161 and for the fast quenches they lie between 1.07720 and 1.47741.

7.3.3 Quenching from the Mott insulator to density wave phase

For large values of U($\gtrsim 9$), there is no superfluid phase, so we choose U to be greater than or equal to 9. For this case, the range of parameters for U and V is given in Table 7.3. Like in the previous case, the on-site interaction remains unchanged for this quench also and the nearest-neighbour interaction changes from V_i to V_f. The values of the interaction parameters are chosen such that the system starts in the Mott insulator phase, far from the Mott insulator-density wave phase boundary, and ends up in the density wave phase. The interval between V_i and V_f is 6 units. The results for Mott-insulator to density wave phase quench are presented in Fig. 7.4. Superfluid to Mott insulator and superfluid to density wave phase transitions are second-order transitions, but the Mott insulator to density wave transition is a first-order transition. Unlike the former two cases, in the latter case the energy gap does not change smoothly, instead there is a sudden jump in the gap at the critical point. Therefore, we expect the Kibble-Zurek coefficient to vary significantly from what it was found to be in the other two cases.

No.	U_i	U_f	V_i	V_f
1	9.00	9.00	1.90	7.90
2	9.50	9.50	2.10	8.10
3	10.00	10.00	2.40	8.40
4	10.50	10.50	2.60	8.60

Table 7.3: Table summarizing the values of the interaction parameters for the Mott insulator to density wave phase quench.

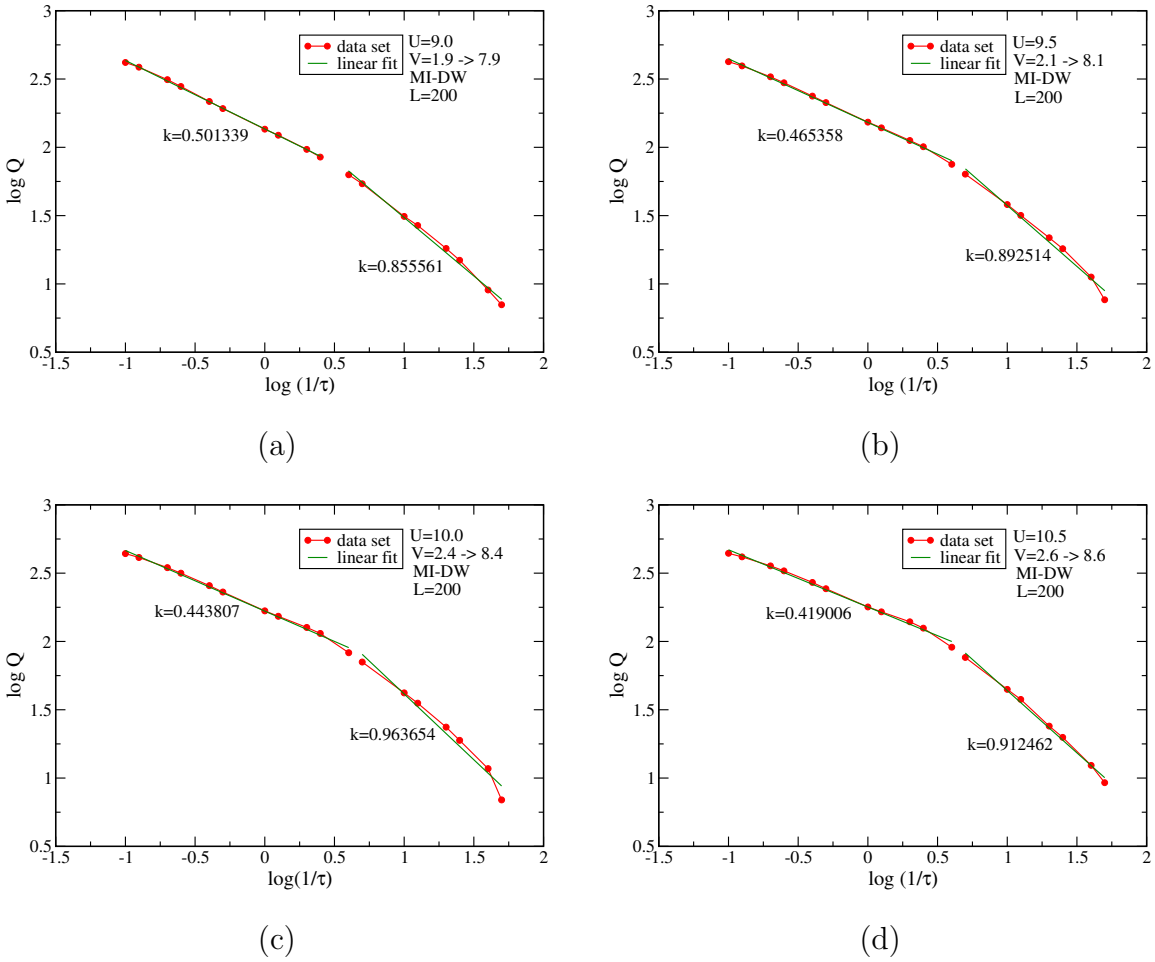

Figure 7.4: Quenching from MI to DW phase for different values of U and V, as indicated in each of the plots. Dots indicate the data obtained from our numerical calculations and solid lines indicates the linear fits for these data points.

Here again the complete data could not be fit using a single linear fit therefore we divide quench region into two convenient parts: (i) slow and (ii) fast to get good linear fits. As can be seen from Fig. 7.4, Kibble-Zurek coefficients for the slow quenches vary from 0.855561 to 0.963654 and for the fast quench they lie between 0.419006 and 0.501339. Unlike the previous two cases of gapless to gapped transitions, where the Kibble-Zurek coefficient was obtained as $\sim$1.4, for the present case which is a gapped to

gapped transition involving the MI and DW phases this coefficient is found to be $\sim$0.5.

7.4 Conclusions

In conclusion, we have studied the effects of the linear quench on a system of ultracold cold atoms in optical lattices within the framework of the extended Bose-Hubbard model. The system was quenched by varying the interactions with respect to time at different rates across the, (i) superfluid-Mott insulator, (ii) superfluid-density wave, and (iii) Mott insulator-density wave phase boundaries. In each case we obtain a power-law behaviour of the residual energy (hence, the generation of defects) with the quench rate. We find that the Kibble-Zurek (power-law) coefficient in each case largely depends on the type of transition.

Bibliography

[1] Ramesh V. Pai and Rahul Pandit, Phys. Rev. B **71**, 104508 (2005).

[2] G. G. Batrouni, R. T. Scalettar, G. T. Zimanyi and A. P. Kampf, Phys. Rev. Lett. **74**, 2527 (1995).

[3] Davide Rossini and Rosario Fazio, New J. Phys. **14**, 065012 (2012).

[4] W.H. Zurek, Nature **317**, 505 (1985).

[5] T.W.B. Kibble, J. Phys. A: Math. Gen. **9**, 1387 (1976).

[6] W.H. Zurek, U. Dorner, and P. Zoller, Phys. Rev. Lett. **95**, 105701 (2005).

[7] S.R. Clark and D. Jaksch, Phys. Rev. A **70**, 043612 (2004).

[8] R. Schützhold, M. Uhlmann, Y. Xu, and U.R. Fischer, Phys. Rev. Lett. **97**, 200601 (2006).

[9] J. Dziarmaga, Phys. Rev. Lett. **95**, 245701 (2005).

[10] R.W. Cherng and L. Levitov, Phys. Rev. A **73**, 043614 (2006).

[11] F.M. Cucchietti, B. Damski, J. Dziarmaga and W.H. Zurek, Phys. Rev. A **75**, 023603 (2007).

[12] L. Cincio, J. Dziarmaga, M.M. Rams, and W.H. Zurek, Phys. Rev. A **75**, 052321 (2007).

[13] T. Caneva, R. Fazio and G.E. Santoro, Phys. Rev. B **76**, 144427 (2007).

[14] T. Caneva, R. Fazio and G.E. Santoro, Phys. Rev. B **78**, 104426 (2008).

[15] F. Pellegrini, S. Montangero, G.E. Santoro, and R. Fazio, Phys. Rev. B **77**, 140404 (R) (2008).

[16] K. Sengupta, D. Sen, and S. Mondal, Phys. Rev. Lett. **100**, 077204 (2008).

[17] S. Deng, G. Ortiz, and L. Viola, Europhys. Lett. **84**, 67008 (2008).

[18] U. Divakaran, A. Dutta, and D. Sen, Phys. Rev. B **78**, 144301 (2008).

[19] A. Polkovnikov and V. Gritsev, Nature Phys. **4**, 477 (2008).

[20] C. De Grandi, R.A. Barankov and A. Polkovnikov, Phys. Rev. Lett. **101**, 230402 (2008).

[21] E. Canovi, D. Rossini, R. Fazio, and G.E. Santoro, J. Stat. Mech. P03038 (2009).

[22] V. Mukherjee and A. Dutta, Europhys. Lett. **92**, 37004 (2010).

[23] F.E. Zimmer and M. Haque, arXiv:1012.4492 (2010); arXiv:1110.0840 (2011).

[24] C. Trefzger and K. Sengupta, Phys. Rev. Lett. **106**, 095702 (2011).

[25] J.-S. Bernier, G. Roux, and C. Kollath, Phys. Rev. Lett. **106**, 200601 (2011).

[26] J.-S. Bernier, D. Poletti, P. Barmettler, G. Roux, and C. Kollath, Phys. Rev. A **85**, 0336

[27] S. Braun, M. Friesdorf, S.S. Hodgman, M. Schreiber, J.P. Ronzheimer, A. Riera, M. del Rey, I. Bloch, J. Eisert, U. Schneider, **arXiv:1403.7199** (2014).

[28] S. Fölling, S. Trotzky, P. Cheinet, M. Feld, R. Saers, A. Widera, T. Müller, and I. Bloch, Nature **448**, 1029 (2007).

[29] M. Cramer, A. Flesch, I.P. McCulloch, U. Schollwöck, and J. Eisert, Phys. Rev. Lett. **101**, 063001 (2008); Phys. Rev. A **78**, 033608 (2008).

[30] S. Trotzky, Y.-A. Chen, A. Flesch, I.P. McCulloch, U. Schollwöck, J. Eisert, and I. Bloch, Nature Phys. **8**, 325 (2012).

[31] A. Polkovnikov, Phys. Rev. B **72**, 161201(R) (2005).

[32] B. Damski, Phys. Rev. Lett. **95**, 035701 (2005).

[33] J. Dziarmaga, Advances in Physics, vol. **59**, issue 6, pp. 1063-1189 (2010).

[34] V. A. Kashurnikov and B. V. Svistunov, Phys. Rev. B **53**, 11776 (1996).

[35] P. Niyaz, R. T. Scalettar, C. Y. Fong and G. G. Batrouni, Phys. Rev. B. **44**, 7143 (1991).

[36] G. G. Batrouni, F. Hebert and R. T. Scaletter, Phys. Rev. Lett. **97**, 087209 (2006).

[37] T. D. Kuhner and H. Monien, Phys. Rev. B **58**, R14741(R) (1998).

[38] T.D. Kuhner, S. R. White, H. Monien, Phys. Rev. B. **61**, 12474 (2000).

[39] Jamshid Moradi Kurdestany, Ramesh V. Pai, Subroto Mukerjee, Rahul Pandit, **arXiv:1403.2315v1** (2014).

[40] Takashi Kimura, J. Phys.: Conf. Ser. **400**, 012032 (2012).

[41] M. Maik, P. Hauke, O. Dutta, J. Zakrzewski, M. Lewenstein, New J. Phys. **15**, 113041 (2013).

[42] J.M. Kurdestany, R.V. Pai, and R. Pandit, Annalen der Physik, **524**, Issue 3-4, 234, (2012).

[43] M. Kumar, S. Sarkar, and S. Ramaseha, Int. J. Mod. Phys. B **25**, 159 (2011).

Chapter 8

Conclusions and Future Directions

8.1 Conclusions

We now summarize the findings of this PhD thesis work. Our goal was to study the behaviour of ultracold atoms loaded in optical lattices and superlattices, interacting via several kinds of interactions, local as well as non-local. Owing to different strengths of interaction parameters, lattice geometries we observe novel quantum phases that have not been studied before. The thesis work has been carried out by using quantum many-body theories and state-of-the art numerical methods.

We started by introducing the theoretical methods used for this PhD thesis work. Mean-field method, cluster mean-field method, Density Matrix Renormalization Group theory and Matrix Product States are elaborated with sufficient details. We follow it up by study of ultracold atoms in optical lattices, within the framework of the Bose-Hubbard model, using mean-field and perturbation theory methods. We show that the results obtained from our mean-field theory are in agreement with those obtained from the perturbation theory. The value of critical point for the superfluid to Mott insulator transition is found to be the same from both the methods. This is followed by the study

of quantum phase transitions in optical superlattices. In the latter case we found that when a superlattice potential is introduced, we get a new type of insulator phase which we call as superlattice induced Mott-insulator phase (SLMI) and it is different from the regular Mott-insulator phase. Turning on the superlattice potential breaks the translational symmetry of the system which is responsible for the SLMI phases. These phases, like MI phases are gapped but arise not because of any change in the interaction between the atoms but because of change in the geometry of the potential wells. Moreover these phases arise at half-integer densities and can be seen below U_c for the SF-MI transition. The regular MI phases are also affected by the superlattice potential λ. For small values of λ the system remains unaffected but for sufficiently high λ the regular MI phase (e.g. $\rho = 1$, [...1 1 1 1...]) undergoes a transition to a SLMI phase ($\rho = 1$, [...0 2 0 2...]) via a SF phase at $\lambda \approx U$.

In Chapter 4, we have shown our findings on how the on-site three-body interaction (W) effects the quantum phase transitions and changes the phase diagrams obtained obtained in previous chapters. We found from our calculations that the effect of W is very small compared to the two-body interaction in the system of bosons in an optical lattice when the filling factor of the system is unity. But as we go on increasing the density the three-body effects become significant and dominating. The introduction of the three-body on-site interaction in the above scenario significantly modifies the phase diagram. The insulating lobes get bigger in the phase diagram. Also the location of the presence of the intermediate superfluid phase gets displaced in the presence of three-body interaction [**?**]. All the results in this chapter were obtained using mean-field theory. In the next chapter we do a follow-up study using the finite size DMRG method and obtain more accurate phase diagrams of the systems mentioned above. The DMRG results confirm the results obtained using the mean-field theory and are in a good qualitative agreement.

Chapter 6 deals with the quantum phases of attractive bosons on a Bose-Hubbard ladder with three-body constraint. The model we considered was that of a two leg ladder,

but with nearest-neighbour interaction present along the rungs only. We find that there exists a transition from the atomic superfluid to the dimer superfluid phase when the density of the system varies from zero to two and interaction is attractive. When the density is two we obtain a gapped phases, MI(2). By introducing nearest neighbour interactions between the particles sitting in the two sites of a rung, we obtain the dimer rung insulator(DRI) phase at unit filling. The DRI phase is gapped in which the particle motion is confined within the rungs of the ladder. This phase appears in the middle of the DSF phase which gets enhanced as the value of the nearest neighbour interaction increases. We also find that the MI(0)-ASF transition boundary is first order. However, the ASF-MI(2) phase boundary is continuous for small values of $|U|$ and becomes first order when $|U|$ is large through a tricritical point. This point shifts towards the smaller values of $|U|$ as the value of V increases. We also complement our prediction of the DRI phase by studying a system of hardcore bosons on a two leg ladder with nearest neighbour repulsions only along the rung. To check the stability of the phases and scaling of the critical points we have done the calculations using 4, 6, 8 and 10 site clusters for the hardcore bosons. For the soft-core bosons with the three-body constraint we have done calculations upto 8-sites keeping V fixed at 1.0. In the case of hard-core bosons on a ladder we find that phase diagram improves with the increase in cluster size and the RI-SF critical point approaches the value as obtained from DMRG and Quantum Monte Carlo calculations. In the case of softcore bosons with the three-body constraint we find that overall the phase diagram remains the same qualitatively and there are only small changes in the phase boundaries with the change in cluster size.

In the last part of the thesis work, we have studied the system of ultracold atoms in optical lattices out of equilibrium within the framework of the extended Bose-Hubbard (EBH) model. We have studied the effects of linear quenches for various phase transitions within the framework of the extended Bose-Hubbard model. The phase transitions considered were, (i) SF-MI, (ii) SF-DW, and (iii) MI-DW. In each case we try to es-

tablish a power-law behaviour of the residual energy (hence, the generation of defects) with the quench rate. We find that the Kibble-Zurek (power-law) coefficient in each case largely depends on the type of transition under consideration. Also we see that the KZ mechanism type of behaviour holds only for intermediate values of quenching rates.

8.2 Future Directions

The field of ultracold atoms is now a rapidly expanding area of research and can be used to study a wire range of important problems. Some of them are listed below:

- To study quantum phase transitions in a system of ultracold atoms in an optical lattice with nearest-neighbour interactions in the presence of the three-body on-site interactions. In our studies we have looked at the phase transitions of ultracold bosonic atoms in the presence of the two-body and three-body on-site interactions [1]. The extended Bose-Hubbard model also has been studied extensively [2, 3, 4, 5, 6]. But a combined study involving on-site two-, three-body and non-local nearest-neighbour interaction has not been investigated to the best of our knowledge. So, it will be instructive to study such a system and search for novel quantum phases by varying the densities and the strengths of the interactions. This will definitely modify the existing phase diagrams and in addition to that we may obtain new phases. The study can be first carried out using the cluster mean-field method and then by the DMRG method in order to verify and obtain more accurate results. In continuation with this, the effect of the superlattice potential can also be investigated.

- To study novel quantum phases of hard-core bosons in 2D optical lattices. The dimensionality of the system also plays a crucial role in determining the phases a system can exhibit. In of our recent studies we found that the attractive bosons with a maxi-

mum occupation of 2 per site, loaded in two coupled 1D optical lattices give rise to dimer phases [7], like dimer superfluid and dimer rung-insulator [13]. Bosons in coupled 1D lattices and square lattices have been extensively studied [7, 8, 9, 10, 11, 12]. Therefore, another interesting problem to study will be the phases of two- and three-body hardcore bosons in a 2D optical lattice with identical as well as different tunnelling strengths in the two planar directions. As an extension of this, the hopping or tunnelling strengths can be made to vary in alternate fashion along one of the directions while keeping it fixed to some other value along the other direction. In both the cases we expect new phases.

- The dynamics of ultracold atoms and molecules remains a relatively unexplored area. It will be worthwhile to investigate the dynamics for the supersolid phase and quenching of systems through multicritical points. In most of these scenarios analytical studies are either not possible or can be performed with support from numerical calculations. Investigating the validity of the Kibble-Zurek mechanism in such evolution scenarios will be interesting.

- Ultracold atoms can be used for mimicking spin-orbit interactions. Engineered spin-orbit coupling in ultracold atoms can be achieved by dressing two atomic spin states with a pair of lasers. In the presence of laser coupling the two dressed atomic states are modified, driving a quantum phase transition from a spatially mixed state (laser off) to a phase separated state (above a critical laser intensity). Such systems can exhibit novel quantum phases like quantum Hall liquids, topological insulators and superfluids. Also, they can improve our understanding of phenomena that have recently been predicted for electron systems in external magnetic fields or with strong spin-orbit interaction [14, 15, 16].

- Development and application of the coupled cluster method to study ultracold

bosonic atoms in optical lattices. The coupled cluster method is a very powerful and versatile quantum many-body theory [17]. This theory has been very successful in determining atomic and molecular properties to a very high degree of accuracy [18, 19]. At first, the coupled cluster method can be applied to study the properties of atoms and molecules in general and compare with known results. After that it can applied to study ultracold bosonic and fermionic atoms in optical lattices for determining novel quantum phase transitions.

The problems proposed above as future directions are extremely relevant in the current scenario and and are worth pursuing. This pursuit will not only improve our understanding of phases of matter at ultracold temperatures but also many condensed matter phenomena. The knowledge gained by the studying these problems will surely be a significant contribution to the scientific community.

Bibliography

[1] M. Singh, A. Dhar, T. Mishra, R. V. Pai, B. P. Das, Phys. Rev. A **85**, 051604(R) (2012).

[2] G. G. Batrouni, R. T. Scalettar, G. T. Zimanyi and A. P. Kampf, Phys. Rev. Lett. **74**, 2527 (1995).

[3] G. G. Batrouni, F. Hebert and R. T. Scaletter, Phys. Rev. Lett. **97**, 087209 (2006).

[4] Ramesh V. Pai and Rahul Pandit, Phys. Rev. B **71**, 104508 (2005).

[5] Davide Rossini and Rosario Fazio, New J. Phys. **14**, 065012 (2012).

[6] J. M. Kurdestany, R. V. Pai, S. Mukerjee, R. Pandit, **arXiv:1403.2315v1** (2014).

[7] A. J. Daley, J. M. Taylor, S. Diehl, M. Baranov, and P. Zoller, Phys. Rev. Lett. **102**, 040402 (2009).

[8] L. Bonnes and S. Wessel, Phys. Rev. Lett. **106**, 185302 (2011).

[9] Y.-W. Lee and M.-F. Yang, Phys. Rev. A **81**, 061604(R) (2010).

[10] Y.-C. Chen, K.-K. Ng, and M.-F. Yang, Phys. Rev. B **84**, 092503 (2011).

[11] S. Greschner, L. Santos, and T. Vekua, Phys. Rev. A **87**, 033609 (2013).

[12] A. J. Daley and J. Simon, arXiv:1311.1783v1

[13] M. Singh, T. Mishra, R. V. Pai, and B. P. Das, Phys. Rev. A **90**, 013625 (2014).

[14] M. Z. Hasan and C. L. Kane, Rev. Mod. Phys. **82**, 3045 (2010).

[15] M. Z. Hasan and J. E. Moore, Ann. Rev. Cond. Matt. Phys. **2**, 55 (2011).

[16] X. L. Qi and S.-C. Zhang, Rev. Mod. Phys. **83**, 1057 (2011).

[17] R. F. Bishop, Microscopic Quantum Many-Body Theories and their Applications, The Coupled Cluster Method **1**, Springer (1997).

[18] B. K. Sahoo, R. K. Chaudhury, B. P. Das, D. Mukherjee, Phys. Rev. Lett. **96**, 163003 (2006).

[19] R. J. Bartlett, and M. Musial, Rev. Mod. Phys. **79**, 291 (2007).